Contributions to the Study of Autism Spectrum Brain Connectivity

By

Moises Martin Silva Choque

Department of Computer Science and Artificial Intelligence

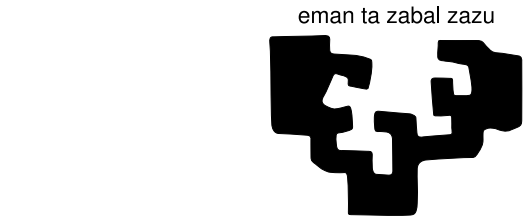

PhD Advisor:

Prof. Dr. Manuel Graña Romay UPV-EHU

Universidad del País Vasco

Euskal Herriko Unibertsitatea

Donostia - San Sebastián

2021

Contributions to the Study of Autism Spectrum Brain Connectivity

by

Moises Silva

Abstract

Abstract Autism Spectrum Disorder (ASD) is a largely prevalent neurodevelopmental condition with a big social and economical impact affecting the entire life of families. There is an intense search for biomarkers that can be assessed as early as possible in order to initiate treatment and preparation of the family to deal with the challenges imposed by the condition. Brain imaging biomarkers have special interest. Specifically, functional connectivity data extracted from resting state functional magnetic resonance imaging (rs-fMRI) should allow to detect brain connectivity alterations. Machine learning pipelines encompass the estimation of the functional connectivity matrix from brain parcellations, feature extraction and building classification models for ASD prediction. The works reported in the literature are very heterogeneous from the computational and methodological point of view. In this Thesis we carry out a comprehensive computational exploration of the impact of the choices involved while building these machine learning pipelines.

Originality Statement

I hereby declare that this submission is my own work and to the best of my knowledge it contains no materials previously published or written by another person, or substantial proportions of material which have been accepted for the award of any other degree or diploma at The University of the Basque Country or any other educational institution, except where due acknowledgement is made in the thesis. Any contribution made to the research by others, with whom I have worked at The University of the Basque Country or elsewhere, is explicitly acknowledged in the thesis. I also declare that the intellectual content of this thesis is the product of my own work, except to the extent that assistance from others in the project's design and conception or in style, presentation and linguistic expression is acknowledged.

The author hereby grants to University of the Basque Country permission to reproduce and to distribute copies of this thesis document in whole or in part.

Signed:_____

Acknowledgements - Agradecimientos

I would like to thank God for his never-ending grace, mercy, and provision in order to finish this research.

I would like to express my deep gratitude to Dr. Manuel Graña, my research supervisor, for their patient guidance, help, encouragement, support, valuable expertise and sharing knowledge of this research work.

I would like to thanks the Carolina Foundation for allowing me to obtain a scholarship for a doctoral stay in the Basque Country.

I thank with love to Yovanna, my wife. She has been my best friend and great companion for finishing this job. To my children, Valeria and Thiago, you are my inspiration with your games and happiness.

Finally, I wish to thank my great family parents and siblings for their support and encouragement throughout my study.

Contents

List of Figures

List of Tables

Chapter 1

Introduction

This chapter presents the background and motivation for this Thesis in section 1.1. Section 1.2 describes the objectives of this research work. A summary of the generated contributions is given in section 1.3. The research environment and context are described in section **??**. The related publications are listed in section 1.4. Section 1.5 presents the structure of this Thesis.

1.1 Background and Motivation

Autism Spectrum Condition (ASC) [8,9] is a highly prevalent, heritable and heterogeneous neurodevelopmental disorder that has distinctive cognitive features often cooccuring with other psychiatric or neurological disorders. It is the subject of a broad and intense research effort, with more than 40 EU funded research projects devoted to some of its aspects in the last 20 years. Similar effort is being done in China, USA, Russia, and South America looking for its causes at various levels: genetic, metabolic, neural or brain based. Searching for the pathogenesis leads also to findings which are also diagnostic indications, i.e. biomarkers of the disorder that can be used to guide early diagnosis, which in its turn may allow to apply therapeutic or palliative treatments from an early age. ASC computer aided diagnosis (CAD) has been gaining interest in the scientific community in the recent years, aiming to contribure to its early detection. In this report we gather the approaches that have been reported in the recent literature trying to be comprehensive, though

keeping pace of the reported results may be difficult. Some CAD approaches are based on behavioral characterizations, while the majority of approaches are based on the analysis of brain neural activity and morphology in some way or another. Most recent studies are focused on the detection of brain functional connectivity anomalies using specific signals such as electroencephalographic (EEG) recordings or functional magnetic resonance imaging (fMRI). The emergence of large public repositories of data is boosting research in this topic.

1.1.1 Prevalence

Across the Autism and Developmental Disabilities Monitoring (ADDM) Network sites, estimated ASC prevalence among children aged 8 years was 23.4 per 1,000 (one in 43) boys and 5.2 per 1,000 (one in 193) girls [10]. Thus ASC appears to require specific research programs contemplating explictly the impact of sex/gender related issues [11, 12]. Some references [13] state that the overall worldwide prevalence of ASC is as high as 1% of the population, while others [14] argue that non specific diagnostic criteria recently included in the diagnostic protocol produce as an artifact the 20-fold increase in its prevalence. Therefore, the heterogeneity in ASC features that hinders the identification of biomarkers could be a side effect of excessively wide diagnostic criteria. A recent normative study [15] on brain cortical structure modeled by a probabilistic predictive model concluded that there is some indication that sexual-related characteristics of the brain are highly correlated with ASC.

1.1.2 Diagnosis

ASC is currently diagnosed on the basis of qualitative information obtained from parent interviews and clinical observation, which leads to disturbing differences between sites [16]. Given its great prevalence, automated approaches to assist diagnosis [17, 18] are highly desirable. Increasingly, clinical neuroscience focus is shifting to find metrics derived from brain imaging [19] that may be useful to predict diagnostic category, disease progression, or response to intervention, e.g. looking for endophenotype using multivariate analysis approaches [20]. These metrics come

from machine learning approaches to the study of brain structure and function. Some of them can be considered as neuroimage based biomarkers that would be helpful to guide early interventions. Currently, the research community has not yet identified reliable and reproducible biomarkers for ASC. Clinical heterogeneity, methodological standardization and cross-site validation raise issues that must be addressed before further progress can be achieved [21].

1.1.3 Datasets

A central role in the effort to obtain robust and reproducible biomarkers is played by the availability of public datasets, such as the Autism Brain Imaging Data Exchange (ABIDE) dataset [22, 23] that includes demographic, clinical information and data from several magnetic resonance imaging (MRI) modalities allowing for a variety of studies such as brain maturity estimation as a biomarker of brain abnormality [24].

1.1.4 Pattern recognition for CAD

A wide variety of machine learning and pattern recognition studies on the development of CAD systems for ASC have been reported [25] exploiting a variety of information sources, including structural, diffusion and functional MRI, as well as electroencephalography (EEG) [26–28], additional demographic and clinical data [29], and behavioral measurements captured by computer vision or other body measurement approaches [30]. There are meta-analysis confirmations of ASC imaging biomarkers from anatomical MRI [31], and diffusion MRI imaging [32, 33]. The latter showing white matter integrity disruption. Connectivity based brain parcellation [34] provided additional evidence of altered white matter connectivity in ASC.

1.1.5 Brain functional connectivity

A main goal of this Thesis is the exploration and validation of ASC biomarker discovery based on brain functional connectivity information using artificial intelligence approaches, namely namely machine learning and deep learning techniques. Brain

functional connectivity analysis based on resting state functional MRI (rs-fMRI) can be done by seed analysis, where the specific connectivity relative to a selected brain region is compared across subjects and populations [34], or on the basis of brain parcellations into a set of regions of interest (ROIs) which can be defined either by anatomical guidelines or by data driven unsupervised segmentation [35]. In any case, rs-fMRI connectivity analysis has been accepted as a source of information for the discovery of biomarkers of psychiatric disorders [36] such as schizophrenia [37] and ASC [21].

Neuroimage biomarker discovery over functional connectivity data may be guided by statistically significant differences between ASC and typically developing (TD) subjects. For instance, t-test on the dynamical network strength of ASC vs. TD was reported to confirm identification of aberrant connectivity in ASC subjects [38], and significant differences between ASC and TD in the level of activation of thalamic connectivity have been identified by independent component analysis (ICA) [39]. In predictive analysis approaches to biomarker identification, the subject's condition (ASC vs. TD) prediction performance achieved is the measure of the biomarker significance. Predictor models are built by machine learning techniques, often consisting of two steps: a dimensionally reduction (aka feature extraction or feature selection) followed by a classification step for class prediction. Though discrimination between ASC and TD is the most common paradigm, some works [40, 41] compare ASC with Schizophrenia over a small cohort, while others consider patterns for discrimination among low-functioning and high-functioning ASC subjects [42].

1.1.6 Computational pipeline

The general pipeline of predictive analysis for brain connectivity based biomarkers is illustrated in Figure 1.1. Functional connectivity matrices are extracted from preprocessed rs-fMRI data as follows:

1. A parcellation of the brain is defined;

2. The time series corresponding to the voxels in each region of the parcellation are aggregated into one representative time series often by averaging;

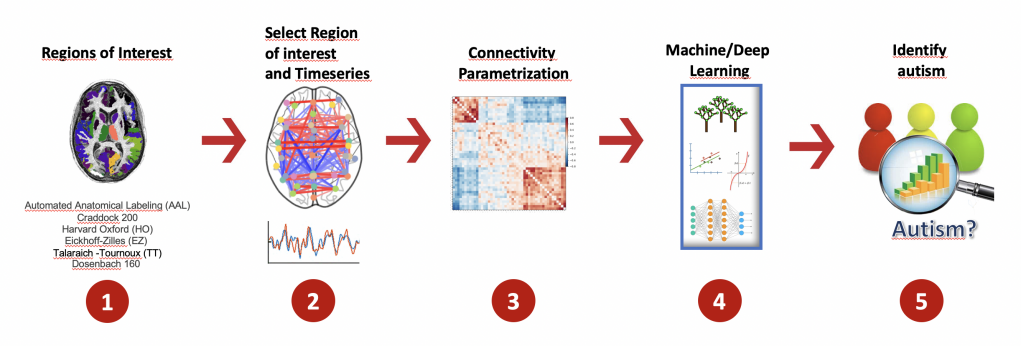

Figure 1.1: Functional connectome predictive analysis pipeline steps after rs-fMRI data preprocessing (not shown): 1) given a parcellation of the brain, 2) obtain the representative time series of each region by averaging the time series of voxels within the region, 3) build the connectivity matrix by computing a similarity measure between each pair of representative time series, 4) carry out cross-validation experiments, using Machine Learning algorithms for feature extraction and classifier training; 5) report test results on the prediction of the ASC vs TD.

3. The connectivity matrix is built computing the similarity among the representatives of each pair of regions in the parcellation. Hence the connectivity matrix is always a symmetric matrix that can be interpreted as the adjacency matrix of a graph representing the relations among brain regions.

4. The connectivity matrix is then used as the raw data for machine learning processes which may involve feature extraction/selection. Feature selection involves the selection of specific connections that may become identified as biomarkers.

5. Predictive performance is estimated by the training/testing of classification models often in a cross-validation scheme.

Predictive performance may be heavily influenced by the decisions made at each step of the study, namely by the cohort selection, the choice of brain volume parcellation, the functional connectivity matrix estimation procedure, the feature selection/extraction algorithm applied, and the classification model building algorithm. After the cross-validation assessment, the cross-validation classification performance results may be used to identify biomarkers in the connectivity matrix.

1.2 Objectives

The main objective of this thesis is to explore the eficiency of machine learning approaches, including more recent deep learning techniques, to the CAD of ASC subjets, stated as a classification problem of ASC versus healthy controls (aka typically developing (TD) children).

We want to assess the impact of the various metaparameter choices in computational pipeline of Figure 1.1. If possible we would like to select the optimal combination of such metaparameter choices.

Operational objectives implemented in the pursue of this general objective are:

- Identifiying and recovering a representative dataset for the realization of the computational experiments
- Implementation of the exploitation of the diverse feature extraction, classifier building algorithms, cross validation procedures, and performance result collection and analysis.
- Carrying out the computational experiments assessing the performance of the various combinations of metaparameter choices, managing the combinatorial complexity of the data coming out from the experiments.

1.3 Contributions

In this Thesis, the functional connectivity matrix computed from rs-fMRI data is the sole source of information for classification.

We explore the impact of choices made in the implementation of the machine learning pipeline of Figure 1.1 for the prediction of ASC vs. TD.

We have carried out extensive cross-validation experiments over the algorithmic choices at each step of the classification model building pipeline.

We report the impact on predictive performance ASC vs TD of all combinations of:

- five feature extraction/selection approaches,

- six brain parcellations,
- five functional connectivity matrix computation methods, and
- ten classification model building techniques.

This comprehensive comparison of classical machine learning approaches encompasses more than eleven thousand (11500) cross-validation experiments.

We report statistically significant differences in performance found as well as direct comparison to state of the art published results.

We found that specific combinations of pipeline choices can boost the performance of ASC vs. TD classification based on brain functional connectivity data.

The software needed to replicate the experiments reported in this Thesis have been published in github[1].

1.4 Publications

Publications related with the content of this Thesis:

- Impact of Machine Learning Pipeline Choices in Autism Prediction From Functional Connectivity Data; Graña, M. & Silva, M. International Journal of Neural Systems , Vol. 31 , pp. 2150009 , 2021
- Impacto y regulación de la inteligencia artificial en el ámbito sanitario Karina Medinaceli, M. S. REVISTA IUS , 2021
- On Machine Learning for Autism prediction from functional connectivityMoises Silva , Manuel Graña, CORES21, The 12th International Conference on Computer Recognition Systems June 28–30, 2021 Bydgoszcz, Poland

1.5 Structure of the thesis

This thesis is structured as follows:

[1] https://github.com/mmscnet/Impact-feature-extraction-in-Autism

- Chapter 2 discusses the role fo computer aided systems in the dignosis of Autism Spectrum Condition. We review several paradigms besides the brain connectivity approach that is the main focus of the Thesis.

- Chapter 3 provides a detailed review of approaches and resources for the analysis of brain connectivity directed to the finding of biomarkers of Autism Spectrum Condition from the point of view of machine learning.

- Chapter 4 provides the descritption of the machine learning tools and techniques applied in the search of optimal classification of Autism Spectrum Condition subjects on the basis of brain connectivity.

- Chapter 5 provides the description of the deep learning approaches tested in the framework of this Thesis, including transfer learning approaches.

- Chapter 6 provides the report of the results achieved with machine learning techniques over the ABIDE database.

- Chapter 7 reports the results achieved over the ABIDE dataset using deep learning techniques.

- Finally, Chapter 8 presents the conclusions and future lines of work.

Chapter 2

State of the art of Autism diagnostic technological tools

In this Chapter we review the state of the art on the use of technological support for the diagnosis of autism. The contents of the Chapter are as follows: Section 2.2 presents behavior measurement based CAD approaches. Section 2.3 presents EEG based CAD approaches. Section 2.4 presents MRI based biomarker finding efforts. Section 2.5 presents MRI based CAD approaches. Section 2.6 presents public available data repositories. Finally, Section 2.7 gives some concluding remarks.

2.1 Introduction

Computer aided diagnosis (CAD) aims to help the clinical practitioner to achieve early and accurate diagnosis of ASC in order to try to apply early treatments hoping to improve the child's condition in some way. Recent randomised control trials [43–48] emphasize the improved effect achieved when the treatment is applied at early ages, even todlers. Here we will not discuss the clinical aspects such as treatment protocols or diagnositic procedures follow in the clinic, focusing only on the technological aspects. A CAD system often is composed of some technological device that allows to measure the behavior or some biological or physiological aspect of the subject, and some classifier system built by machine learning techniques that provides the diagnosis suggestion. Machine leraning can be used to build hi-

erarchies of categories which may help to refine diagnostic process [49], but mostly is used to give a response to the question "Is this child at high risk of ASC?". It is important to keep in mind that ASC is a quite heterogeneous condition that is still under revision by the clinical experts, therefore all the technological solutions would be always limited in their scope by some a priori selection of measures and expected observations. Regarding the kind of knowledge modeling approach used, the literature offers a wide variety:

- Rule based expert systems [50].
- Deep learning architectures [51, 52] and shallow artificial neural networks [53].
- Support Vector Machines [52, 54–57].
- Statistical inference (i.e. ANOVA) is traditionally used in biomarker identification.

Regarding the kind of information used, the literature refers the following at least:

- Qualitative information produced by reports from parents and caregivers [50, 58].
- Genetic and metabolic information such as the selection of microarray expression data [54, 55, 59, 60], or the detection of specific metabolites that are hypothesized to be related to ASC [56].
- Brain imaging data, often from diverse MRI modalities [21]. Structural brain imaging is widely recognized as a rich source of information for the neuropsychological analysis of the brain [61–65]. Also, brain functional imaging may be providing a wealth of information on the effects on brain connectivity that may be at the root of the ASC [66–72]. Diffussion spectrum MRI have been also proposed [73–75] for high precision white matter fiber tracking. Finally, there are increasingly facilities for multimodal data processing [76].
- Diverse motion capture devices which provide quantitative information about the subject responses and motion.

- EEG data that can be used either for brain functional connectivity analysis or as features for classification processes.

- Functional near-infrared spectroscopy (fNIRS) is a recent approach to measure the brain activitiy wich already gives some discrimination results regarding the processing of faces by ASC children [77].

Most of the CAD approaches are developed over small local datasets, posing problems of reproducibility and generalization of the results. In some areas, such as brain imaging, there are efforts to collect big repositories of data coming from many research centers. As will be discussed later, these efforts pose the additional difficulty of dealing with inter center variability of data recording procedures and methods.

2.2 Behavior measurement based CAD approaches.

Some approaches use behavioral information measured by computer vision or another sensing technique. They can be rooted in an enactive approach to autism understanding [101], focusing on disruptions to action perception [102]. Table 2.1 summarizes the literature found so far[1]. Some approaches measure the response of the child to stylized representations, such as the discrimination of geometric figures from visualization of grasping [103]. In general, a wide variety of sensors can and have been used to monitor the behavior and assess the risk of ASC [104–106] either in isolation or in some kind of information fusion. For instance, in [79] authors propose the measurement using computer vision of the imitation response of ASC children versus neurotypical children to discriminate them. Another non intrusive approach to discriminate ASC children uses the inertial information of a smart tablet [80]. The authors find definitive patterns of motion that are compatible with the ASC clinical characterization, larger and faster motions, stronger forces at contact, with

[1]Explanation of acronyms: CA conversation analyis, CV computer vision, EMT eye motion tracking, EOG electrooculogram, FD face detection, FER facial expression recognition, MoCap Motion Capture, MA mobile application, WA wrist accelerometers, GE gaze estimation, HPE head pose estimation, LE landmark extraction, MI Magneto-Inertial, MMN mismatch negativity, OMC object motion capture, PA pupil analysis, POMDP Partially Observable Markov Decision Process SR speech recognition.

Table 2.1: Behavioral approaches to CAD for ASC characterization.

ref	sensor	approach	robot?
[78]		CA	
[79]	CV		
[80]	tablet	dynamical analysis	
[81]	kinect	MoCap	
[82]	WA	dynamical analysis	
[83]	CV	FD,LE,GE, HPE,FER	
[84], [85], [86, 87]	CV	MoCap	
[88]	CV	GE,PA	y
[89]	EOG	EMT	
[90]	MA	pictograms	
[91]	CV,SR	name calling	
[92]	CV	OMC	
[93]		CA, MMN	
[94]		EMT	
[95]	CV	FD	
[96]	CV	POMDP	y
[97]	Haptic, kinect		
[98]	tablet	target tracking	
[99]	MI		
[100]	CV	MoCap	y

more distal use of space. Another approach uses the Kinect V2 sensor in order to measure the motions of the subjects and try to detect stereotypical motor reactions which are the hallmark of autism in clinical diagnosis processes. The experiments reported with motion captured from professional actors promised that this detection can be achieved with great probability [81]. Detection of motion by means of wrist accelerometers has been reported by [82] achieving discrimination of children at high risk versus low risk of ASC in the realization of some motor tasks. A comprehensive behavior observation system encompasing face detection, landmark extraction, gaze estimation, head pose estimation and facial expression recognition has been proposed in [83] to make a continuous assessment of the evolution of the ASC subjects under treatment. Another motion analysis system, tracking the motion of diverse body parts while the subjects are inmersed in an interactive discussion involving turn taking, has demonstrated significant differences between ASC and TD subjects [84]. Similarly, tracking body motion while engaging with a social robot was found discriminant in [85]. Computing the dynamic time warping (DTW) distance between the robot motion and the child motion while engaging in an imitation game was intended as a measure of impairment in [100]. The examination of the gaze and the pupil while interacting with a robotic avatar has been also shown to be lead to moderate classification accuracy [88]. The measurement of eye motion when tracking objects by means of an electrooculogram has been also show capable of high accuracy discrimination of ASC subjects [89], while serving also to train the subjects to perform more accurate object tracking. Also it showed that the ASC children retain intact shape appreciation while losing emotional content [94]. From a different point of view, proposal in [96] consists in the modeling of child behavior by means of Partially Observable Markov Decision Process (POMCP) from the incomplete observations made by a robot interacting with the child.

In a different approach, a mobile application is proposed [90] that helps in the screening of children by evaluating their responses to pictogram based questionaire. Childs with high risk of ASC are referred to a specialized centre. Another early screening proposal involves the close monitoring of classroom to study the reaction to name calling of the children [91]. This system has voice recognition as well

as human body posture and reaction monitoring. For instance, subject vitality is measured by tracking object motion speed using hidden infrared markers with six infrared cameras, while the subjects are performing simple picking tasks [92]. The measurement of stereotypical motion was also a way to characterize ASC interacting skills [86, 87]. The measurement of reaching acts mediated by a robotic arm was found to differ from ASC to TD young adults [107] with better performance for ASC when the error refers to properctive senses, while it is the converse when error is measured by visión. The analysis of brain volumes through MRI indicates that there are significant variations of volume in lobule VI, and parts of lobule VIII.

The responses to a mismatch experiment of sounds (vowel, vowel duration, consonant, syllable frequency, syllable intensity) showed significant differences in children (8-12 year old) with asperger syndrome in intensity and frequency relative to typically developing children [93] leading to conclude aberrant cortical sound-speech discrimination in Asperger syndrome children. Conversation analysis is used while a ASC child is interacting with a robot trying to ascertain if he has perseverative talking features [78] one of the traits of high performing ASC children. The sequential analysis showed that recurrence may be driven by the interaction scenario. Other experiments measured the response of ASC versus TD children when viewing silouhettes of human and robotic [108] measuring the mimicry as the project results.

Target tracking in a tablet device provides behavioral information that can be used for assessment of sensorial impairment [98], while a magneto-inertial platform is proposed in [99] for the assessment of motor skills.

2.3 EEG based CAD approaches.

Electroencephalographic (EEG) sensors of neural activity have been also used to explore the feasibility of identifying brain biomarkers of ASC or to implement CAD systems based on their readings. Some works have achieved discrimination between ASC and TD children in small cohorts [109] applying some feature extraction procedures that include the techniques from non-linear chaotic time series analysis and time frequency decomposition, such as the fractal dimension. Another proposed

computational pipeline involves wavelet decomposition, entropy feature extraction from each EEG sub-band and a classifier based on ANNs [53]. Another kind of ANN, uses the self-organizing map (SOM) for feature extraction reporting results of a number of conventional classifiers upon the SOM features [110]. Classification oriented research, however, does not provide clinical or biological insights because it is often impossible to translate back the significative features into biological causes or biomarkers that can be useful to understand the condition and propose treatments. Looking for biomarkers, a recent systematic review of studies that have used EEG and magnetoencephalography (MEG) data for brain connectivity analysis reports underconnectivity in long-range connections for ASC subjects, while local connections seem to be unafected [111]. Recent approaches fuse EEG information with other sources such as MRI information [112].

2.4 MRI based biomarkers.

Another track for research into the existence of anomalies in brain morphology and functionality connectivity is the use of various modalities of magnetic resonance imaging (MRI), namely structural (T1-weighted) MRI, resting state functional MRI (rs-fMRI) and diffusion weighted imaging (DWI), and magnetic resonance spectroscopy (MRS) are the most relevant modalities found in the literature aiming to identify ASC biomarkers [126, 134]. Table 2.1 provides a summary of the literature worked out so far[2].

The neural circuit mechanisms taking care of the regulation of social behaviors are key to find such biomarkers [135]. For instance, structural MRI has provided

[2]Explanation of acronyms: **Machine learning** RF: Random Forest; SVM: Support Vector Machine; CART: Classification and Regression Trees; GBM: Gradient Boosting Machine; RFE: Recursive Features Elimination; PSO: Particle Swarm Optimization; DBN: Deep Belief Network; DNN: Deep Neural Network; ICA: Independent Component Analysis; GCT Granger Causality Test; LSTM: Long Short-Rerm Memory; ROI: Region of Interest; GLM: General Linear Model; RW: Random Walk; WBA: voxel-wise Whole Brain Analysis; **Anatomical references** RSFG: Right Superior Frontal Gyrus, MFG: Middle Frontal Gyrus; IFG: Inferior Frontal Gyrus; FFA: Fusiform Face Area; OFA: Occipital Face Area; EBA: Extrastriate Body Area; STS: Sulcus Temporal Superior; CC: Corpus Callosum; LUF: Left Uncinate Fasciculus; SLF : Superior Longitudinal Fasciculus; CP: Cerebral Peduncle; SCC: Splenium Corpus Callosum; PCC : Posterior Cingulate Cortex; SFG/mPFC: Superior Frontal Gyrus/Medial Prefrontal Cortex; LPC: Left Parietal Cortex; RPC: Right parietal Cortex; Hipp: Hhippocampal formation; RSN: Resting State Network; CB: Cingulum Bundle; A/SL-F: Arcuate/Superior Longitudinal Fasciculus; UF: Uncinate Fasciculus.

Table 2.2: Summary of Biomarker and CAD findings for autism.

ref	Mod.	BD	Anal.	Findings	review
[113]	fMRI	IMAGEN		RSFG, rMFG	
[114]	sMRI,DTI				y
[115]	DTI		ROI, WBA	CC, CB, A/SL-F, UF, STG	y
[116]	rs-fMRI	ABIDE	LSTM		
[117]	rs-fMRI	ABIDE	ROI, DNN		
[118]	rs-fMRI, sMRI	ABIDE	ROI, DBN		
[119]	rs-fMRI	ABIDE	RW		
[120]	rs-fMRI	ABIDE	SVM(+PSO, RFE)		
[121]	rs-fMRI	13ASC-13TD	ICA, GCT, GLM		
[122]	fMRI	ABIDE	ROI	PCC, mPC	
[123]	sMRI, DTI,1H-MRS	15ADS:18TD	CART, ROI	CC, IFG	
[112]	fMRI, DTI, EGG	3 ASC	ROI, ICA	PCUN/PCC, SFG/mPFC, LPC, RPC	
[124]	DTI		voxel	CP, SCC	y
[125]	DTI			SLF, LUF, CC	y
[126]	sMRI, fMRI, rs-fMRI, DTI				y
[127]	DTI, MRI	22ASC;10TD	voxel	Amigdala, Hipp	
[128]	sMRI	ABIDE	RF, GBM	VIQ, AS	
[129]	sMRI	ABIDE	RF, SVM, GBM		
[130]	fMRI	15ASC;14TD	RFE, SVM, voxel	FFA, OFA, EBA, STS	
[131]	DTI	30ASC, 30TD		CC,sACC	
[132]		ABIDE	deep learn		
[133]	rsfMRI				

evidence of atypical brain lateralization of subjects with ASC [136] in a cohort of 67 ASC subjects and 69 neurotypical subjects with matching IQ and relevant personal characteristics.

The study of brain regions related to language [137] suggests that the child can discern the social quality of behavior, but he has limited capability to explain and rationalize it. These findings confirm the general assessment [138] that ASC subjects suffer impairments of audio processing at neural level. Other approaches focus on the motor disabilities searching for correlated regions and performance in the brain [139]. Other neurophysiological models such as the mirror neurons [140] seem to have been abandoned in the recent years [141].

Image biomarker findings are quite diverse [134]. Structural MRI findings using voxel based differences are sometimes contradictory and inconsistent, and heavily dependent on the technique used and the age of subjects, though some increase in gray matter and white matter volume was consistently reported, as well as corpus callosum decrease in volume. Morphological differences in thalamus and striatum have been also reported using structural features [142]. A long term longitudinal (accross late childhood, adolescence and adulthood) big scale study of cortical thickness is reported in [143]. Increased cortical thickness was reported for ASC in the range between 6 years and adolescence [143], with differences decreasing towards adulthood. Other authors report significant differences in temporoparietal regions [144]. One of the questions raised is whether the differences in measurements found in older children may be due to the actual ASC effects or the years of social disfunction. Hence, the current preferences of researchers looking for ASC biomarkers is to do the observations in very early ages, even toddlers. Tractography analysis based on fractional anisotropy coefficients extracted from DWI data have shown consistent degradation of main neural tracts, pointing to a degradation of brain connectivity. Fusion of DTI and sMRI volumetric information has shown differences in preschool ASC children [127]. The study of brain connectivity in toddlers comparing ASC with other developmental disorders has been reported using DWI and streamlined tractography [145]. Over an anatomical parcellation of the brain, the neural pathways between them were extracted, and the connectivity strength between brain

regions was estimated. The results point to overconnectivity in ASC toddlers versus other developmental disorders.

The analysis of functional connectivity based on rs-fMRI data has found also many incoherent or contradictory results heavily dependent on the heterogeneity of population samples, analysis methods and design of the resting state scan [146]. The accepted conclusion so far is that there is some form of compensation between reduced long-range connectivity and increased short-range connectivity [111]. The functional parcellation of the insula allowed to find differences of insula functional connectivity between ASC and neurotypical subjects [147]. Another study detected effects in the extrastriate body area (EBA) [148] in fMRI when the task is the contigency detection of one's movements with others. Other studies found altered connectivity from/to the superior temporal sulcus (STS) [149, 150].

In reviews of white matter connectivity studies [32,114,124,125], mostly done on DTI data, it was found recently that there is evidence of alterations in the connectivity of the limbic system, contributing to ASC social impairment, while previous reviews emphasized decreased connectivity of the corpus callosum, cingulum, and temporal lobe [115]. On a functional MRI study [151] involving age and IQ matching ASC and TD subjects playing "stone paper scissor" against human/robot/random computer some reversed effect on the hypothalamus activity was found in ASC subjects. On the other hand, other authors focus on the motor functional system [139] as the key to improve the ASC subject outcomes. A recent work points in the direction of alterations of the brain microstructure while the macrostructural features are mostly preservated as the neurological causes for ASC [152].

The spatial shifting of resting state networks, such as the default mode network, has been also tested as a biomarker for ASC [153]. The parcellation of the brain activity into intrinsic connectivity networks allowed to assess their spatial variability and its discriminant power, finding that ASC showed greater spatial variability. These results help to harmonize the contradictory findings of underconnectivity and overconnectivity in several studies [154]. Increase in intrasubject variability brain connectivity in time, due to diverse factors such as caffeine intake between sessions, has been found a potential biomarker for ASC [122]. Connectivity of the thalamus

cortex has been studied by rs-fMRI brain networks and anatomical connectivity computed by diffusion weighted imaging tractography [155] finding diverse patterns of underconnectivity. On other effort, the connectivity between the cerebellum and the temporoparietal junction was analyzed in detail using both independent component analysis and seed based connectivity analysis [156] finding perturbed input to the temporal-parietal regions from the cerebelar areas. Some task oriented studies, such as the longitudinal study in [113] looks at the reward processing brain related regions and functional connections.

2.5 MRI based CAD approaches

Biomarker identification aims to detect brain regions, connections or biochemical signatures that show significant differences between ASC and neurotypical populations. CAD goes one step further, it produces a decision on the diagnosis that can be used by the clinical practitioner with some confidence. CAD systems require sophisticated machine learning tools, such as multiview multitask ensembles of classifiers [157]. Classification experiments based on structural MRI morphological features extracted using FreeSurfer give low scores [129].

A tensor based approach to estimate connectivity in rs-fMRI is proposed in [158] that it is able to extract both the connectome representation and the dynamic functional connectivity for each subject finding discriminant effects on the putamen connectivity for ASC subjects. Fine temporal analysis of the rs-fMRI time series, by clustering them into short time intervals that may be shared between brain regions, allows more precise classification [159,160]. On the other hand, structural features of brain cortex were used by random forest classifier to produce reliable predictions in toddlers [161]. Independent component analysis (ICA) and Granger Connectivity Analysis (GCA) of rs-fMRI from high functioning autism showed discriminating differences that can lead to automated classification [121].

A multimodal approach, involving structural and functional MRI is followed in [52] where nonstationary independent components are extracted as fMRI features and an sparse autoencoder extracts texture features from the structural MRI.

These features are used to train/test a SVM classifier. SVM and recursive feature extraction (RFE) allow to classifiy children into ASC and control [130]. In another study [123] a decision tree classification was applied to features extracted from multimodal MRI information, though the sample is very small (#ASC=19, #TD= 18). On other study, the use of random forest classifiers give a much better classification accuracy that SVM+RFE [120]. It was claimed in [162] that it is possible to discriminate ASC from controls on the basis of a few abnormal functional connections, however conclusions do not seem well supported to us.

Deep learning is having also a definitive impact in the recent attempts to construct CAD systems. For instance, Deep Belief Networks have been reported [51,117] to achieve ASC children discrimination fusing structural MRI imaging data and rs-fMRI data. Another approach [52] uses sparse autoencoders to extract feature filters from structural MRI, which are applied to the 3D structural MRI by a convolution neural network for feature extraction. A linear decomposition by ICA is applied to extract rs-fMRI connectivity features after appropriate signal bandpass. Structural and functional features are finally entered to a linear support vector machine (SVM) classifier. However, deep learning approaches are blind, in the sense that no biological information is provided by them, so there is no explanation that may lead the clinical practice to find treatments. Long Short-Term Memories (LSTM) have been applied to classification of ASC children [116] using ABIDE data.

The brain dynamics of ASC young adults is compared with TD matched in IQ and age [119] looking for significant differences. It is found that dynamic transitions identified from rs-fMRI data are differently coorelated with IQ in TD and ASC subjects: for TD subjects IQ is correlated to the frequency of transitions, while for ASC subjects is correlated with brain dinamics stability.

2.6 Public data resources

Looking forward to achieve more robust classification results [157, 163], big repositories of multi-center information are becoming available, most including several modalities of brain imaging data [164]. However, inter-site variability seriously im-

pedes the data analysis [165]. After removing inter-center variability predictive classification results reported are close to random noise, enforcing the conclusion that more specific differential diagnostic tools are needed because of the actual heterogeneity of the brain structures in ASC subjects. Also, fine subdivisions of the disorder are proposed as a way to improve automated diagonistic decisions [128]. The state of the publicly available data resources until 2017 was summarized in [166], here we review some of the most relevant up to date

Simons Foundation Autism Research Initiative (SFARI) SFARI is a repository of genetic samples of 2700 families with at least a descentdant that has ASC traits. A subset of subjects called the Simons Variation in Individuals Project (VIP), 200 cases, have also fMRI and sMRI data. The data website is `http://www.sfari.org`. The data can be accessed after registration.

Autism Brain Imaging Data Exchange (ABIDE) The first collection ABIDE I is presented in [167]. It was built up aggregating data available from several institutions. It contains data from 1112 subjects, 539 with ASC and 573 healthy, aging range is from 7 up to 64 years. There are rs-fMRI and sMRI data as well as phenotipic information. The second collection ABIDE II is presented in [168] after adding 487 ASC and 557 healthy subjects from additional institutions. The new data collection includes DWI data for 284 subjects, as well as psychological variables for all new subjets. Both datasets are available from `http://fcon_1000.projects.nitrc.org/indi/abide/`, where a curated bibliographic list is also given (up to March 2017), including publications about ABIDE availability (up to August 2016).

IMAGEN It is a result of EU FP6 funded project LSHM-CT- 2007-037286 in the period 2007-2012. The main goal of the project was to identify the genetic and neurobiological roots of the ASC in european adolescents. The consortium was composed of 20 institutions from UK, Germany, France, Norway, Canda and Ireland. The dataset contains stratified data from three main periods of subjects life: Phase 1: adolescents 15-16 years old; Phase 2: the same subjects in the range 18-20 years,

and Phase 3: at 22 years. It contains data from 2223 subjects. It is not specific for ASC subjects. The data includes biological and psychological tests data. The data can be accessed, after registration, from `http://www.imagen-europe.com`.

2.7 Concluding remarks

Computer aided diagnosis (CAD) systems for ASC are currently a hot focus of research, because they may provide early detection leading to improved treatment. CAD systems provide the clinical practitioner with a recommendation of the diagnosis, which may (or may not) be based on accepted biomarkers. Black-box CAD systems are not easily accepted because the medical staff requires understanding the recommendation from a causality point of view. Therefore, future efforts must emphasize explainability in order to get acceptance in the medical community.

Chapter 3

State of the art of brain connectivity analysis for Autism

This Chapter summarizes the state of the art in the analysis of brain connectivity looking for biomarkers or computer aided diagnostic systems for Autism spectrum condition (ASC). Section 3.1 provides a brief revision of protocols of magetic resonance imaging (MRI) for the brain. Section 3.2 provides a review of previous works focused on the brain MRI data, specifically based on the data from the ABIDE dataset that has been used also in our experiments.

3.1 Brain imaging

Brain imaging technologies are divided into two main categories: structural imaging and functional imaging. Structural imaging techniques are used for studying the anatomy of the brain and diagnosing disorders, for example, detecting tumors or physical injuries. Functional brain imaging techniques are used to measure the activity of the brain and analyze how it changes overtime to understand the brain functions and dynamics. Magnetic Resonance Imaging (MRI) can be used for both structural and functional brain imaging, the latter usually denoted as fMRI. Additional techniques for functional brain data aquisition are electroencephalography (EEG) and magnetoencephalography (MEG). fMRI has become a popular tool for psychologists trying to examine normal and abnormal brain function. Over the last

decade it has provided new insight to the investigation of how memories are formed, language, pain, learning and emotion to name but a few areas of research. fMRI is also being applied in clinical and commercial settings. Recently, machine learning techniques are extensively applied to extract useful information from fMRI [169]. In the following subsections we will give a short revision of the fundamentals of processing MRI data for brain imaging applications.

3.1.1 Kinds of noise found in brain MRI

As with almost all types of physical measurements, MRI data can be corrupted by acquisition artifacts. These artifacts arise from a variety of sources, including head movement, brain internal motion, such as the vascular effects related to periodic physiological fluctuations, and computational errors introduced by reconstruction and interpolation processes. In particular, MRI data often contain transient spike artifacts and slow drift over time related to a variety of sources, including magnetic gradient instability, radio frequency interference, and movement induced and physiologically induced in homogeneities in the magnetic field. These artifacts will likely lead to violations of the assumptions of normally and identically distributed errors that are commonly made in subsequent statistical analysis. Unless these sources of noise are properly tackled with, they will reduce statistical power in group level analysis, and will increase false positives in single-subject inference. Of course, the effect in machine learning predictive approaches will be catastrophic. It is very important to perform a careful examination of the data, in order to have an early detection of these problems. However, for some modalities such as fMRI the large amount of data prevents this exhaustive examination. For instance, fMRI often presents a substantial slow drift of the signal over time, which may induce significant signal variations that may confound the statistical analysis or the predictive models. The introductory chapter in [1] collects visualization of some types of MRI artifacts that are reproduced in Figure 3.1.

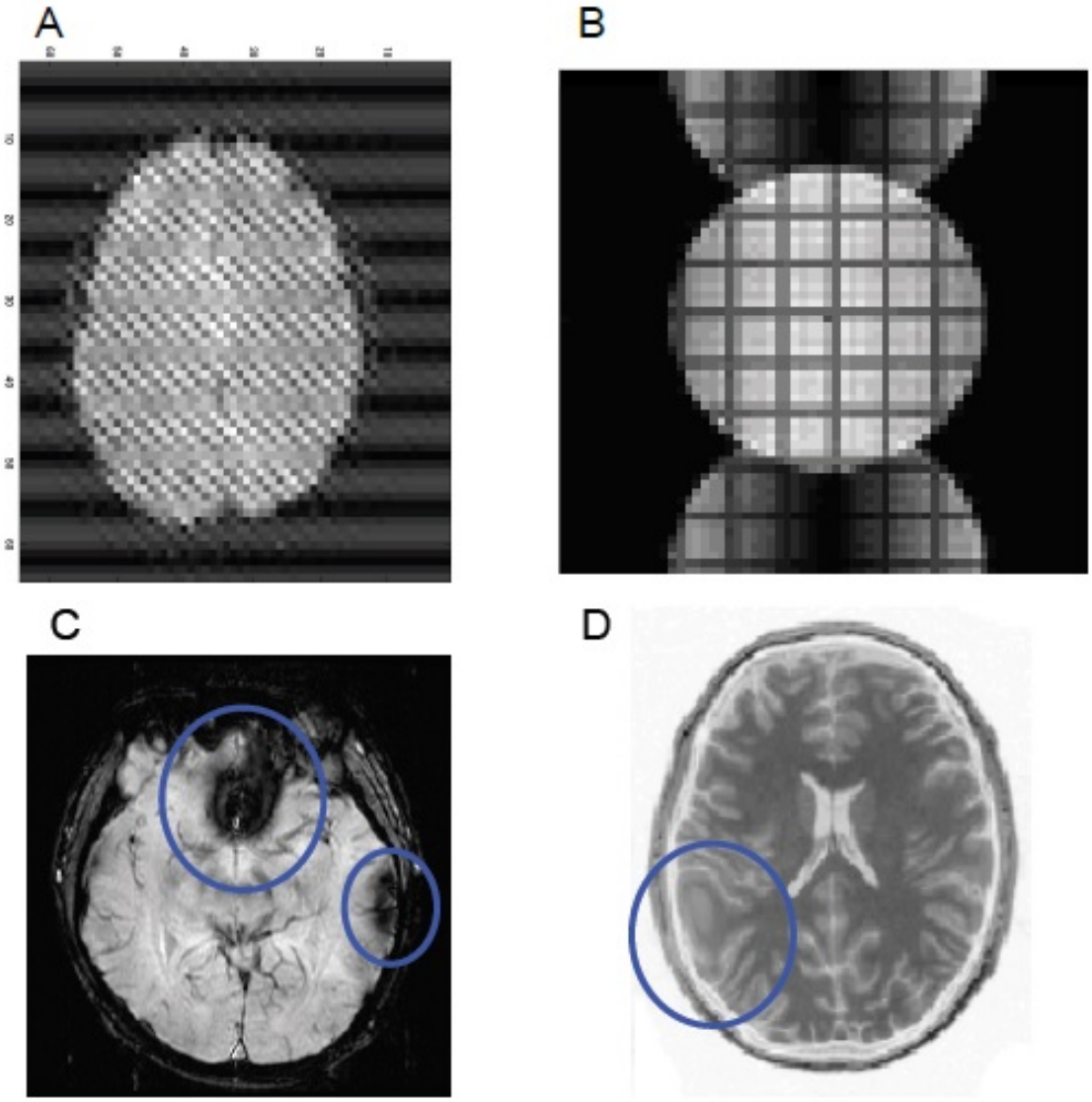

Figure 3.1: Examples of common MRI artifacts: (A) k-space artifact; (B) ghosting in a phantom; (C) susceptibility artifact; and (D) spatial normalization artifact. [1]

3.1.2 The fMRI experiment

The fMRI signal is produced by the variable presence of oxigen in the blood as a reponse to the need of energy due to activation of the neurons carrying some cognitive task. The Blood-oxygen-level-dependent (BOLD) signal captures the haemodynamic response that provides more oxygen to working neurons than to inactive neurons.

The typical fMRI task activation experiment utilizes visual, auditory or other stimuli to induce two or more different cognitive states in the subject following an alternating sequence, while collecting MRI volumes continuously [170]. In a task with a two-condition design, one cognitve state corresponds to the experimental condition, while the other corresponds to the control condition. The aim of the experiment and data processing is to assess if there are specific locations in the brain that have specific neural responses to the task, i.e. that change their activity according to the change in proposed cognitive state. This is done through multiple statistical tests carried out over all the brain space that try to falsify the null hypothesis of no change in the BOLD signal correlated with the task.

When the experiment follows a block design, the alternation between the experimental and control conditions are shown in Figure 3.2. Each block typically lasts in the order of tens of seconds. A jittered event-related (ER) design (not shown) may be useful to characterize the amplitude or timing of the hemodynamic response. In the ER design, task events are relatively brief happening at non-constant intervals of control condition so long that allow a more fully return of the hemodynamic response to baseline state. The detail of the design of the task greatly influences the degree to which valid inferences can be drawn from the measured time series data. The research must ensure of separating the effect of interest changes between experimental and control conditions from confounding effects, like the attention of the subject or his emotional valence.

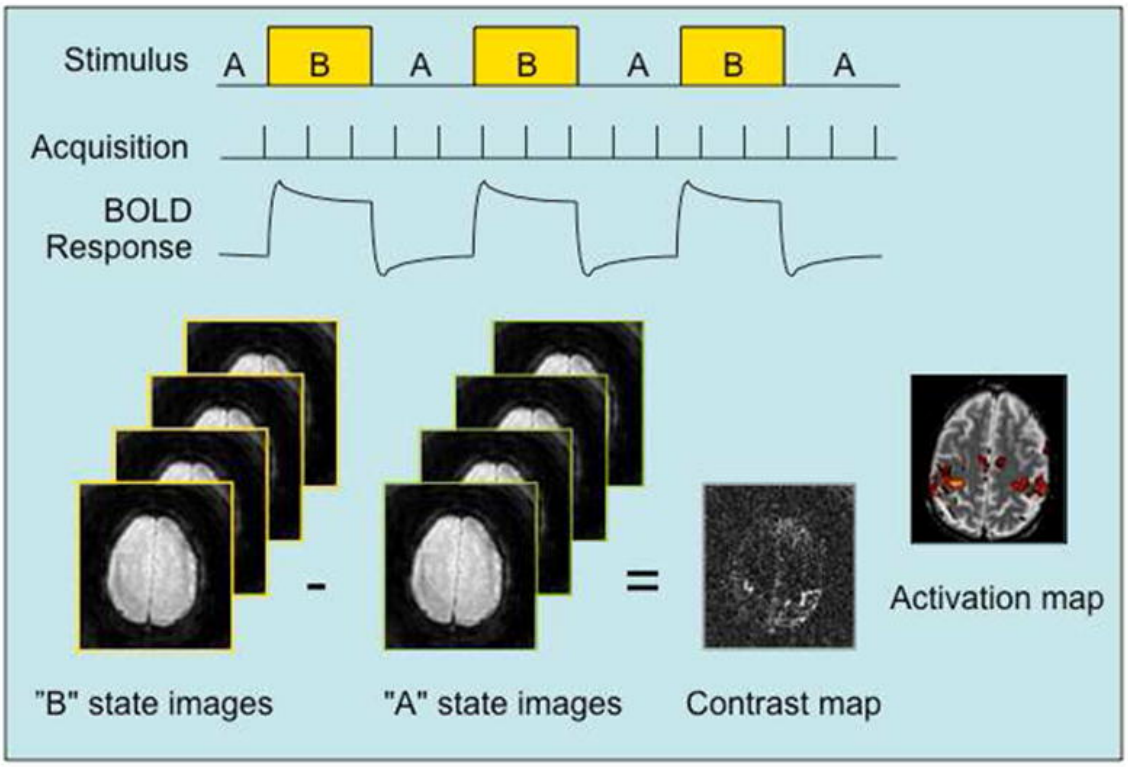

Figure 3.2: Block design fMRI experiment. A neural response to the state change from A to B in the stimulus is accompanied by a hemodynamic response that is detected by the rapid and continuous acquisition of MR images sensitized to BOLD signal changes. Using single- or multi-variate time series analysis methods, the average signal difference between the two states is computed for the scan and a contrast map generated. A statistical activation map is finally obtained using a suitable threshold for the difference; the map depicts the probability that a voxel is activated given the uncertainty due to noise and the small BOLD signal differences.

3.1.3 The resting state fMRI experiment

Contrary to the task oriented fMRI experiments, the resting state fMRI (rs-fMRI) experiments do not impose any cognitive or motor task to the subject. Subjects are instructed to stay relaxed, doing nothing and trying not to fall sleep or loss conscience. The aim is to examine the ground state of the brain and its connectivity. It has the advantage that any kind of subjects can perform the experiment, whatever their cognitive impedements, if they can stay quiet for a while. The analysis of the rs-fMRI data has been tackled with diverse approaches, for instance independent component analysis (ICA) allowed to discover the default mode networks (DMN). A common approach is to compute the average signal of each region of a given brain parcellation and to estimate the connection strength between regions as some measure of correlation or similarity among these representative signals. The latter is the approach pursued in this Thesis.

3.1.4 Preprocesing

The preprocessing methods customarily applied to the fMRI data include skull stripping, spatial normalization, realignment for motion correction, and smoothing for noise reduction [**?**]:

- Skull stripping. After all the brain images in the fMRI sequence have been converted to a predefined shape and size, the structure of the skull along with other parts of the body (i.e. eyes, spinal cord and the muscles in the face and neck) are removed because they do not provide any useful information.

- Spatial normalization. The size and shape of the human brain varies from subject to subject. We must ensure that each point in one brain volume corresponds to the same location in another brain volume, in order to have anatomically comparable values (i.e. we do not compare different brain structures in the subjects). Therefore, all the brain volumes must be registered and warped to a standard template. The most conventional is the Montreal Neurological Institute (MNI) for structural MRI.

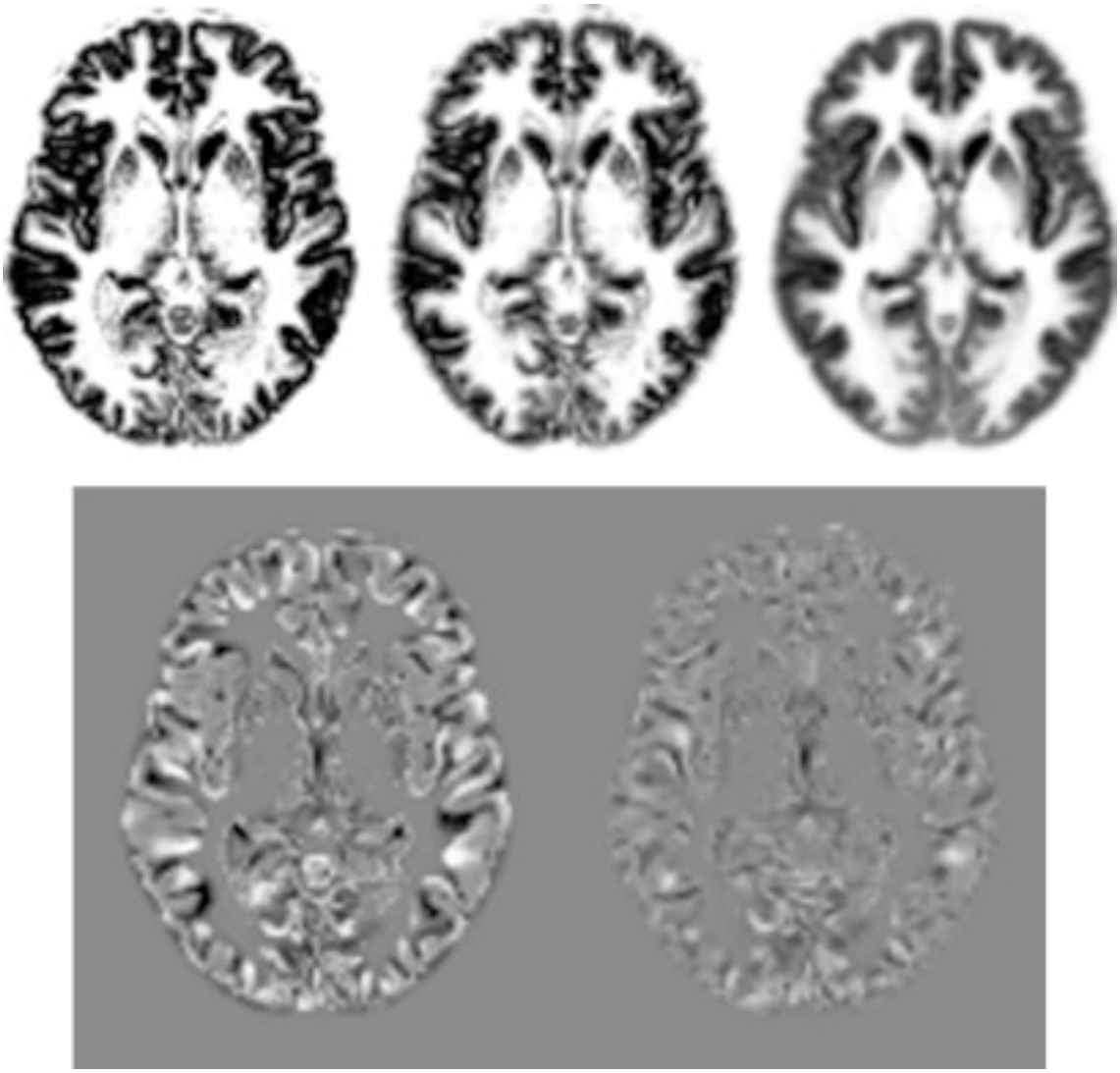

Figure 3.3: An image (top left) is warped to match a template (top right) to produce a spatially normalized version (top center). For clarity, the original image was approximately aligned with the template, and the warping was only done in two dimensions. The bottom row shows the difference between the template and image, both before and after the warping [2].

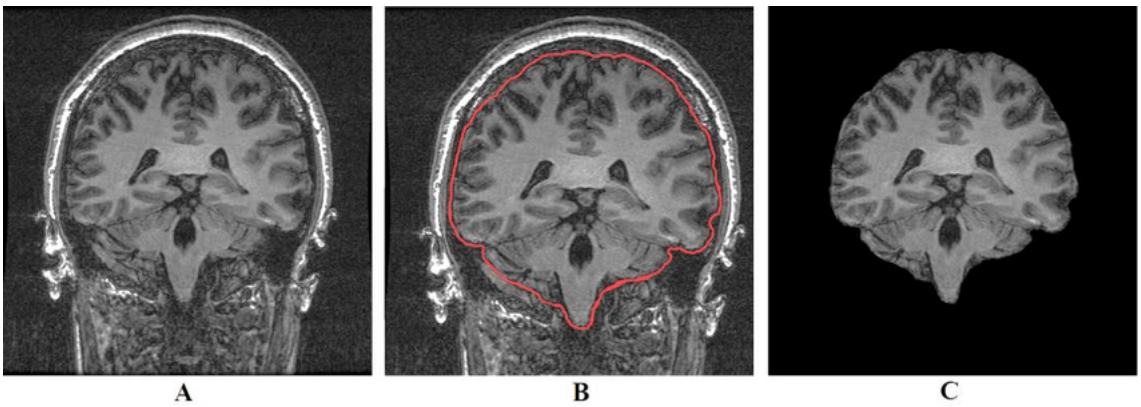

Figure 3.4: Skull-stripping steps: (A) input images, (B) brain contouring, and (C) removal of nonbrain tissues [3].

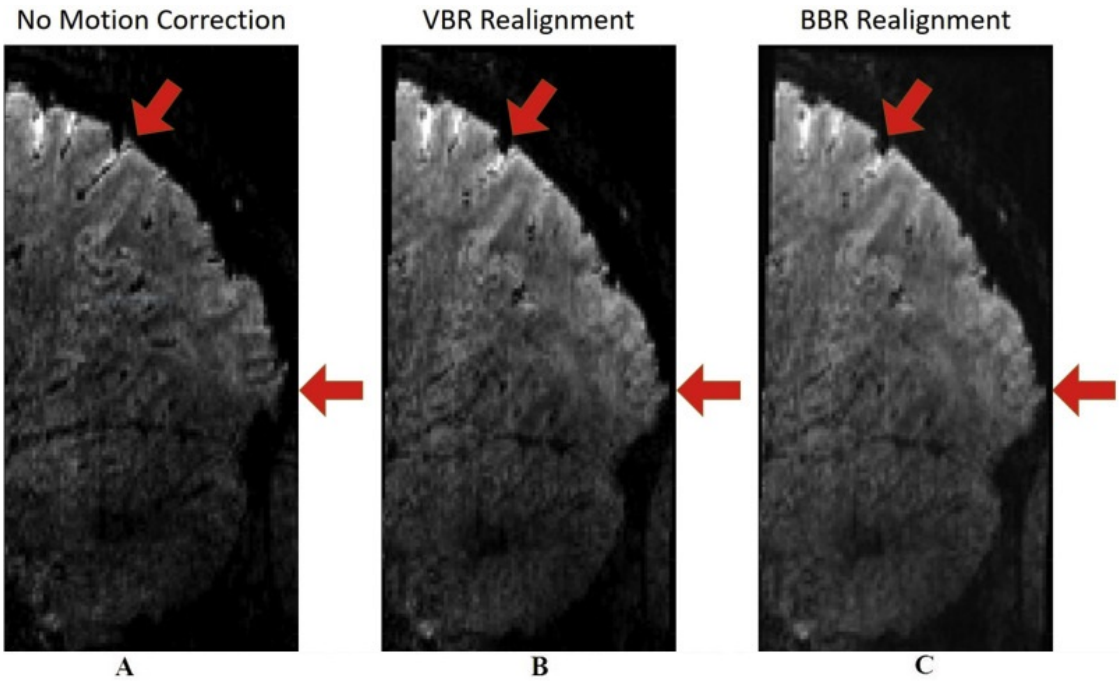

Figure 3.5: Realigment: (A) input image, (B) Voxel-Based Registration Method, and (C) Boundary-Based Registration Method [4]

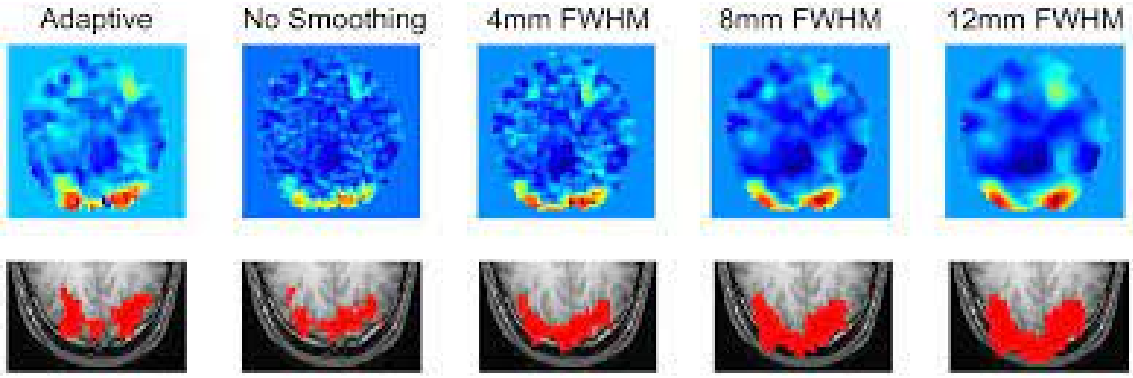

Figure 3.6: Results of the smoothing data analysis: t-maps (top) and thresholded images (bottom) obtained using spatially adaptive smoothing and fixed Gaussian kernels with various widths from [5].

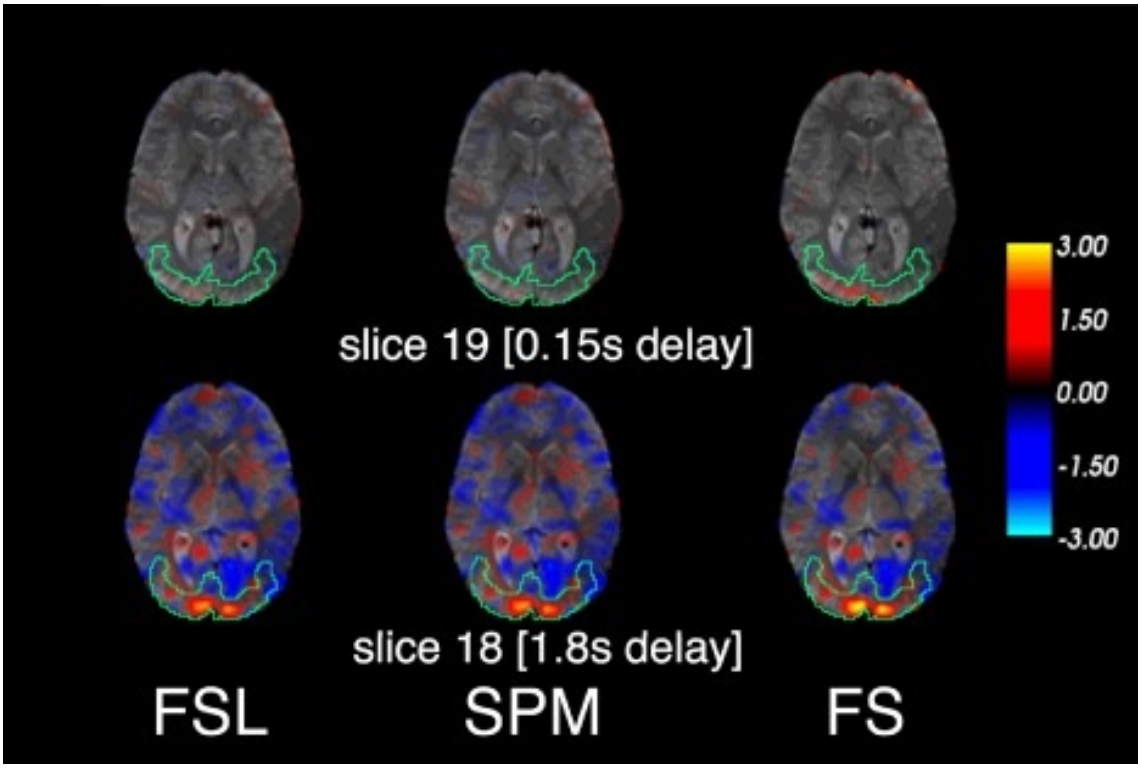

Figure 3.7: Different methods of Slice time correction: A) FSL B)SPM and C)FS

- Realignment. When the head moves during an experimental run or between runs (also termed within-run vs. between runs head movements), the correspondence between image location and brain anatomical region will be changing slightly between MRI volume captures, i.e. motions can cause a given voxel to contain signal from two different types of tissue or a loss of data. This effect is more easy to visualize at the edges of the imaging volume. Furthermore, movement of the head will alter the uniformity of the magnetic field that has been shimmed for one particular head position. Finally, head motion can have consequences for activation timing/pattern of excitation, given that each excitation pulse is targeted to one slice at a time and the head is moving through different slices during acquisition. Motion correction adjusts the series of MRI volumes to ensure that the brain appears in the same position by a process called co-registration [171].

- Smoothing (Noise reduction). The spatial noise present in the fMRI scans is assumed to be Gaussian noise, independent for each voxel, and zero-mean. We expect that convolving the BOLD volumes, after realignment, with a Gaussian smoothing kernel will remove most of this Gaussian noise improving the Signal to Noise Ratio (SNR). The main inconvenient of this process is that for very low SNR, the amount of smoothing required may damage the information content of the fMRI volumes.

- Slice time correction. The fMRI data for each subject is a time series of MRI scans. Each scan should correspond to a particular point in time recording the instantaneous BOLD information. However, recording each slice in the volume requires some time. Therefore, the data captured at different brain regions are obtained at different points in time. Slice time correction method uses the Fourier transform of the signal at each voxel across time to perform the time series interpolation in order to obtain time homogeneous BOLD volumes.

- Coregistration. The anatomical label maps of the brain are created to over an sMRI template. Therefore, the sMRI scan is used to coregister the fMRI data to the right dimensions allowing to overlaid the anatomical labe lel map

Table 3.1: Number of regions of the brain parcellations used in this Thesis.

Atlas	#ROIs
Automated Anatomical Labeling (AAL)	116
Eickhoff-Zilles (EZ)	116
Harvard-Oxford (HO)	110
Talarach and Tournoux (TT)	110
Dosenbach 160	160
Craddock 200 (CC200)	200

on the fMRI data in order to produce the brain parcellations discussed below. This is required so that we can have a one to one match of the ROIs defined in the atlas with the areas in the fMRI data.

3.1.5 Brain parcellations

Korbinian Brodmann subdivided the cerebral cortex into numerous areas based on regional differences in the distribution, density, shape, and size of cell bodies [172, 173] providing one of the first brain anatomical parcellation allowing researchers to investigate brain-behavioral associations with developmental [174], cognitive , and clinical phenotypes [175].

In our works on the functional connectivity analysis, the parcellations presented in Table 3.1 were applied in order to obtain the region representative time series for each of the regions of the selected parcellations. As discussed in [35] there are several approaches to the definition of the brain parcellation which may lead to significant differences in the computational experiments outcomes [175, 176]. On the one hand, we consider in this paper the anatomically guided parcellations such as the Tailarach and Tournoux (TT), Eickhoff-Zilles [177], Harvard Oxford (HO) [178], and the Automated Anatomical Labeling (AAL) [179, 180] defined from the brain segmentation of selected control populations. On the other hand, we consider parcellations are produced from the segmentation of the rs-fMRI time series of the brain volume using clustering techniques, such as the Dosenbach [174] and Craddok [181] parcellations. All these atlases were defined at the conventional resolution of sMRI of $1mm^3$. In order to reduce their resolution to conventional fMRI resolution of $3mm^3$ nearest neighbor interpolation was used.

- Tailarach and Tournoux. The Co-Planar Stereotactic Atlas of the Human Brain by Talairach and Tournoux (1988) [**?**] is based on the anteroposterior commissural system and contains gross anatomy onaxial, coronal, and sagittal sections. The Talairach and Tournoux (TT) atlas has widespread familiarity and utilization, and the associated Talairach transformation is a practical way for normalizing brain images. Developed initially for stereotactic and functional neurosurgery, the TT atlas iswidely used in human brain mapping for brain comparison across subjects [**?**] and the number of references to it has been growing exponentially [**?**]. In addition, the Talairach system is the most frequently used coordinate system in human brain mapping [182]. The TT atlas distributed with AFNI was coregistered and warped into template space.

- Eickhoff-Zilles. The Eickhoff-Zilles(EZ) atlas [177] was derived from the max-propagation atlas distributed with the SPM Anatomy Toolbox. The atlas was transformed into template space using the Colin 27 template (also distributed with the toolbox) as an intermediary.

- Harvard-Oxford. The Harvard-Oxford (HO) atlas [178] was developed at the Center for Morphometric Analysis (CMA), and distributed with the FMRIB Software Library (FSL). It comes with a probability distribution for each brain region obtained from a Maximum A posteriori (MAP) estimate. The HO atlas is split into cortical and subcortical probabilistic atlases. A 25% threshold was applied to each of these atlases and they were subsequently bisected into left and right hemispheres at the midline ($x = 0$). ROIs representing left/right WM, left/right GM, left/right CSF and brainstem were removed from the subcortical atlas.

- Automated Anatomical Labeling (AAL). The AAL atlas [179, 180] is distributed with the AAL Toolbox.

- Dosenbach 160. The Dosenbach 160 atlas [174] distributed with DPARSF/DPABI includes 160 4.5-mm radius spheres placed at coordinates extracted from Table S6 in Dosenbach et al., 20104. These regions were identified from meta-analyses of task-related fMRI studies.

- Craddock 200 (CC200) [183]: Functional parcellation was accomplished using a two-stage spatially-constrained functional procedure applied to preprocessed and unfiltered resting state data corresponding to 41 individuals from an independent dataset. A grey matter mask was constructed by averaging individual-level grey matter masks derived by automated segmentation. Individual-level connectivity graphs were constructed by treating each gray matter voxel as a node and defining edges between nodes whose temporal correlation among 3D neighborhoods was above a preset threshold. Each graph was partitioned into 200 regions using normalized cut spectral clustering. Association matrices were constructed from the clustering results by setting the connectivity between voxels to 1 if they are in the same ROI and 0 otherwise. A group-level correspondence matrix was constructed by averaging the individual level association matrices and subsequently partitioned into 200 regions using normalized cut clustering. Labels were generated for each of the resulting ROIs from their overlap with AAL, EZ, HO, and TT atlases using the cluster naming script distributed with the pyClusterROI toolbox .

3.1.6 Connectivity matrices

The first step of a computational pipeline dealing with rsfMRI data is the estimation of the connectivity matrices. In the experimental works reported in Chapters 6 and 76 we have considered five similarity metrics to build the connectivity matrices from the time series representatives of the brain parcellations which are available from the nilearn python package (`https://nilearn.github.io/modules/generated/nilearn.connectome.ConnectivityMeasure.html`). At the root of these computations is the robust estimation of the covariance matrix of the time series. We use the Ledoit-Wolf shrinkage estimator [184] following methodological recommendations in [175, 176]. The connectivity matrices are constructed according to the following connectivity measures:

- The covariance matrix computed using the Ledoit-Wolf shrinkage estimator [184],

- The Pearson Correlation Coefficient (PCC) [185] among each pair of ROI time series, which is computed as the normalization of the covariance matrix [186].
- The precision computed as the inverse of the covariance matrix.
- The partial correlation obtained regressing out all other connections for each pair of regions [187].
- The tangent space representation of the matrices obtained by whitening them [188].

Hence, for each subject in the ABIDE dataset and brain parcellation we have five different connectivity matrices as input for the feature extraction and classifier cross-validation.

3.2 Related works

Artificial intelligence tools and problem solving approaches [208] are contributing to the understanding and predictive analysis of ASC. Overall, there is increasing evidence that specific features extracted from MRI neuroimaging can be used to discriminate ASC from TD. However, there is a wide variety of methodological and computational approaches tested on widely different cohorts and imaging modalities [21, 209].

3.2.1 Anatomical brain imaging

Regarding anatomical brain imaging, predictive models can be built based on anatomical differences computed by voxel based morphometry (VBM) over gray and white matter segmentations of T1-weighted MRI data. Experiments over a small cohort have reported average accuracies cross-validation experiments below 70% for a series of stratified computational experiments [210]. However, a similar study [211] using voxel based morphometry (VBM) significative differences of diverse stratifications of female and male subjects of the ABIDE dataset reported much higher accuracies, above 90% in several subgroups. On the other hand, the use of 3D convolutional

Table 3.2: State of the art results of the classification ASC vs. TD on the functional connectivity data of ABIDE I dataset. 24ISC=24 inter-hemispheric selected connections, Acc=Accuracy, ADM=additional demographic features, AUC= Area under the ROC, BASC=Bootstrap Analysis of Stable Clusters, CC200=Craddock200, DNN= Deep neural network, E3DCNN=ensemble 3D convolutional networks, ECM=eigenvalues of connectivity matrix; EGC=Ensemble of GCNs, GNB=Gaussian naive Bayes, GNG=G naive graph, HO= Harvard Oxford, kNN=k-Nearest Neighbors, LDA=linear discriminant analysis, LR= logistic regression, LSTM=Long Short-Term Memory networks, maLRR= multisite adaptation low rank decomposition, MODL= massive online dictionary learning, MSDL=multi-subject dictionary learning, MTGM= multi-task graphical model, NC= network centralities; RF=random forest, RRC=ridge regression classification, SFM=spatial feature detection method, SFS= sequential feature selection, SGC=spectral graph convolution, SP=stochastic parcellation, TT=Teilarach & Tournoux, WC=Ward's clustering.

Ref.	Year	Classifier Method	Feature extraction/selection	Brain Parcellation	Best Result
[189]	2018	GCN	PCA, MLP, ADM	HO	Acc=70.4 AUC=0.75
[190]	2017	GCN	PCA, GCN	HO	Acc=62.9
[132]	2018	DN, RF,SVC		AAL, CC200, D160, EZ, HO, TT	Acc=70.0
[191]	2016	GCN	RFE	HO	Acc=69.5
[192]	2019	SVC, GCN, EGCN	RFE	HO	Acc=70.86
[193]	2015	DT, RF, SVC, LR, kNN,MLP		PCD features	Acc=62.0, AUC=0.65
[176]	2019	kNN, GNB, RF, SVC, RRC, LR	ANOVA-SVC	AAL, HO, BASC, MODL,	Median AUC=0.71
[194]	2017	LSTM		CC200	Acc=68.5
[195]	2017	SVC, RF, GNB, MLP		CC200	Acc=61.8
[196]	2017	SCVC		AAL	Acc=62.0
[197]	2017	LR	structural MRI		Acc=62.0
[175]	2017	SVC, RRC		HO, Yao, CC200, kM, WC, ICA, MSDL	Acc=69.7
[198]	2017	MTGM		dosenbach 40	Acc=58.6
[199]	2019	E3DCNN		SP, HO, TT, EZ, CC200, CC400	Acc=73
[200]	2019	LR	subnetwork extraction		Acc=66.74
[201]	2019	SVM	24ISC		Acc=88 (intrasite)
[202]	2018	SGC	PCA	HO	AUC=0.58, Acc<70
[203]	2020	Ensemble CNN (300)		AAL	AUC=0.67, Acc=67
[204]	2020	SVM	graph measures	Glassner	Acc=60
[205]	2017	SVM	SFM	AAL (90)	Acc=77
[206]	2020	ensemble MLP	autoencoders	AAL,CC200	Acc=75
[207]	2020	kNN	maLRR	AAL	Acc=73

neural networks (3D-CNN) [212] on the complete ABIDE structural MRI dataset reported an accuracy of 70%. Hence, there is a strong selection effect that may bias significantly the reported results. Significance weighted principal component analysis allows to remove the effects of site data acquisition improving discrimination based on anatomical imaging [213].

3.2.2 Functional connectivity

Works based on functional connectivity information extracted from rs-fMRI data have been predominant in the latter times. They have been carried out over a wide variety of cohorts, testing many computational approaches. Relevant brain connection selection using logistic regression [162] achieved accuracy of 85% by a linear classifier in a leave one out validation over a small cohort (74 high-functioning adult ASCs and 107 adult TDs). Further validation on an independent subset of the ABIDE dataset (N=88) achieved a remarkable accuracy of 75%. Another work [214] reports accuracies over 80% on a small cohort of paired 20 ASC and 20 TD children using hyperconnectivity networks as features for a SVM classifier, while other authors [215] reported on the results of multilinear regression over the functional connectivity matrices after PCA dimensionality reduction of a cohort of 85 ASC and 163 TD children finding specific imbalances in brain connectivity for ASC children. However, the heterogeneity of the cohorts points to powerful selection bias in the results. In other words, the selection of which subjects are used for the experiments has a strong effect in the results reported.

3.2.3 Dataset heterogeneity

The heterogeneity of the data in ABIDE as illustrated by the demographic information shown in Table 6.1 is a source of bad results for machine learning approaches. Experiments concerning single sites report overly optimistic results that can not be achieved with the entire ABIDE dataset or a large subsample [216]. For instance, some works carry out separate intra-site cross-validation experiments reporting as the global result over the database the average of the separate intra-site

results [201,217]. This selection strategy overlooks the differences among sites, doing the crossvalidation on coherent data.

The selection of the experimental cohort among the ABIDE subjects varies among studies, often for unexplained reasons. For instance, the benchmarking work [176] selected 871 subjects, after visual quality inspection of the data, while our own selection includes 884 subjects because our exclussion reason is diagnostic. Therefore we have excluded from Table 3.2 references such as the recursive feature selection on 532 subjects [218], the time series clustering approach tested on 814 subjects [219], and others that report results on ABIDE subsamples of 209 [220], 365 [39], 182 [221], 211 [222], and 119 [223] subjects .

3.2.4 Summary information

Table 3.2 summarizes the state of the art regarding the classification of subjects into ASC or TD on the basis of functional connectivity matrices extracted from the rs-fMRI data published in the ABIDE I dataset [22,23]. The criteria for inclusion in this table are (1) that the references report results on the (almost) complete ABIDE I dataset in order to be comparable to our own results reported below, and (2) that they report results using only features extracted from the functional connectivity matrices. We have excluded results obtained adding other kinds of information, such as the graph convolutional networks (GCN) enriched with demographic information [189], and the features extracted from structural and MRI data [206].

The selected references of Table 3.2 apply the conventional machine learning validation methodology uniformly. Works report the average results of repetitions of k-fold cross-validation results where the training and any feature extraction is restricted to the training dataset avoiding the double dipping issues [224, 225], with training and testing datasets selected across original sites contributing to ABIDE listed in Table 6.1. The performance reports in the references of Table 3.2 are usually in terms of the average Accuracy. Some works report the AUC as a more robust performance measure [176,189,202], and some report the median and 5% and 95% percentiles of the AUC [202]. Maximal accuracy and AUC results found in the literature are 77% and .75, respectively. Regarding reproducibility of the results,

one key issue is the availability of the actual data used in the experiments, which is heavily dependent on rs-fMRI preprocessing, brain parcellation, and functional connectivity matrix estimation. In many instances, obtaining the same dataset is not possible, so we prefer to work on the publicly available preprocessed connectomes. We feel that results reported over this dataset are fairly comparable.

Columns of Table 3.2 reflect the choices made in the steps of the process of Figure 1.1, namely on brain parcellation, feature extraction, and classification method. Most works do not report on the specific functional connectivity matrix estimation procedure. The most popular brain parcellations are the HO [178], and the AAL [179, 180], whose definitions are guided by anatomical criteria. However, data driven parcellations have also been assessed in the literature applying dictionary learning, independent component analysis (ICA), clustering approaches, stochastic parcellations according to a random selection of sites (SP), and the selections of sites following biomarkers reported in the literature, such as [173]. The feature extraction processes applied are widely varying among references. Some works report graph measures, other PCA and recursive feature selection (RFE), sequential feature selection (SFS), or the use of ANOVA to select the most relevant connections [176]. Unlike conventional machine learning classifier model building approaches, studies using deep learning [203] do not have a separate feature extraction process. Convolutional Neural Networks (CNN) that learn from the data to carry out a hierarchy of feature extraction processes have been also applied to the task of defining ASC classification systems [226–232].

Chapter 4

Machine learning background

This Chapter provides some background ideas and definitions on Machine Learning techniques that have been used in the computational pipeline proposed in Figure 1.1. Section 4.1 gives some introductory terminology. Section 4.2 provides details on the classifier building models. Section 4.3 provides details on the feature extraction and feature selection methods that have been applied to the brain connectivity matrices. Section 4.4 describes the performance evaluation procedures and metrics used to report results in Chapter 6.

4.1 Introduction

Machine learning is a field of artificial intelligence that provides the machine with theability to learn from data without providing specific instructions. Machine learning is divided into three broad categories: supervised learning, unsupervised learning, and semi-supervised learning. In machine learning terms, this goal is formulated as the supervised learning task of inferring from collected data a model that predicts the value of an output variable based on the observedvalues of input variables. As such, finding an appropriate model is based on the assumption that the output variable does not take its value at random and that there exists a relation between the inputs and the output [233]. Unlike supervised learning, in unsupervised learning, there is no corresponding output for the input data. The goal of unsupervised learning is to draw inference and learn the structure and patterns of the data. Cluster

analysis is the most common example of unsupervised learning. Semi-supervised learning is a category of machine learning which falls between supervised and unsupervised learning. In semi-supervised learning techniques, besides using labeled data, unlabeled is used the learning process [169].

4.2 Classifier model building methods

We have applied classifier building methods that are available from the open and free source Python library scikit-learn v0.22 (`https://scikit-learn.org/`) [234]. In this section we describe the classifiers that have been tested:

4.2.1 Random Forest (RF)

Random Forest (RF) [235] is a supervised learning algorithm and a popular ensemble method that combines by majority voting the response from a committee of decision trees [236] trained upon bootstrapped versions of the training data. The "forest" it builds, is an ensemble of decision trees; usually trained with the “bagging” method. Moreover, the variables used to compute each node split are randomly selected. The basic premise of the algorithm is that building a small decision tree with few features is a computationally cheap process [237]. A tree-based model involves recursively partitioning the given dataset into two groups based on a certain criterion until a predetermined stopping condition is met. At the bottom of decision trees are the leaf nodes where the decision on the class is performed. Figure 4.1 illustrates a recursive partitioning of a two-dimensional input space with axis-aligned boundaries. Each time the input space is partitioned in a direction parallel to one of the axes. In the figure, the first split is defined by $x2 \geq a2$. Then, the two resulting subspaces are partitioned: The left branch corresponds to the split on $x1 \geq a4$. The right branch is first split by the rule $x1 \geq a1$, and then one of its subbranches is split by the ryle $x2 > a3$. Figure 4.2 is a graphical representation of the space partition in figure 4.1.

Depending on how the partition and stopping criteria are set, decision trees can be designed for both classification tasks (categorical outcome, for example, logistic regression) and regression tasks (continuous outcome).

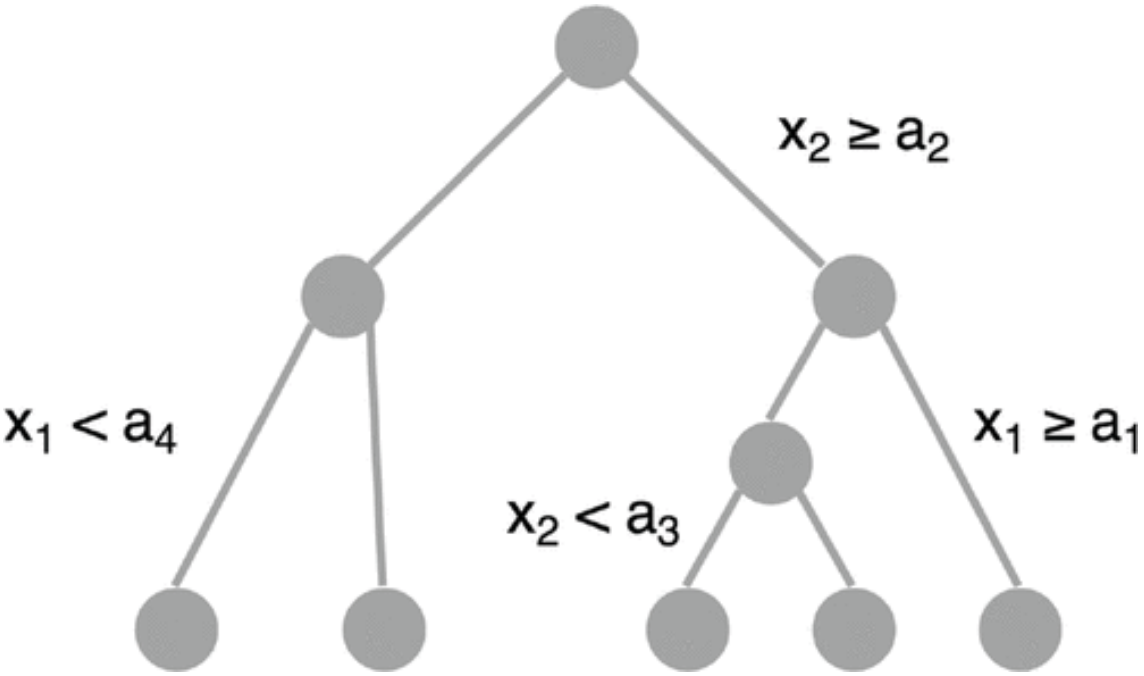

Figure 4.1: A graphical representation of a binary decision tree splitting the space recursively.

For both classification and regression problems, the subset of predictor variables selected to split an internal node depends on predetermined splitting criteria that are formulated as an optimization problem. A common splitting criterion in classification problems is entropy, which is the practical application of Shannon's source coding theorem that specifies the lower bound on the length of a random variable's bit representation. At each internal node of the decision tree, entropy is given by the equation (4.1) where c is the number of unique classes and p_i is the prior probability of each given class. This value is maximized to gain the most information at every split of the decision tree. For regression problems, a commonly used splitting criterion is the mean squared error at each internal node:

$$E = -\sum_{i=1}^{c} p_i \times log(p_i) \tag{4.1}$$

A drawback of decision trees is that they are prone to overfitting, which means that the model follows the idiosyncrasies of the training dataset too closely and performs poorly on the test data, i.e. unknown data at training time. Overfitted decision trees lead to low generalization performance.

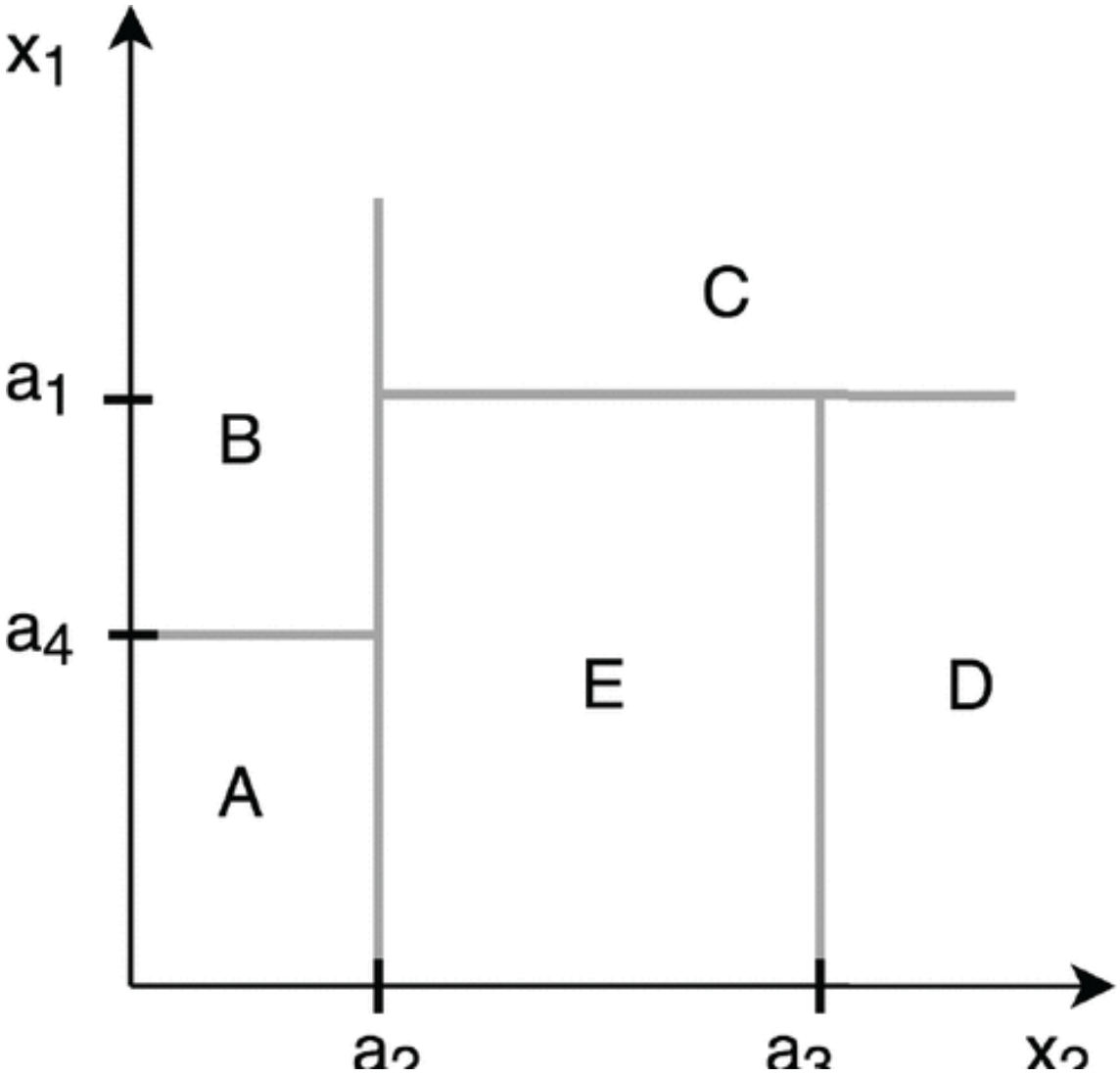

Figure 4.2: Recursive binary partition of a two-dimensional space obtained as a result of the binary tree in 4.1.

One way to increase generalization accuracy is to consider only a subset of the observations and build up many individual trees. First introduced by [238], this idea of the random-subspace method was later extended and formally presented as the random forest by [239]. The random forest model is an ensemble tree-based learning algorithm; that is, the algorithm averages predictions over many individual trees. The individual trees are built on bootstraped samples from the original sample. This is called bootstrap aggregating or simply bagging, and it reduces overfitting. It is performed in order to obtain additional randomization of the training of individual decision trees, expecting a more diverse ensemble of classifiers. It is a common understanding (though there are scarce formal proofs) that diversity improves the generalization performance of the ensemble, decreasing overfitting effects.

Individual decision trees are easily interpretable, but this interpretability is lost in random forests because many decision trees are aggregated. However, in exchange, random forests often perform much better on prediction tasks. The random forest algorithm more accurately estimates the error rate compared with decision trees. More specifically, the error rate has been mathematically proven to always converge to zero as the number of trees increases [239].

The error of the RF is approximated by the out-of-bag error during the training process, wich is computed as follows. Each decision tree is built on a different bootstrap sample. Each bootstrap sample randomly leaves out a number of the observations in the original sample. These left-out observations for a given tree are referred to as the out-of-bag sample. Finding parameters that would produce a low out-of-bag error is often a good strategy for model selection and parameter tuning. Note that in the RF algorithm, the size of the subset of predictor variables strongly determines the final depth of the trees. Hence, it is a parameter that needs to be tuned during model selection [237].

4.2.2 K-Nearest Neighbors (KNN)

K-Nearest Neighbors (KNN) [240] is the basic non parametric classifier building approach where the test sample class is assigned by majority voting among the class labels of the K closest training samples according to the Euclidean distance. Fix &

Hodges were the first to propose a KNN classifier algorithm as early as the year of 1951 for performing pattern classification task [241].

The KNN algorithm essentially boils down to forming a majority vote between the K most similar instances to a given "unseen" observation. Similarity is defined according to a distance metric between two data points. A popular choice is the Euclidean distance, but other measures can be more suitable for a given setting, such as the Manhattan, Chebyshev and Hamming distances. More formally, given a positive integer K, a stored training data sample of feature vectors with associated class labels $S = \{\mathbf{y}_i, \omega_i\}_{i=1}^{N}$, an unseen observation x, and a similarity metric $\phi(\mathbf{y}, \mathbf{x})$, a KNN classifier performs [242] the following steps:

1. It runs through the whole dataset computing $\{d_i = \phi(\mathbf{y}_i, \mathbf{x})\}_{i=1}^{N}$. The nearest neighboring set **A** is composed of the K points in the training data that are closest to x, . K is usually odd to prevent tie situations.

2. It then estimates the conditional probability for each class, that is, the fraction of points in **A** with that given class label. ($I(z)$ is the indicator function which evaluates to I when the argument z is true and 0 otherwise)

$$P(\omega_{\mathbf{x}} = j, X = \mathbf{x}) = \frac{1}{k}\sum_{i \in A} I(\omega_i = j)) \tag{4.2}$$

3. Finally, input x gets assigned to the class with the largest probability.

4.2.3 Gaussian Naive Bayes (GNB)

Gaussian Naive Bayes (GNB) [240] assumes the statistical independence of the features, so that the classifier can be built as an aggregation of one dimensional not interacting classifiers modeled by a loose mixture of Gaussians. Naive Bayes is used widely [243] in many applications such as: text categorization [244], document judgment and data stream classification [245]. Naive Bayes is a generative model based classifier [246] with a fast learning and testing process.

Bayesian classifiers are straightforwardly derived from the Bayes rule and probability theorems. It has been proven that learning the optimal Bayesian classifier

from training data is an NP-hard problem [247]. A simplified version of Bayesian classifier called naive Bayes uses two assumptions. The first is that attributes are conditionally independent given the class label. The second is that, no latent attribute affects the label prediction process [248].

Assume, the vector $(x_1, \ldots, x_n)$ represents the n attributes of the instance $\mathbf{x}$. Let it be c the class label of the instance $\mathbf{x}$. The probability of observing $\mathbf{x}$ given the class label c can be computed by as follows:

$$p(x_1, \ldots, x_n \,|c) = \prod_{i=1}^{n} = p(x_i \,|c) \tag{4.3}$$

In order to predict the class label of instance x, its probability to belong to each class is computed. The class with the maximum probability is identified as the class label of the instance x. Formally:

$$C(x)_{NB} = \arg\max_{c} \{p(x_1, \ldots, x_n \,|c)\}_c \tag{4.4}$$

The conditional independence assumption between the attributes in naive Bayes is weak, and rarely correct in most real problems except of situations in which the attributes are extracted from independent stochastic processes. Some methods have been introduced for improving the conditional independence assumption in naive Bayes.

Gaussian naive Bayes classification is an instance of naive Bayes method assuming that each the attribute follows a Gaussian distribution given the class label. For example, suppose that i^{th} attribute is continuous and its class conditional mean and variance are denoted by $u_{c,i}$ and $\sigma^2_{c,i}$, respectively, given the class label c. Hence, the probability of observing the value x_i in i^{th} attribute given the class label c, is given by the normal distribution:

$$p(x_i|c) = \frac{1}{\sqrt{2\pi\sigma^2_{c,i}}} exp^{(-\frac{(x_i-\mu_{c,i})^2}{2\sigma^2_{c,i})}} \tag{4.5}$$

4.2.4 Support Vector Classifier (SVC)

Support Vector Classifier (SVC) [249,250] looks for the maximum margin hyperplane discriminating the sample into two classes solving a linear programing problem on the relevance of the samples to this class boundary. We use the linear kernel version because its response is more stable, needs less parameter tuning, and is more efficient computationally. In some instances we carry out a variable selection procedure based on their statistical significance in an ANOVA analysis [251]. We consider both sparse (ℓ_1) and non-sparse (ℓ_2) regularization terms. We test the two implementations available from scikit-learn, based respectively on libsvm (`https://www.csie.ntu.edu.tw/~cjlin/libsvm/`) and liblinear (`https://www.csie.ntu.edu.tw/~cjlin/liblinear/`) libraries.

The foundations of Support Vector Machines (SVM) have been developed by Vapnik [252] and gained popularity due to many promising features such as better empirical performance. The formulation uses the Structural Risk Minimization (SRM) principle, which has been shown to be superior [253], to traditional Empirical Risk Minimization (ERM) principle, used by conventional neural networks. SRM minimizes an upper bound on the expected risk, whereas ERM minimizes the error on the training data. It is this difference which equips SVM with a greater ability to generalize, which is the goal in statistical learning. SVMs were developed to solve the classification problem, but recently they have been extended to solve regression problems [254].

4.2.5 Logistic regression (LR)

Logistic regression (LR) [255–257] is the classical approach that models the probability of the binary classes by a logistic linear function, enabling linear regression solvers to cope with classification problems. We apply both sparse (ℓ_1) and non-sparse (ℓ_2) regularizations. Unlike linear regression which outputs continuous number values, logistic regression transforms its output using the logistic sigmoid function to return a probability value which can then be mapped to two or more discrete classes. There are thre types of logistic regression: Binary, Multi and Ordinal.

In linear regression we tried to predict the value of $y^{(i)}$ for the i-th example $\mathrm{x}^{(i)}$ using a linear function $y = h_{\boldsymbol{\theta}}(\mathbf{x}) = \boldsymbol{\theta}^\top \mathbf{x}$. This is clearly not a solution for predicting binary-valued labels ($y(i) \in \{0, 1\}$). In logistic regression we use a different hypothesis class to try to predict the probability of a given example belonging to the "1" class versus the probability that it belongs to the "0" class. Specifically, LR tries to learn a function of the form:

$$P(y = 1 \,|\mathbf{x}) = h_{\boldsymbol{\theta}}(\mathbf{x}) = \frac{1}{1 + exp\left(\boldsymbol{\theta}^\top \mathbf{x}\right)} \equiv \sigma\left(\boldsymbol{\theta}^\top \mathbf{x}\right) \tag{4.6}$$

$$P(y = 0 \,|\mathbf{x}) = 1 - P(y = 1 \,|\mathbf{x}) = 1 - h_{\boldsymbol{\theta}}(\mathbf{x}) \tag{4.7}$$

The function $\sigma(z) \equiv \frac{1}{1+exp(-z)}$ is often called the "sigmoid" or "logistic" function. It is an S-shaped function that "squashes" the value of $\left(\boldsymbol{\theta}^\top \mathbf{x}\right)$ into the range $[0, 1]$ so that we may interpret $h_{\boldsymbol{\theta}}(\mathbf{x})$ as a probability. Our goal is to search for a value of $\boldsymbol{\theta}$ so that the probability $P(y = 1 \,|\mathbf{x}) = h_{\boldsymbol{\theta}}(\mathbf{x})$ is large when x belongs to the "1" class and small when x belongs to the "0" class (so that $P(y = 0 \,|\mathbf{x})$ is large). For a set of training examples with binary labels $\left\{(\mathbf{x}^{(i)}, y^{(i)}) : i = 1, \ldots, m\right\}$ the following cost function measures how well a given h_θ does this prediction:

$$J(\boldsymbol{\theta}) = -\sum_i (y^{(i)} log(h_\theta(\mathbf{x}^{(i)})) + (1 - y^{(i)}) log(1 - h_\theta(\mathbf{x}^{(i)}))) \tag{4.8}$$

When $y^{(i)} = 1$ minimizing the cost function means that we need to make $h_{\boldsymbol{\theta}}(\mathbf{x}^{(i)})$ large, and when $y^{(i)} = 0$ we want to make $1 - h_\theta$ large as explained above. We can learn to classify our training data by minimizing $J(\boldsymbol{\theta})$ to find the best choice of $\boldsymbol{\theta}$. Once we have done so, we can classify a new test point as "1" or "0" by checking which of these two class labels is most probable: if $P(y = 1|x) > P(y = 0|x)$ then we label the example as a "1", and "0" otherwise. This is the same as checking whether $h_\theta(\mathbf{x}) > 0.5$

To minimize $J(\theta)$ we can use the tools of linear regression. We need to provide a function that computes $J(\boldsymbol{\theta})$ and $\nabla_\theta J(\boldsymbol{\theta})$ for any requested choice of $\boldsymbol{\theta}$. The

derivative of $J(\boldsymbol{\theta})$ as given above with respect to θ_j is as follows:

$$\frac{\partial J(\theta)}{\partial \theta_j} = \sum_i x_j^{(i)}(h_\theta(\mathbf{x}^{(i)}) - y^{(i)}) \tag{4.9}$$

Written in its vector form, the entire gradient can be expressed as follows:

$$\nabla_\theta J(\boldsymbol{\theta}) = \sum_i \mathbf{x}^{(i)}(h_\theta(\mathbf{x}^{(i)}) - y^{(i)}). \tag{4.10}$$

This is essentially the same as the gradient for linear regression except that now

$$h_\theta(\mathbf{x}) = \sigma(\boldsymbol{\theta}^\top \mathbf{x}) \tag{4.11}$$

.

4.2.6 Least absolute shrinkage and selection operator (LASSO)

Least absolute shrinkage and selection operator (LASSO) [258] is a sparse (ℓ_1) regularized regression method that performs simultaneously variable selection and regularization. The lasso is a shrinkage method like ridge, with subtle but important differences. The lasso estimate is defined by

$$\hat{\beta}^{lasso} = \arg\min_\beta \sum_{i=1}^{N} (y_i - \beta_0 - \sum x_{ij}\beta_0)^2 \tag{4.12}$$

subject to

$$X_{pj} = |\beta_j| \leq t \tag{4.13}$$

It is possible to re-parametrize the constant β_0 by standardizing the predictors; the solution for $\hat{\beta}_0$ is $\overline{y}$, and thereafter the model is fitted without an intercept. In the signal processing literature, the lasso is also known as basis pursuit [259]. We can also write the lasso problem in the equivalent Lagrangian form

$$\beta^{lasso} = \arg\min_\beta \left\{ \frac{1}{2} \sum_{i=1}^{N} (y_i - \beta_0 - \sum_j x_{ij}\beta_j)^2 + \lambda \sum_{j=1}^{p} |\beta_j| \right\} \tag{4.14}$$

.

The L_2 ridge penalty term $\sum_{j=1}^{p} \beta_j^2$ is replaced by the L_1 lasso penalty $\sum_{j=1}^{p} |\beta_j|$. This modified constraint makes the solutions nonlinear in the y_i, and there is no closed form expression like the one available to solve ridge regression. Computing the lasso solution is a quadratic programming problem, that efficient algorithms are available for computing the entire path of solutions as λ is varied. Because of the nature of the constraint, making t sufficiently small will cause some of the coefficients to be exactly zero. Thus the lasso does a kind of continuous subset selection. If t is chosen larger than $t_0 = \sum_{j=1}^{p} \left|\hat{\beta}_j\right|$ (where $\beta_j = \hat{\beta}_j^{ls}$, i.e. the least squares estimates), then the lasso estimates are the $\hat{\beta}$. On the other hand, for $t = t_0/2$ say, then the least squares coefficients are shrunk by about 50% on average.

4.2.7 Ridge Classifier (RC)

Ridge Classifier (RC) [260,261] treats the classification problem as a straightforward regression in the $[-1, 1]$ interval with a penalty on the size of the coefficients. The ridge coefficients minimize a penalized residual sum of squares,

$$\hat{\beta}^{ridge} = \arg\min_{\beta} \left\{ \sum_{i=1}^{N} (y_i - \beta_0 - \sum_{j=1}^{p} x_{ij}\beta_j)^2 + \lambda \sum_{j=1}^{p} \beta_j^2 \right\} \tag{4.15}$$

Here $\lambda \geq 0$ is a complexity parameter that controls the amount of shrinkage: the larger the value of λ, the greater the amount of shrinkage. The coefficients are shrunk toward zero (and each other). The idea of penalizing according to the sum of squares of the parameters is also used in neural networks, where it is known as weight decay. An equivalent way to write the ridge problem is

$$\hat{\beta}^{ridge} = \arg\min_{\beta} \sum_{i=1}^{N} (y_i - \beta_0 - \sum_{j=1}^{p} x_{ij}\beta_j)^2, \tag{4.16}$$

subject to

$$\lambda \geq \sum_{j=1}^{p} \beta_j^2 \tag{4.17}$$

which makes explicit the size constraint on the parameters. When there are many correlated variables in a linear regression model, their coefficients can become poorly determined and exhibit high variance. A wildly large positive coefficient on one

variable can be canceled by a similarly large negative coefficient on its correlated cousin. By imposing a size constraint on the coefficients, this problem is alleviated. The ridge solutions are not equivariant under scaling of the inputs, and so one normally standardizes the inputs before solving equation (4.15). In addition notice that the intercept β_0 has been left out of the penalty term. Penalization of the intercept would make the procedure depend on the origin chosen for Y ; that is, adding a constant c to each of the targets y_i would not simply result in a shift of the predictions by the same amount c. It can be shown that the solution to equation (4.15) can be separated into two parts, after reparametrization using centered inputs: each x_{ij} gets replaced by $x_{ij} - \overline{x}_j$. We estimate $\beta_0 by \bar{y} = \frac{1}{N}\sum_1^N y_i$. The remaining coefficients get estimated by a ridge regression without intercept, using the centered xij . Henceforth we assume that this centering has been done, so that the input matrix X has p (rather than $p+1$) columns.

Writing the criterion of equation (4.15) in matrix form, we have

$$RSS(\lambda) = (y - X\beta)T(y - X\beta) + \lambda\beta^T\beta, \tag{4.18}$$

and the ridge regression solutions are easily seen to be given by the following expression:

$$\hat{\beta}^{ridge} = (X^TX + \lambda I)^{-1}X^Ty, \tag{4.19}$$

where I is the $p \times p$ identity matrix. Notice that with the choice of quadratic penalty $\beta^T\beta$, the ridge regression solution is again a linear function of y. The solution adds a positive constant to the diagonal of X^TX before inversion. This makes the problem nonsingular, even if X^TX is not of full rank, and was the main motivation for ridge regression when it was first introduced in statistics [262]. In the case of orthonormal inputs, the ridge estimates are just a scaled version of the least squares estimates, that is, $\hat{\beta}^{ridge} = \hat{\beta}/(1+\lambda)$.

Ridge regression can also be derived as the mean or mode of a posterior distribution, with a suitably chosen prior distribution. In detail, suppose $y_i \sim N(\beta_0 + \mathbf{x}_i^T\beta, \sigma^2)$, and the parameters β_j are each distributed as $N(0, \tau^2)$, independently of one another. Then the (negative) log-posterior density of β, with τ^2 and σ^2 assumed

known, is equal to the expression in curly braces in eq. (4.15), with $\lambda = \sigma^2/\tau^2$. Thus the ridge estimate is the mode of the posterior distribution; since the distribution is Gaussian, it is also the posterior mean.

The singular value decomposition (SVD) of the centered input matrix X gives us some additional insight into the nature of ridge regression. This de- composition is extremely useful in the analysis of many statistical methods. The SVD of the $N \times p$ matrix X has the form

$$X = UDV^T. \tag{4.20}$$

Here U and V are $N \times p$ and $p \times p$ orthogonal matrices, with the columns of U spanning the column space of X, and the columns of V spanning the row space. D is a $p \times p$ diagonal matrix, with diagonal entries $d_1 \geq d_2 \geq ... \geq d_p \geq 0$ called the singular values of X. If one or more values $d_j = 0$, then X is singular. Using the singular value decomposition we can write the least squares fitted vector as

$$X\hat{\beta}_{ls} = X(X^TX)^{-1}X^Ty = UU^Ty, \tag{4.21}$$

after some simplification. Note that U^Ty are the coordinates of y with respect to the orthonormal basis U. Q and U are generally different orthogonal bases for the column space of X. Note that since $\lambda \geq 0$, we have $d_j^2/(d_j^2 + \lambda) \leq 1$. Like linear regression, ridge regression computes the coordinates of y with respect to the orthonormal basis U. It then shrinks these coordinates by the factors $d_j^2/(d_j^2 + \lambda)$. This means that a greater amount of shrinkage is applied to the coordinates of basis vectors with smaller d_j^2. The SVD of the centered matrix X is another way of expressing the principal components of the variables in X. The sample covariance matrix is given by $S = X^TX/N$, and from eq. (4.15) we have

$$X^TX = VD^2V^T, \tag{4.22}$$

which is the eigen decomposition of X^TX (and of S, up to a factor N). The eigenvectors v_j (columns of V) are also called the principal components of X. The first principal component direction v_1 has the property that $z_1 = X_{v_1}$ has the largest

sample variance amongst all normalized linear combinations of the columns of X. This sample variance is easily seen to be

$$Var(z_1) = Var(X_{v_1}) = \frac{d_1^2}{N}, \tag{4.23}$$

and in fact $z_1 = X_{v_1} = u_1 d_1$. The derived variable z_1 is called the first principal component of X, and hence u_1 is the normalized first principal component. Subsequent principal components z_j have maximum variance d_j^2/N, subject to being orthogonal to the earlier ones. Conversely the last principal component has minimum variance. Hence the small singular val- ues dj correspond to directions in the column space of X having small variance, and ridge regression shrinks these directions the most. If we consider fitting a linear surface over this domain (the Y -axis is sticking out of the page), the configuration of the data allow us to determine its gradient more accurately in the long direction than the short. Ridge regression protects against the potentially high variance of gradients estimated in the short directions. The implicit assumption is that the response will tend to vary most in the directions of high variance of the inputs. This is often a reasonable assumption, since predictors are often chosen for study because they vary with the response variable, but need not hold in general.

The following monotone decreasing function of λ is the effective degrees of freedom of the ridge regression fit.

$$df(\lambda) = tr\left[X(X^T X + \lambda I)^{-1} X^T\right] = tr(H_\lambda) = \sum_{j=1}^{p} \frac{d2j}{2j + \lambda}. \tag{4.24}$$

Usually in a linear-regression fit with p variables, the degrees-of-freedom of the fit is p, the number of free parameters. The idea is that although all p coefficients in a ridge fit will be non-zero, they are fit in a restricted fashion controlled by λ. Note that $df(\lambda) = p$ when $\lambda = 0$ (no regularization) and $df(\lambda) \to 0$ as $\lambda \to \infty$. Of course there is always an additional one degree of freedom for the intercept, which was removed apriori.

4.2.8 Bayesian Ridge Classifier (BRC)

Bayesian Ridge Classifier (BRC) [263] performs the ridge regression in a Bayesian framework modeling the priors of the coefficients as a spherical Gaussian distribution whose parameters follow prior Gamma distributions. Model fit and hyper-parameter estimation is carried out concurrently allowing for better adaptability to the data at hand. Bayesian regression allows a natural mechanism to survive insufficient data or poorly distributed data by formulating linear regression using probability distributors rather than point estimates. The output or response y is assumed to drawn from a probability distribution rather than estimated as a single value. Mathematically, to obtain a fully probabilistic model the response y is assumed to be Gaussian distributed around X_w as follows:

$$p(y\,|X, w, \alpha\,) = N(y\,|X_w, \alpha\,) \tag{4.25}$$

.

One of the most useful type of Bayesian regression is Bayesian Ridge regression which estimates a probabilistic model of the regression problem. Here the prior for the coefficient w is given by spherical Gaussian as follows:

$$p\,(w\,|\lambda\,) = N\left(w\,\middle|0, \lambda^{-1}Ip\right). \tag{4.26}$$

4.2.9 Multi-layer Perceptron (MLP)

Multi-Layer Perceptron (MLP) [264] implements the classical artificial neural network architecture with sigmoid activation functions in the hidden and output layers trained by backpropagation of the error at the output layer. We apply both the adam and the L-BFGS solvers. We explore MLP architectures with 5 and 10 hidden layers in order to assess the impact of different hierarchical representational depths.

Historically, MLP were motivated by the functionality of the human brain. Indeed, the first neural network was devised by McCulloch and Pitts [265] in an attempt to model a biological neuron. A McCulloch and Pitts neuron is a function

of the form

$$x \notin \mathbb{R}^d \mapsto 1_{\mathbb{R}^+} \sum_{i=1}^{d} w_i x_i - \theta, \tag{4.27}$$

where $d \in N$, $1_{\mathbb{R}^+} : \mathbb{R} \longrightarrow \mathbb{R}$, with $1_{\mathbb{R}} + (x) = 0$ for $x < 0$ and $1_{\mathbb{R}^+}(x) = 1$ elsewhere, and $w_i, \theta \in \mathbb{R}$ for $i = 1, ...d$. The function $1_{\mathbb{R}^+}$ is a so called activation function θ, is called a *threshold*, and w_i are *weights*. The McCulloch and Pitts neuron, receives d input signals. If their combined weighted strength exceeds the threshold then the neuron fires. Otherwise the neuron remains inactive. A network of neurons can be constructed by linking multiple neurons together in the sense that the output of one neuron forms an input to another. A simple model for such a network is the multilayer perceptron as introduced by Rosenblatt [266].

A multilayer perceptron (MLP) with d-dimensional input, L layers, and activation function

$$isafunction$$

F$thatcanbewrittenasx \mapsto F(x) := T_L(\varrho(4.28))$ where $T_\ell(x) = A_{\ell x} + b_\ell$, and $(A_\ell)_{\ell=1}^{L} \in \mathbb{R}^{N\ell}$, for $N_\ell \in \mathbb{N}$, $N_0 = d$ and $\ell = 1, ..., L$. Here$\varrho : \mathbb{R} \to \mathbb{R}$ is applied coordinate-wise.

The neurons in the MLP correspond again, to the applications of

$$even though, in contrast to the McCulloch and Pitts neuron, the MLP allows arbitrary$$

ϱ. We should notice that the MLP does not allow arbitrary connections between neurons, but only between those, that are in adjacent layers, and only from lower layers to higher layers. While the MLP or variations thereof, are probably the most widely used type of neural network in practice, they are very different from their biological motivation. Connections only between layers and arbitrary activation functions make for an efficient numerical scheme but are not a good representation of the biological reality.

4.3 Feature extraction/selection

We have considered several dimensional reduction procedures which are either feature extraction or feature selection techniques. Feature extraction usually involve

some transformation of the feature space where the meaning of the original variables is lost unless there is some backprojection transformation. Feature selection preserves some of the original variables discarding others. As feature extraction techniques we have applied the following ones available in the scikit-learn Python package:

4.3.1 Probabilistic Principal Component Analysis (PCA)

Probabilistic Principal Component Analysis (PCA) [267] is a probabilistic approach to the estimation of the eigendecomposition of the feature vectors covariance matrix instead of the conventional singular value decomposition (SVD) approach. A maximum likelihood approach is followed for this estimation under the assumption of a Gaussian multivariate model.

Principal component analysis (PCA) [268] is a well-established technique for dimensionality reduction, and a chapter on the subject may be found in numerous texts on multivariate analysis. Examples of its many applications include data compression, image processing, visualisation, exploratory data analysis, pattern recognition and time series prediction.

The most common derivation of PCA is in terms of a standardised linear projection which maximises the variance in the projected space [269, 270]. For a set of observed d-dimensional data vectors $\{t_n\}$, $n \in \{1...N\}$ the q principal axes w_j, $j \in \{1...N\}$, are those orthonormal axes onto which the retained variance under projection is maximal. It can be shown that the vectors w_j are given by the q dominant eigenvectors of the sample covariance matrix $S = \sum_n (t_n - \bar{t})(t_n - \bar{t})^T/N$, where $\bar{t}$ is the data sample mean, such that $Sw_j = \lambda w_j$. The q principal components of the observed vector t_n are given by the vector $x_n = W^T(t_n - t)$, where $W = (w_1, w_2, ..., w_q)$. The variables x_j are then uncorrellated such that the covariance matrix $\sum x_n x_n^T/N$ is diagonal with elements λ_j.

A complementary property of PCA, and that most closely related to the original discussions of [271] is that, of all orthogonal linear projections $x_0 = W^T(t_0 - \bar{t})$, the principal component projection minimises the squared reconstruction error $\sum_n \left\| t_n - \hat{t}_n \right\|^2$, where the optimal linear reconstruction of tn is given by $t_n = Wx_n + \bar{t}$

.

4.3.2 Isometric Mapping (Isomap)

Isometric Mapping (Isomap) [272] looks for a low dimension embedding of the feature space which preserves the geodesic distances among the data samples. It involves the search for the nearest neighbors, the shortest-path search between samples, and the computation of the partial eigendecomposition.

Assume a cloud of high dimensional data points$\{x_1, x_2, ..., x_N\}, x_i \in R^M$ that lie on a smooth K-dimensional manifold. In most cases of practical interest K is much smaller than the data dimension $M(K \ll M)$. Isomap builds upon MDS but attempts to compute the low-dimensional representation by estimating pairwise geodesic distances. For sufficiently close pairs, referred to as neighboring points, the euclidean distance provides a good approximation of geodesic distance [273], [274]. For faraway points, one needs to walk through these neighboring pairs in the shortest way possible to evaluate the geodesic distance. That can be achieve defficiently by applying a shortest path algorithm on a graph comprising edges that connect neighboring points. Here we introduce notations for these concepts. The graph is denoted as $G = (V, E)$ in which $V = \{x_1, x_2, ..., x_N\}$ denotes the set of nodes, and E is the set of edges connecting neighboring samples. There are two ways of determining the neighbors of a point are K-nearest neighbors [275], or all points within a fixed range ϵ. For neighboring nodes x_i and x_j, the weight is taken to be $w_{i,j} = ||x_i - x_j||^2$. If we take $x_i x_j$ to be the shortest route between x_i and x_j, we could compute geodesic distances as $d^G(x_i, x_j) = w(x_i \rightsquigarrow x_j)$ in which $w(.)$ denotes weight of the path. Finally, we seek a set of low-dimensional point denoted by $\{y_1, y_2, ..., y_N\}$ in R^K t hat preserves pair wise geodesic distances [276].

4.3.3 Local Linear Embedding (LLE)

Local Linear Embedding (LLE) is manifold learning approach that can be assimilated to a sequence of PCA transformations, which try to benefit from and enhance the local linear structure of the data [277].

The high-dimensional coordinates of each patch can be mapped into corresponding local co-ordinates by means of an essentially linear tmation. LLE attempts to find a global transformation of the high-dimensional coordinates into low dimensional ones by exploiting adjacencyinformation about closely located data points, this information being aform of summarisation of the local transformations between the high and low dimensional co-ordinates. Suppose that the data set comprises vectors $\{x_1, ..., x_N\} \in \mathbb{R}^D$. In the first step, for each $1 \leq i \leq N$, nearest neighbours of x_i are identified by using a preselected criterion for close proximity and further indexed by a set $N(i) \subset 1, ..., N$. In the second step, weights $w_{ij_j} \in N_{(i)}$ are found that optimally reconstruct x_i from ts nearest neighbours. These weights minimise the local reconstruction error

$$E_{loc}^{(i)}(\{w_{ij}\}_{j\in N(i)}) = \left\| xi - \sum_{j\in N(i)} w_{ij}x_j \right\|,^2 \tag{4.29}$$

where $\|\cdot\|$ is the Euclidean norm, subject to the condition $\sum_{j\in N(i)} w_{ij} = 1$.

A key property of the optimal weights is that they are invariant to three types of transformation:

1. Scaling. Multiplying all co-ordinates by a scalar factor scales the errors $E_{loc}^{(i)}$ uniformly and hence yields the same weights

2. Orthogonal transformation. Distances are invariant to rotation and mirror-reflection and so too is each $E_{loc}^{(i)}$

3. Translation. The weights are constrained to sum to one, so an offset to all co-ordinates does not affect the value of any $E_{loc}^{(i)}$

Suppose that the data points are sampled densely from the underlying low-dimensional manifold. Then, for each point x_i, there exists a linear map composed of a translation, rotation and scaling, that maps the high-dimensional coordinates of a close neighbourhood of x_i to corresponding local coordinates on the manifold. Since the weights computed in the high dimensional space are invariant to the three constituent mappings, it is natural to take these weights as a basis for there construction

of the local co-ordinates. In fact, all local neighbourhoods can be reconstructed simultaneously if a specific optimisation problem is solved. The cost function for this problem measures how well low dimensional coordinates of any given point $yi \in \mathbb{R}^d$ are reconstructed from the neighbouring points $y_{j\,j\in N(i)}$ using the weights computed in the previous step; here d is a dimension index fixed beforehand, usually at a value much smaller than D. More specifically, in the third step, LLE minimises the reconstruction error. This optimisation is similar to that in the first step, except that now the weights are fixed and the low dimensional coordinates are sought. To obtain an essentially unique solution, the y_i are constrained to have zero mean and an identity covariance matrix [278].

4.3.4 Multi-Dimensional Scaling (MDS)

Multi-Dimensional Scaling (MDS) [279] looks for a dimensional reduction of the feature space such that the relative ordering of the distances between samples in the original space are preserved in the reduced dimension space.

Proximity data, the input to MDS, consist of dissimilarity information for pairs of objects. This contrasts with multivariate data that consist of attribute information forindividualobjects. If the objects are labeled $i = 1, ..., N$, we will assume that proximity data are given by dissimilarity values $D_{i,j}$. (If the data are given as similarities, a monotone decreasingtransformation will convert them to dissimilarities.) The goal of MDS is to map the objects $i = 1, ..., N$ to "configuration" or "embedding" points $\{x_1, ..., x_N\} \in \mathbb{R}^k$in such a way that the given dissimilarities $D_{i,j}$ are well approximated by the distances $\|x_i - x_j\|$. The choice ofembedding dimension k is arbitrary in principle, but low in practice: $k = 1, 2, 3$ are the most frequently used dimensions, for the simple reason that the points serve as easily visualized representors of the objects. In realdata, there are typically many more objects, and the dissimilarities usually contain error as well as bias with regard to the fitted distances.

The oldest version of MDS, called classical scaling, is due to Torgerson (1952). It is, however, a later version due to [280, 281] that has become the leading MDS method. Kruskal defined MDS in terms of minimization of a loss function called

"Stress", which issimply a measure of lack of fit between dissimilarities $D_{i,j}$ and fitted distances $\|x_i - x_j\|$. In the simplest case, Stress is a residual sum of squares

$$Stress_D(x_1, ..., x_N) = (\sum_{i \neq j = 1..N} (D_{i,j} - \|x_i - x_j\|)^2)^{1/2}, \tag{4.30}$$

where the outer square root is just a convenience that gives greater spread to small values. For a given dissimilarity matrix $D = (D_{i,j})$, MDS minimizes Stress over all configurations $(x_1, ..., x_N)^T$, thought of as $N \times k$-dimensional hypervectors of unknown parameters. The minimization can be carried out by straightforward gradient descent applied to $Stress_D$, viewed as a function on $\mathbb{R}^{Nk}$.

We note that MDS is blind to asymmetries in the dissimilarity data because

$$(D_{i,j} - \|x_i - x_j\|)^2 + (D_{j,i} - \|x_j - x_i\|)^2 = 2 \cdot ((D_{i,j} + D_{j,i})/2 - \|x_i - x_j\|)^2 + C, \tag{4.31}$$

where C is an expression that does not depend on $\|x_i - x_j\|$. We therefore assume from now on that the dissimilarities are symmetrized. The assumption of symmetry will later be brokening one special case, when one of the two values is permitted to be missing.

There exist several types of MDS, and they differ mostly in the loss function they use. Here are two dichotomies that allow us to structure some possibilities:

- Kruskal-Shepard distance scaling versus classical Torgerson-Gower inner-product scaling: In distance scaling dissimilarities are fitted by distances $\|x_i - x_j\|$, where as classical scaling transforms the dissimilarities D_{ij} to aform that is naturally fitted by inner products $\langle x_i, x_j \rangle$. The transformation of dissimilarity data D_{ij} to "inner-product data B_{ij} satisfies $D_{ij}^2 = B_{ii} - 2B_{ij} + B_{jj}$, there by mimicking the corresponding identities for $\|x_i - x_j\|$ and $\langle x_i, x_j \rangle$

- Metric scaling versus non metric scaling: Metric scaling uses the actual values of the dissimilarities, while non metric scaling effectively uses only their ranks [280, 282]. Nonmetric MDS is realized by estimating an optimal monotone transformation $f(D_{i,j})$ of the dissimilarities simultaneously with the configuration

A difference between classical and distance scaling is that inner products rely on an origin in the coordinate system, while distances do not; a set of inner products determines uniquely a set of distances, but a set of distances determines a set of inner products only modulo change of origin. To avoid arbitrariness, one constrains classical scaling to mean-centered configurations. Another difference between classical and distance scaling is that distance scaling requires iterative minimization while classical scaling can be solved with inexpensive eigendecompositions. Just the same, we implemented classical scaling with iterative gradient descent on a loss function called “Strain”, which parallels gradient descent on Stress in distance scaling. This computational uniformity has advantages because it is straightforward to introduceweights and missing values in Strain and Stress, which is not possible in eigen decompositions [283].

4.3.5 Factor Analyisis (FA)

Factor Analysis (FA) [284, 285] tries to explain the observed variables as a linear model of unseen latent variables. The conventional approach assumes a Gaussian prior for the distribution of the latent variables. Changing the prior distribution gives way to diverse algorithms

Factor analysis is a statistical method used to describe variability among observed, correlated variables in terms of apotentially lower number of unobserved variables called factors. The observed variables are modeled as linear combinations of the potential factors, plus "error" terms. The information gained about the interdependencies between observed variables can be used later to reduce the set of variables in a dataset. Computationally this technique is equivalent to low rank approximation of the matrix of observed variables. Factor analysis originated in psychometrics, and is used in behavioral sciences, social sciences, marketing, product management, operations research, and other applied sciences that deal with large quantities of data.

Suppose we have a set of observable random variables $\{x_1, ..., x_n\}$, with means $\{\mu_1, ..., \mu_n\}$. Suppose for some unknown constants l_{ij} and $k-$unobserved random

variables F_j, where $i \in, ..., p$ and $j \in, ..., k$, where $k < p$, that we have

$$x_i - \mu_i = l_{i1}F_1 + ... + l_{ik}F^k + \varepsilon_i. \tag{4.32}$$

Here, the ε_i are independently distributed error terms with zero mean and finite variance, which may not be the same for all i. Let $Var(\varepsilon_i) = \psi_i$, so that we have $cov(\varepsilon) = Diag(\psi_1, ..., \psi_p) = \psi$ and $E(\varepsilon) = 0$. In matrix expresion, we have $x - \mu = LF + \varepsilon$

If we have observations, then we will have the dimensions x_{pxn}, L_{pxk}, and F_{kxn}. Each column of x and F denote values for one particular observation, and matrix L does not vary across observations. Also we will impose the following assumptions on F.

1. F and ε are independent

2. $E(F) = 0$

3. $Cov(F) = I$ (to make sure that the factors are uncorrelated)

4. Any solution of the above set of equations following the constraints F for is defined as the factors, and L as the loading matrix.

Suppose $Cov(x - \mu) = \sum$. Then note that from the conditions just imposed on, either we have

$$Cov(x - \mu) = Cov(LF + \varepsilon)$$

or

$$\sum = LCov(F)L^T + Cov(\varepsilon)$$

or

$$\sum = LL^T + \psi$$

Note that for any orthogonal matrix Q if we set $L = LQ$ and $F = Q^T F$, the criteria for being factors and factor loadings still hold. Hence a set of factors and factor loadings is identical only up to orthogonal transformations.

4.4 Classification performance evaluation

In the computational experiments reported in Chapter 6, we carry out one hundred repetitions of the 10-fold cross-validation for each combination of experimental factors. Feature extraction/selection parameters are always computed only on the training dataset and applied in the test dataset to avoid double dipping issues [224, 225]. Most of the papers in the literature report the accuracy (Acc) of the classification results averaged after the repetition of 10-fold cross-validation experiments. Accuracy is computed as

$$A_{cc} = (TP + TN)/N$$

where N is the number of test samples, and TP and TN are the number of correct positive and negative predictions on the test set, respectively. Some papers on ASC prediction based on brain connectivity [176] report the area under the receiver operating curve (ROC) (AUC) [286] as a more general and robust measure of the classifier performance. The accuracy is determined by the actual decision threshold applied to classify the test samples, while the ROC plots the balance of false positives (FP) versus TP across the entire range of decision threshold values. Following the lead of [176] we report in Chapter 6 the median, 5% and 95% percentile values of the cross-validation repetitions results instead of the average value as a better description of their distribution. We plot the densities of the median AUC results across the repetitions of cross-validation experiments in order to visualize their distribution for different pipeline choices. The plots use the density() function in R that generates smooth curves that are not always bounded in the interval $[0, 1]$. To provide a quantitative ranking of the choices, we carry out one sided non-parametric Wilcoxon's rank sum tests among all pairwise combinations of choices for each pipeline module. For each test we consider the results of all cross-validation repetitions with all possible choice combinations for the remaining pipeline modules. We present the p-values of these tests in tables organized as follows: for each table entry the null hypothesis is that the median AUC of the row choice is greater than that of the column choice. We specify (row>column) at each table caption as a

reminder to the reader.

Chapter 5

Deep Learning Background

This Chapter provides some background information about Deep Learning (DL) architecture and approaches applied to our problem of computer aided diagnostic of ASC. Section 5.1 gives some introductory remarks. Section 5.6 discusses the ideas of transfer learning. Section 5.6 presents the architectures used for transfer learning

5.1 Introduction

Allowing computers to model our world well enough to exhibit what we call intelligence has been the focus of more than half a century of research [287], [288]. Since 2006, deep structured learning, or more commonly called DL or hierarchical learning, has emerged as a new area of machine learning research [289], [288]. DL is a branch of machine learning which is based on artificial neural networks. It is referred as DL in contrast with shallow ANNs. The deep ANNs (DNNs) have more layers than ever before that enable learning hierarchical structures in different granularity and a greater amount of composition of learned functions or learned concepts than conventional machine learning algorithms [290], [291]. It is a type of representation learning that discovers a hierarchy of structures in the data. Trained with large amount of data, DL shows outstanding performance with enormous model capacity, and performs well on diverse structured and unstructured, and even interconnected data sets [292].

One of the objectives of neuroimaging research is to find biomarkers that may

assist the diagnosis of brain disorders and/or help treat these disorders [292]. Using DL algorithms to investigate neurological malfunctions has the advantage of alleviating feature engineering, and an ever-increasing number of neuroimaging studies are turning to DL enabled methods in order to demystify these neurological disorders [293], [294], [295], [199], [296], [297], [298]. DL methods are penetrating clinical practice and reshaping medical imaging research community, and research articles involving DL are accumulating at a fast pace. In this Thesis, we do not attempt an exhaustive review on DL, but mainly focus on fMRI images based brain disorder diagnosis and show the landscape of the active research initiatives. There are many different approaches to analyze fMRI images from different perspectives. Features can be extracted from fMRI images to perform disorder classifications. Different feature extraction methods and data analysis tools can result in different DL models [292].

5.2 Traditional Machine learning, Transfer learning and Fine tunning

Traditional machine learning techniques are based on the model of isolated, single task learning wherein knowledge from a past task is not leveraged for other tasks; however, many machine learning methods work well only under a common assumption: the training and test data are drawn from the same feature space and the same distribution [299]. No knowledge is retained which can be transferred from one paradigm to another [300]. When the distribution changes, most statistical models need to be rebuilt from scratch using newly collected training data. In many real world applications, it is expensive or impossible to re-collect the needed training data and rebuild the models [299].

Transfer learning or Domain Adaptation, related to the difference in the distribution of the train and test set. The need for transfer learning may arise when the data can be frequently outdated. In this case, the labeled data obtained inone time period may not follow the same distribution in a later time period [299]. This can be understood the same as a projecting all new inputs through a pre-trained

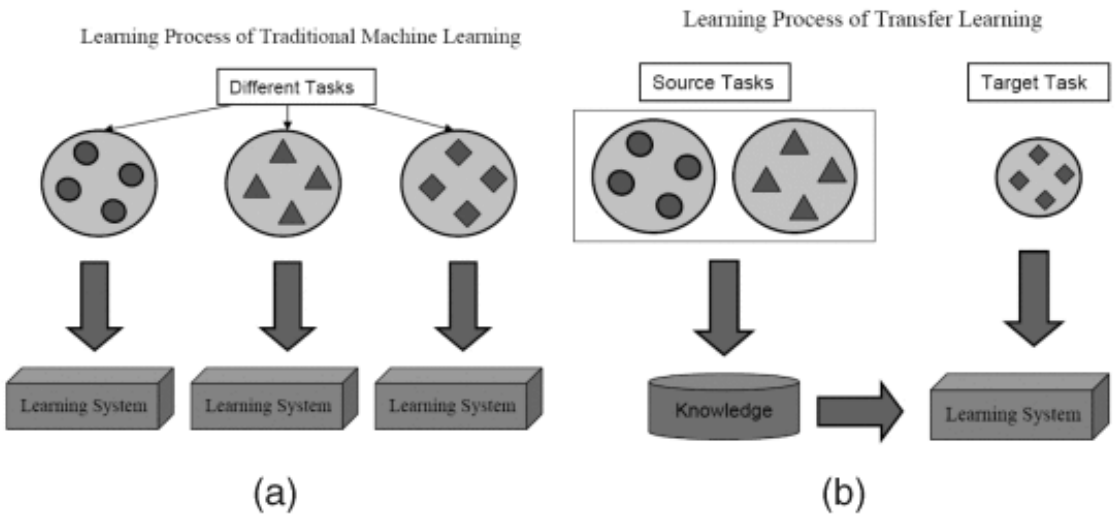

Figure 5.1: Different learning processes (a) traditional machine learning, and (b) transfer learning.

model. Like if we have a pre-trained model function $f()$ and wish to learn a new function $g()$, we can simplify $g()$ by $g(f(x))$. This way $g()$ sees all the data through $f()$. Figure 5.1 shows the difference between the learning processes of traditional and transfer learning techniques. As we can see, traditional machine learning techniques try to learn each task from scratch, while transfer learning techniques try to transfer the knowledge from some previous tasks to a target task when the latter has fewer high-quality training data. Transfer learning can be further segregated into transductive and inductive [299]. It is further divided into domain adaption, cross-lingual learning, multi-task learning and sequential transfer learning. Figure 5.2 ilustrates this taxonomy.

Fine-tuning means making small adjustments to a process to achieve the desired output or performance. Fine-tuning DL involves using weights of a previous DL algorithm for programming another similar DL process. Weights are used to connect each neuron in one layer to every neuron in the next layer in the neural network. The fine-tuning process significantly decreases the time required for programming and processing a new DL algorithm as it already contains vital information from a pre-existing DL algorithm. Fine tuning consists of the following four steps (ilustrated in figure 5.1.):

1. Pre-train a neural network model;

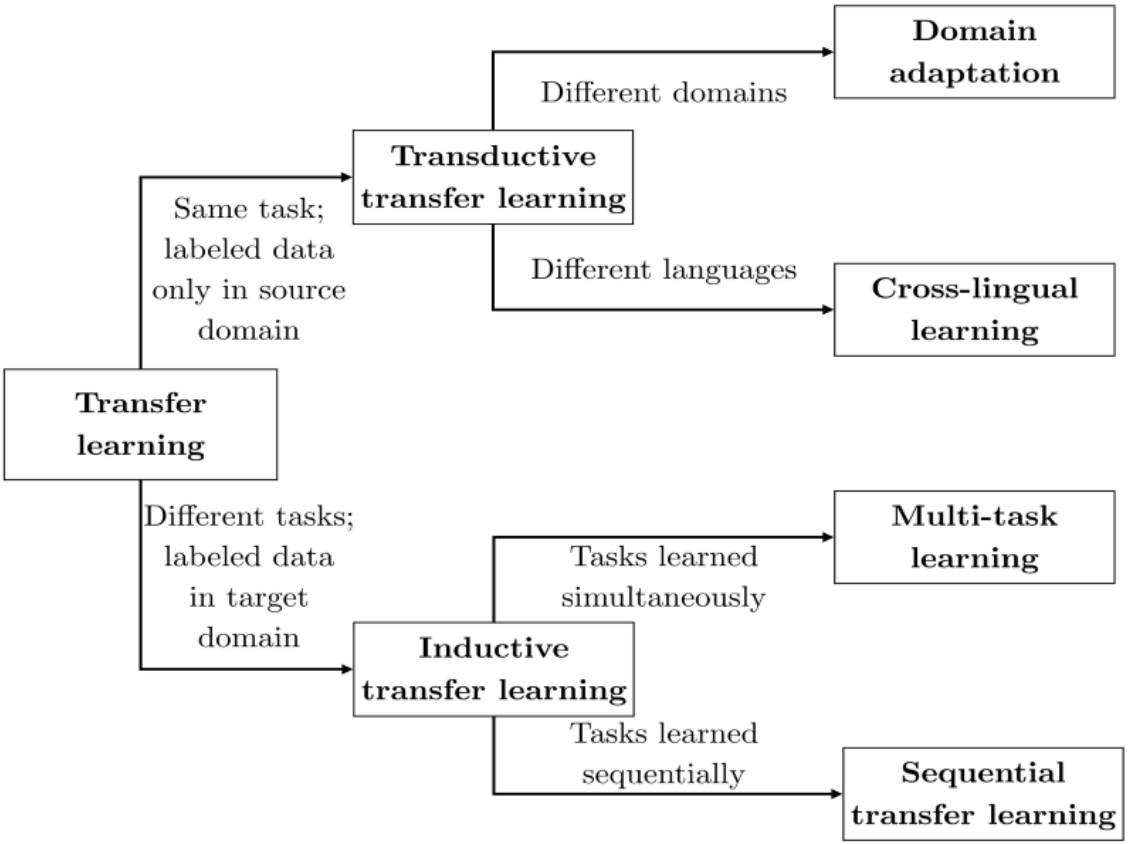

Figure 5.2: Types of transfer learning [6]

Algorithm 5.1 Fine tuning process in transfer learning.

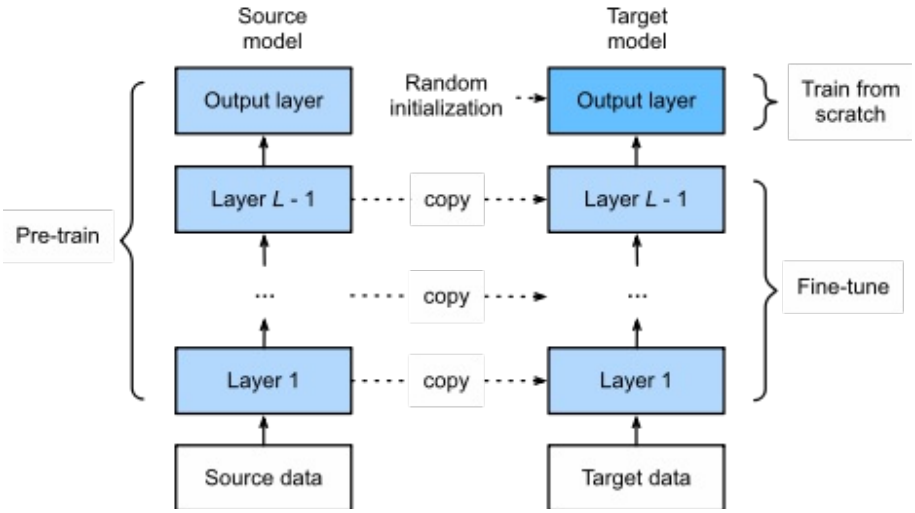

2. Create a new neural network model (We assume that these model parameters contain the knowledge learned from the source dataset and this knowledge will be equally applicable to the target dataset);

3. Add an output layer whose output size is the number of target dataset categories to the target model, and randomly initialize the model parameters of this layer and the last

4. Train the target model on a target dataset, such as a chair dataset.

5.3 Architectures used

5.3.1 VGG16 and VGG19

In 2014 the Visual Geometry Group from Oxford University as second in the ILSVRC challenge for classification using a very deep but simple convolutional neural network architecture that has come to be known as VGG [301]. VGG is used as a pre-processing model. Compared with traditional convolutional neural networks, it has been improved in network depth. It uses an alternating structure of multiple convolutional layers and non-linear activation layers, which is better than a single convolution The layer structure can better extract image features, use Maxpooling for downsampling, and modify the linear unit (ReLU) as the activation function,

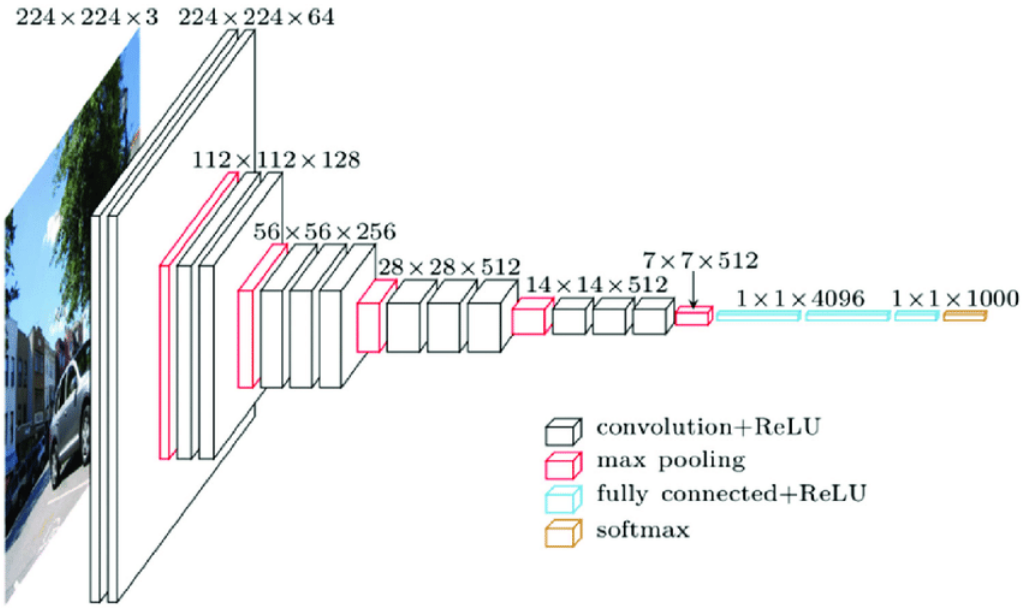

Figure 5.3: An overview of the VGG-16 model architecture, this model uses simple convolutional blocks to transform the input image to a 1000class vector representing the classes of the ILSVRC.

that is, select the largest value in the image area as the pooled value of the area. The down sampling layer is mainly used to improve the anti-distortion ability of the network to the image, while retaining the main features of the sample and reducing the number of parameters [7]. This model has become very popular inthe research community due to its simple approach and becausethe pre-trained weights were made freely available online, facilitating thefine-tuning of this powerful model on new tasks [302]. Several of the papers reviewed make use of this model, and so its network architecture is provided in Figure 5.3.

The structure of the VGG network shown in Figure 5.3 is explained [302] as follows:

- The first and second convolutional layers are comprised of 64 feature kernel filters and size of the filter is 3×3. As input image (RGB image with depth 3) passed into first and second convolutional layer, dimensions changes to 224x224x64. Then the resulting output is passed to max pooling layer with a stride of 2.

- The third and fourth convolutional layers are of 124 feature kernel filters and size of filter is 3×3. These two layers are followed by a max pooling layer with

stride 2 and the resulting output will be reduced to 56x56x128.

- The fifth, sixth and seventh layers are convolutional layers with kernel size 3×3. All three use 256 feature maps. These layers are followed by a max pooling layer with stride 2.

- Eighth to thirteen are two sets of convolutional layers with kernel size 3×3. All these sets of convolutional layers have 512 kernel filters. These layers are followed by max pooling layer with stride of 1.

- Fourteen and fifteen layers are fully connected hidden layers of 4096 units followed by a softmax output layer (Sixteenth layer) of 1000 units.

In another work [7] found training VGG16 and VGG19 challenging (specifically regarding convergence on the deeper networks), so in order to make training easier, they first trained smaller versions of VGG with less weight layers (columns A and C) first. They experiment with 6 models, with different numbers of trainable layers. Based on the number of models the two most popular models are VGG16 and VGG19. The specifics of the architectures are in Figure 5.2.

5.3.2 Resnet

In 2012, [303] rolled out the red carpet for the Deep Convolutional Neural Network. This was the first time this architecture was more successful that traditional, hand-crafted feature learning on the ImageNet. Their DCNN, named AlexNet, contained 8 neural network layers, 5 convolutional and 3 fully-connected. This laid the foundational for the traditional CNN, a convolutional layer followed by an activation function followed by a max pooling operation [304]. Deep networks naturally integrate low/mid/high-level features [305] and classifiers in an end-to-end multi-layer fashion, and the "levels" of features can be enrichedby the number of stacked layers (depth). When deeper networks are able to start converging, a degradation problem has been exposed: with the network depth increasing, accuracy gets saturated (which might beunsurprising) and then degrades rapidly [306]. Unexpectedly, such degradation is not caused by overfitting, and adding more layers to a suitably deep

ConvNet Configuration					
A	A-LRN	B	C	D	E
11 weight layers	11 weight layers	13 weight layers	16 weight layers	16 weight layers	19 weight layers
input (224 × 224 RGB image)					
conv3-64	conv3-64 **LRN**	conv3-64 **conv3-64**	conv3-64 conv3-64	conv3-64 conv3-64	conv3-64 conv3-64
maxpool					
conv3-128	conv3-128	conv3-128 **conv3-128**	conv3-128 conv3-128	conv3-128 conv3-128	conv3-128 conv3-128
maxpool					
conv3-256 conv3-256	conv3-256 conv3-256	conv3-256 conv3-256	conv3-256 conv3-256 **conv1-256**	conv3-256 conv3-256 **conv3-256**	conv3-256 conv3-256 conv3-256 **conv3-256**
maxpool					
conv3-512 conv3-512	conv3-512 conv3-512	conv3-512 conv3-512	conv3-512 conv3-512 **conv1-512**	conv3-512 conv3-512 **conv3-512**	conv3-512 conv3-512 conv3-512 **conv3-512**
maxpool					
conv3-512 conv3-512	conv3-512 conv3-512	conv3-512 conv3-512	conv3-512 conv3-512 **conv1-512**	conv3-512 conv3-512 **conv3-512**	conv3-512 conv3-512 conv3-512 **conv3-512**
maxpool					
FC-4096					
FC-4096					
FC-1000					
soft-max					

Figure 5.4: Different ConvNet Architectures [7].

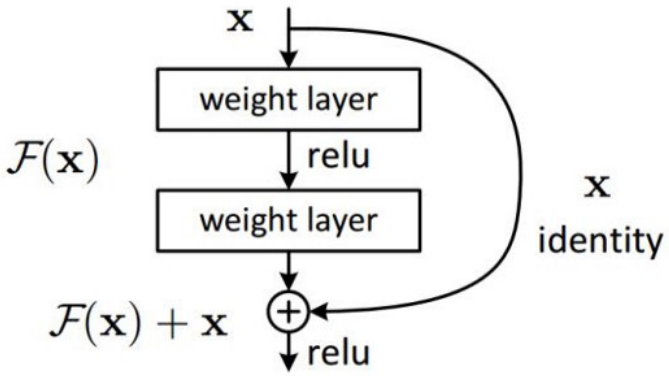

Figure 5.5: Residual learning a building block

model leads to higher training error [307], [308]. This problem of training very deep networks has been alleviated with the introduction of ResNet or residual networks and these Resnets are made up from Residual Blocks, such as the one illustrated in Figure 5.6.

The very first thing we notice to be different is that there is a direct connection which skips some layers (may vary in different models) in between. This "skip connection" is the core of residual blocks. Due to this skip connection, the output of the layer is not the same now. Without using this skip connection, the input x gets multiplied by the weights of the layer followed by adding a bias term. Next, this term goes through the activation function, $F()$ and we get our output as $H(x)$. i.e. $H(x)$=$f(wx + b)$ or $H(x) = F(x)$. Now with the introduction of skip connection, the output is changed to $H(x) = F(x) + x$

There appears to be a slight problem with this approach when the dimensions of the input vary from that of the output which can happen with convolutional and pooling layers. In this case, when dimensions of $F(x)$ are different from x, we can take the following approach: The skip connection is padded with extra zero entries to increase its dimensions. The projection method is used to match the dimension which is done by adding 1×1 convolutional layers to input. In such a case, the output is: $H(x) = F(x) + w_1x$. Here we add an additional parameter w_1 whereas no additional parameter is added when using the first approach.

ResNet network uses a 34-layer plain network architecture inspired by VGG-19

in which then the shortcut connection is added. The skip connections in ResNet solve the problem of vanishing gradient in deep neural networks by allowing this alternate shortcut path for the gradient to flow through. The other way that these connections help is by allowing the model to learn the identity functions which ensures that the higher layer will perform at least as good as the lower layer, and not worse [304]. These shortcut connections then convert the architecture into the residual network as shown in the figure 5.6.

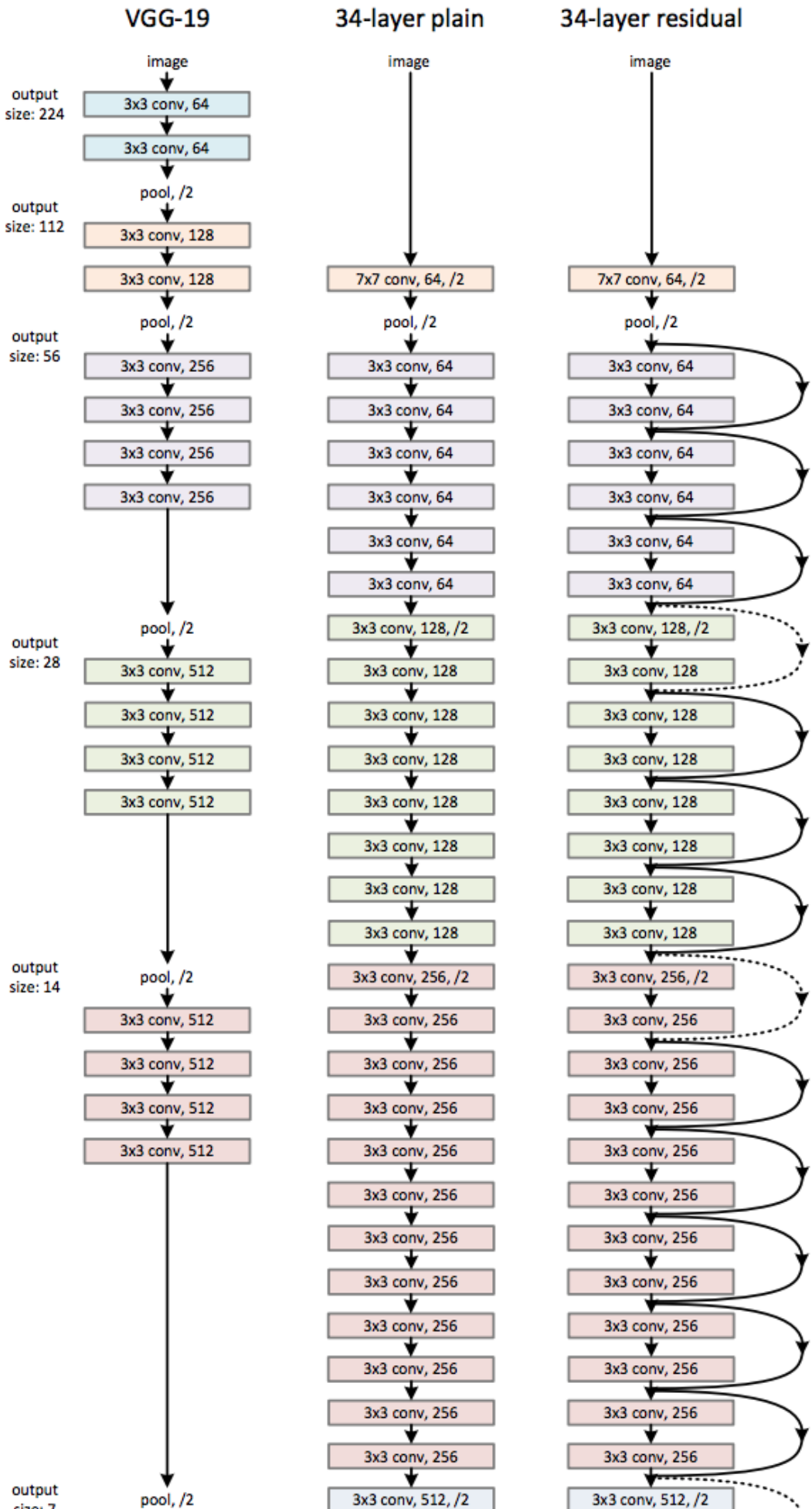
VGG-19
34-layer plain
34-layer residual
image
output size: 224
3x3 conv, 64
3x3 conv, 64
pool, /2
output size: 112
3x3 conv, 128
3x3 conv, 128
pool, /2
output size: 56
3x3 conv, 256
3x3 conv, 256
3x3 conv, 256
3x3 conv, 256
pool, /2
output size: 28
3x3 conv, 512
3x3 conv, 512
3x3 conv, 512
3x3 conv, 512
pool, /2
output size: 14
3x3 conv, 512
3x3 conv, 512
3x3 conv, 512
3x3 conv, 512
pool, /2
output
7x7 conv, 64, /2
pool, /2
3x3 conv, 64
3x3 conv, 128, /2
3x3 conv, 128
3x3 conv, 256, /2
3x3 conv, 256
3x3 conv, 512, /2

Chapter 6

Results of Machine Learning Approaches

In this Chapter we provide experimental results of a large combination of choices in the design of the computational pipeline introduced in Figure 1.1. Section 6.1 describes the experimental dataset extracted from the ABIDE repository. Section 6.2 provides some general remarks on the experimental results. Section 6.3 examines the effect of the brain parcelation. Section 6.3 discusses the effect of the connectivity matrix definition. Section 6.5 presents the effect of the classification model chosen. Section 6.6 shows the effect of the choice of the feature selection method. Section 6.7 summarizes the best results of the experimental work. Finally, the best results are compared with the state of the art of Table 3.2.

6.1 The experimental dataset

In this section we will first introduce the dataset used, then we comment on the brain parcellations and functional connectivity measures considered. The next subsections describes the classifier building methods employed, and the feature extraction and feature selection methods examined. Finally, we comment on the performance measures selected to report results.

The dataset analyzed in the study is extracted from the Autism Brain Imaging Data Exchange (ABIDE) [22, 23] that provides rsfMRI acquisitions of 1112 subjects

Table 6.1: Demographics distribution per site of the ABIDE I dataset. Test = the subject underwent DSM IV TR test. A = Autism, C = Control

				Male		Female		test		Male		Female	
Site	N	A	C	A	C	A	C	Y	N	A	C	A	C
CALTECH	38	19	19	15	15	4	4	37	1	15	14	4	4
CMU	27	14	13	11	10	3	3	5	22	3	1		1
KKI	55	22	33	18	24	4	9	39	16	9	20	3	7
LEUVEN1	29	14	15	14	15			29		14	15		
LEUVEN2	35	15	20	12	15	3	5	32	3	11	14	2	5
MAX_MUN	57	24	33	21	29	3	4	42	15	15	23	3	1
NYU	184	79	105	68	79	11	26	171	13	64	72	9	26
OHSU	28	13	15	13	15			23	5	12	11		
OLIN	36	20	16	17	14	3	2	25	11	11	9	3	2
PITT	57	30	27	26	23	4	4	45	12	18	20	4	3
SBL	30	15	15	15	15			26	4	14	12		
SDSU	36	14	22	13	16	1	6	33	3	12	15		6
STANFORD	40	20	20	16	16	4	4	36	4	13	15	4	4
TRINITY	49	24	25	24	25			44	5	21	23		
UCLA_1	82	49	33	42	29	7	4	55	27	26	23	2	4
UCLA_2	27	13	14	13	12		2	20	7	8	10		2
UM_1	110	55	55	46	38	9	17	82	28	28	31	8	15
UM_2	35	13	22	12	21	1	1	31	4	11	18	1	1
USM	101	58	43	58	43			61	40	38	23		
YALE	56	28	28	20	20	8	8	48	8	15	19	7	7
	1112	539	573	474	474	65	99	884	228	358	388	50	88

either diagnosed with ASC or TD. This dataset collects data from 10 sites as detailed in Table 6.1. We have excluded cases with diagnosis as Asperger or PDD-NOS according to the fourth Diagnostic and Statistical Manual of Mental Disorders (DSM IV TR). We have selected and processed the 884 subjects (ASC n=408,TD n=476) that underwent the DSM IV TR test for the computational experiments in this Thesis.

In order to have a fair comparison with the published literature, we have resorted to the pre-processed acquisitions which are available as part of the Pre-processed Connectome Project (`http://preprocessed-connectomes-project.org/abide/`) [309]. The raw rs-fMRI data has been processed using the Configurable Pipeline for the Analysis of Connectomes (C-PAC) (`http://fcp-indi.github.io/`) in order to obtain the corrected and spatially normalized rs-fMRI volumes. C-PAC applies skull striping, slice timing correction, motion correction, global mean intensity normalization, nuisance signal regression, band-pass filtering (0.01–0.1 Hz) and registration of fMRI images to standard anatomical MNI space.

6.2 General remarks on the results

Before proceeding with the detailed discussion of the effect of each pipeline module, we note an effect that is common to all of them: All the presented distribution density approximations of the median AUC have a big peak around the value 0.5, which is equivalent to random choice. This is a clear indication of the difficulty of the problem. Most pipeline combinations are poor performers and results are quite unstable in general, with big variations between crossvalidation repetitions. We think that this is the most salient empirical demonstration of the data heterogeneity and the need for careful design of large scale data collection efforts. Data heterogeneity is due to site differences on data capture devices and procedures, as well as implementation of diagnostic criteria. Another source of heterogeneity is the openess of the diagnostic criteria leading to the inclussion of subjects with widely diverse cognitive signatures. Clustering analysis [310] of data from a mentalizing task has revealed the existence of at least six well differentiated subgroups in a large

Table 6.2: One sided (row>column) Wilcoxon's rank sum test p-values between median AUC results achieved from the different parcellations used to extract representative time series for the connectivity matrices.

	AAL	CC200	D160	EZ	HO	TT	max AUC
AAL		2.06e-15	2.404e-68	1.632e-30	2.127e-31	1.340e-36	0.753
CC200	1		6.098e-30	4.169e-06	1.164e-05	2.089e-10	0.767
D160	1	1		1	1	1	0.669
EZ	1	1	4.032e-14		4.721e-01	2.372e-02	0.748
HO	1	1	8.746e-15	5.278e-01		2.602e-02	0.739
TT	1	1	1.032e-08	9.762e-01	9.739e-01		0.734

sample of ASC and controls. Finally, sex is a demonstrated source of heterogenity. Sex has bee proven to have a significant effect on the neurobiology of autism [11].

Figure 6.1 summarizes the impact of feature selection/extraction methods versus the classifiers. It can be easily appreciated that the effect of feature extraction is greater than that of the classifier of choice, specifically the factor analysis, PCA and correlation based selection are quite comparable feature computation methods. Figure 6.2 summarizes the impact of feature computation versus the brain parcelation applied to extract brain regions. Results show the greater effect of feature computation methods, with the same qualitative results as above. Figure 6.3 summarizes the impact of classifiers versus the chosen connectivity measure, the results for the tangent and correlation measures show the greatest variances. Other than that theclassifiers do not have a clear ranking, except for the lower performance of k-NN and random forest.

6.3 Effect of the brain parcellation

Figure 6.4 shows the density plots corresponding to the aggregation of the median AUC results per brain parcellation used. As expected, these distributions are not Gaussian shaped, some of them are markedly multimodal. In the case of AAL, the distribution is pretty close to an uniform distribution. Most parcellation distributions have a big peak at the 0.5 value of the median AUC with a low tail of values above 0.7. We use one sided Wilcoxon's rank sum test to assess quantitatively the improvement of results achieved with each parcellation. Table 6.2 shows the p-values

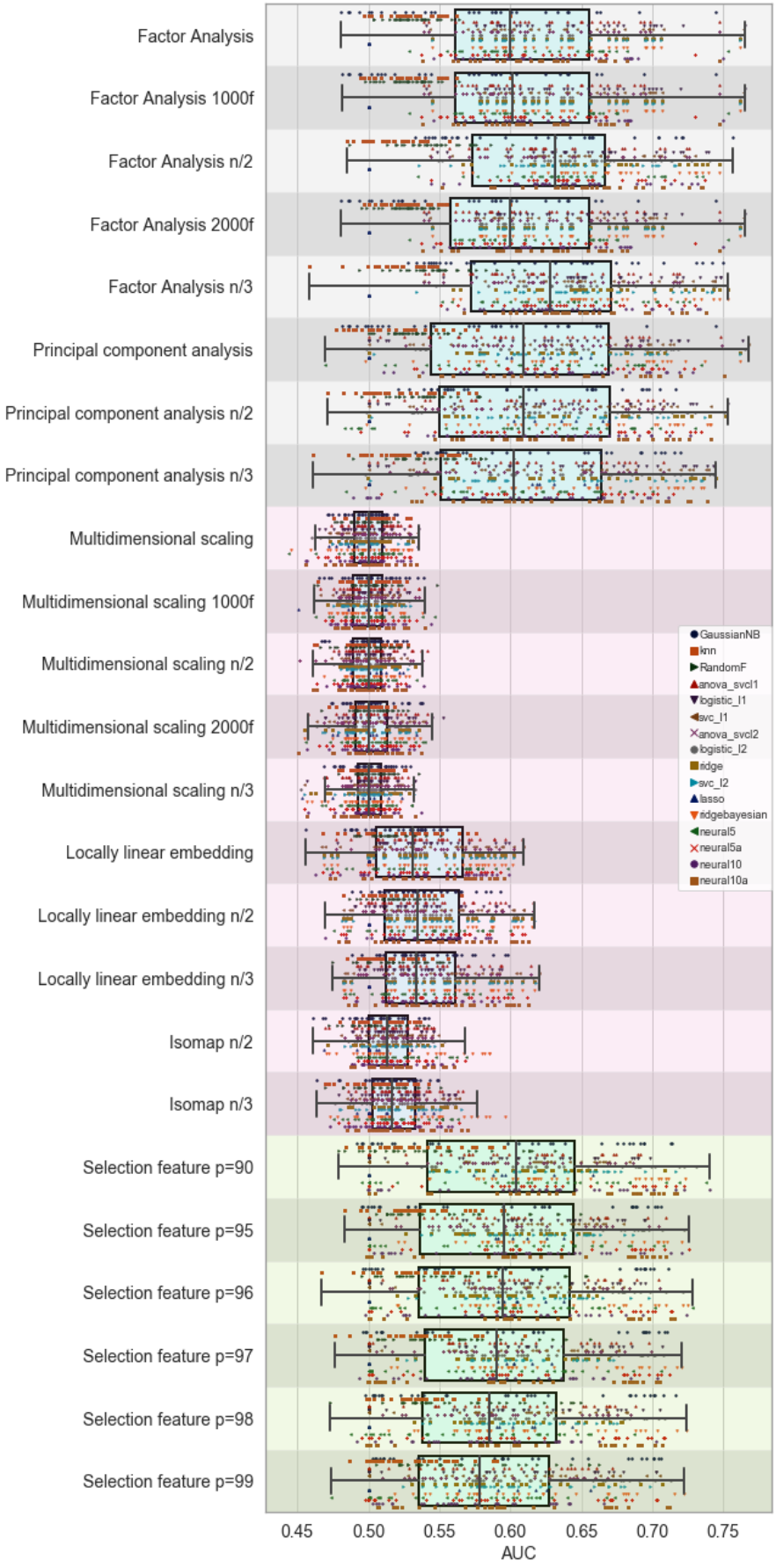

Figure 6.1: Impact of feature selection versus classifiers.

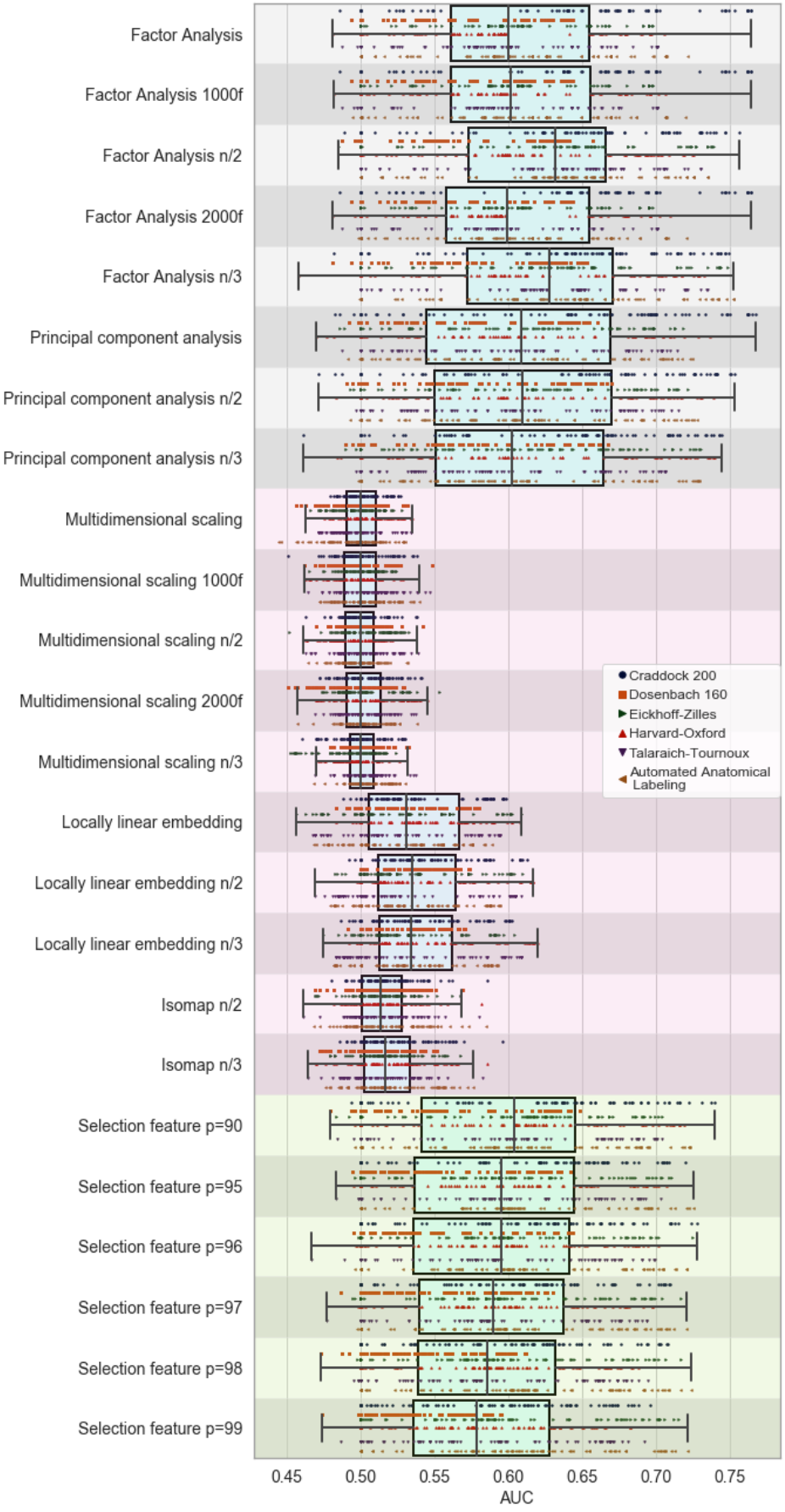

Figure 6.2: Impact of features versus the atlas parcelation of the brain

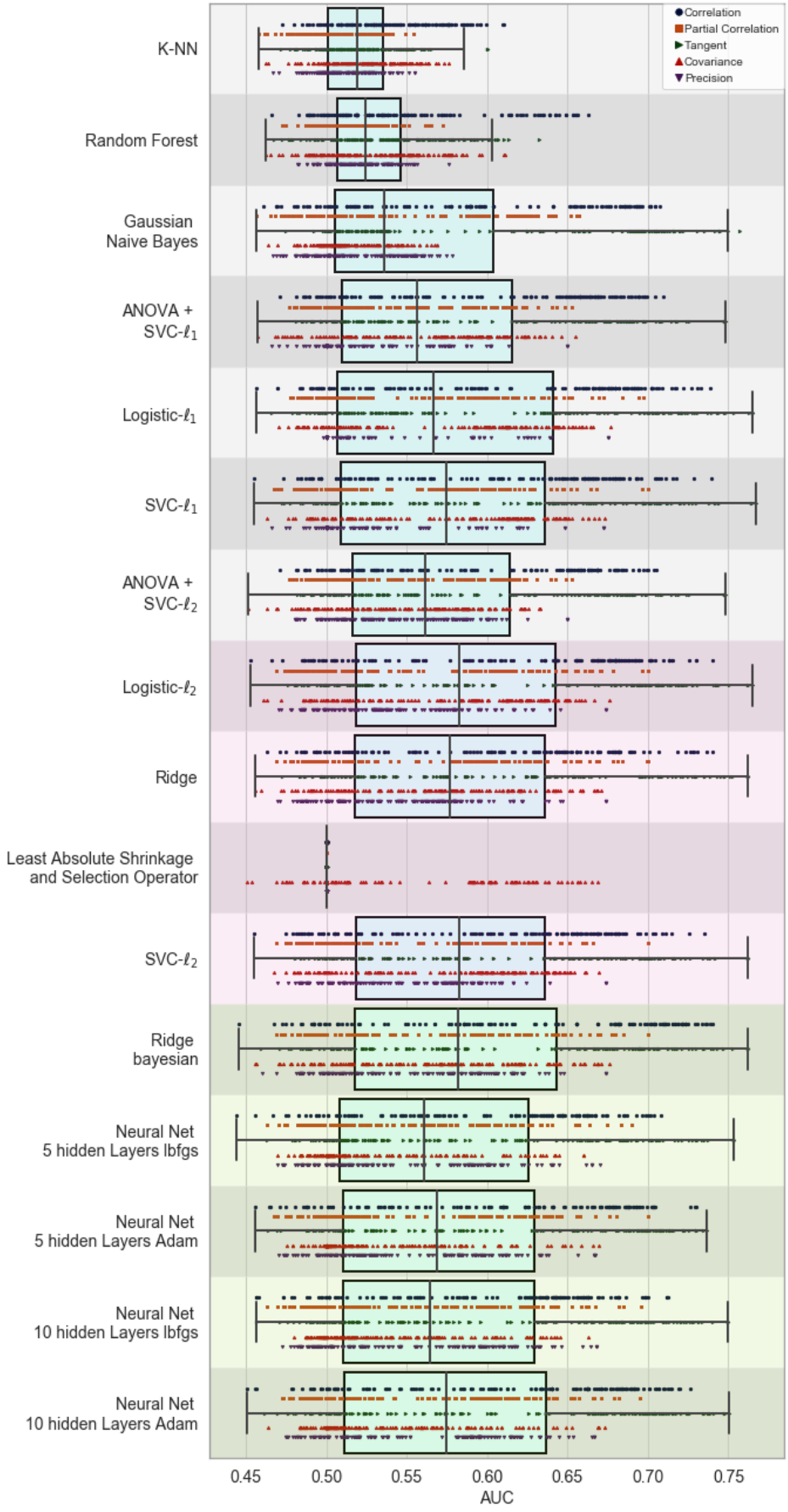

Figure 6.3: Impact of classifiers versus the connectivity measure

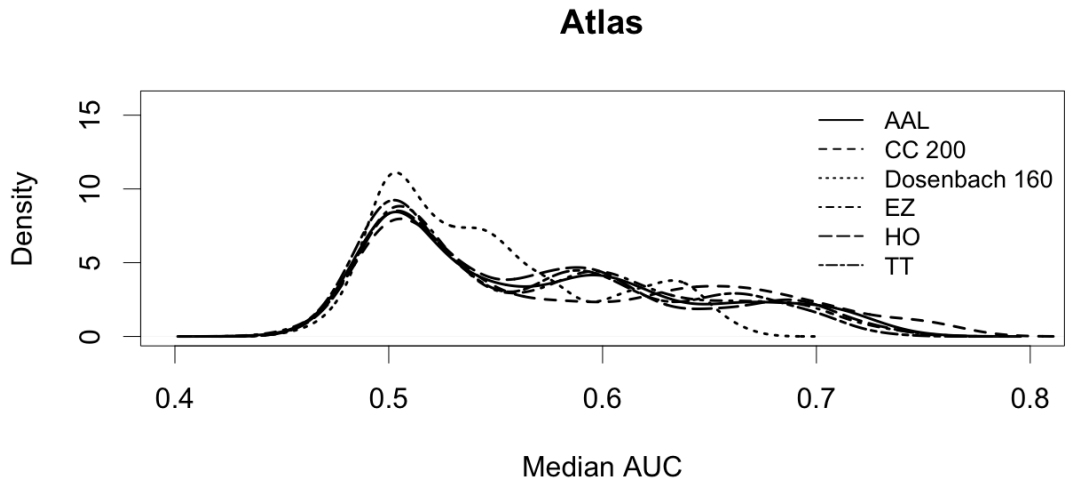

Figure 6.4: Density plots of the median AUC results achieved from the different brain parcellations tested in the experiments.

Table 6.3: One sided (row>column) Wilcoxon's rank sum test p-values between median AUC results achieved from the different measures used to build the connectivity matrices: cv=covariance, pc=partial correlation, p= precision, t=tangent, c=correlation, max=maximum median AUC achieved.

	cv	pc	p	t	c	Max AUC
cv	-	0.011	2.2e-16	1	1	0.67704
pc	0.988	-	8.69e-10	1	1	0.70
p	1	1	-	1	1	0.67
t	2.2e-16	2.2e-16	2.2e-16	-	0.059	0.76
c	2.2e-16	2.2e-16	2.2e-16	0.9408	-	0.74

of paired comparisons among the parcellations. It is quite apparent that the AAL parcellation improves over all others, followed by the CC200 parcellation. However, the maximum median AUC is greater for CC200 parcellation (0.767). The worse results are obtained from the Dosenbach parcellation, which has the greatest concentration of results around AUC=0.5. These findings are quite interesting since the AAL parcellation has a direct anatomical interpretation, allowing results of feature selection to be reported as anatomical biomarkers naturally.

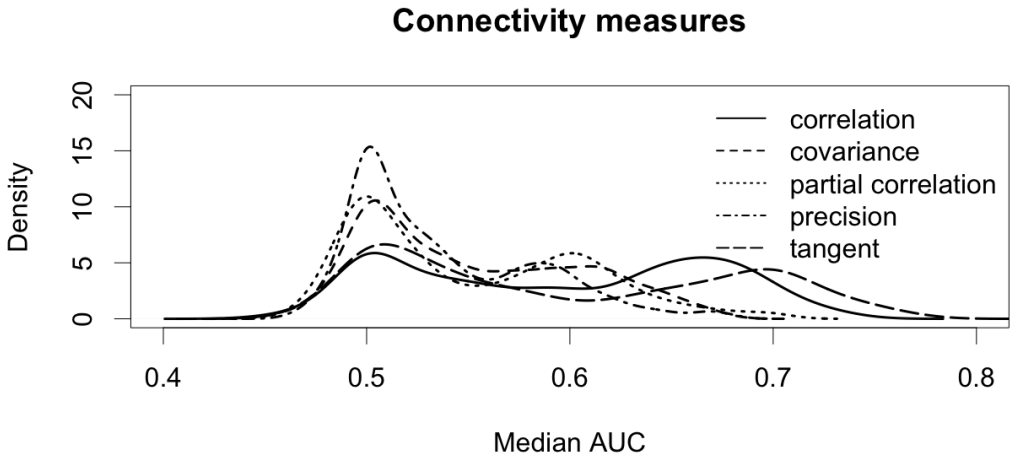

Figure 6.5: Density plots of the median AUC results achieved from the different measures used to build the connectivity matrices.

6.4 Effect of the connectivity matrix estimation

Figure 6.5 shows the distribution plots of the cross-validation repetitions median AUC aggregated by the kind of approach applied to compute the connectivity matrix per individual. It can be appreciated that these distributions are bimodal, with a high peak in 0.5. The tangent measure has the greatest second peak, around 0.7, consequently having the greatest maximum value of the median AUC. We use the one sided Wilcoxon's rank sum test for a quantitative comparison shown in Table 6.3. The PCC based connectivity and the tangent space connectivity allow to achieve much better results than the others, as reflected in the p-values reported in Table 6.3. Tangent space connectivity has a slightly significative improvement (p=0.059) over the correlation based connectivity, which is reflected in the best median AUC achieved (0.76).

6.5 Effect of the classifier building method

We have selected several classifiers to carry out the cross-validation experiments, some exploratory analysis (not reported here) of their performance results was carried out in order to select model building representatives for the comparison here. Figure 6.6 presents the plots of the densities of the selected classifiers, where two

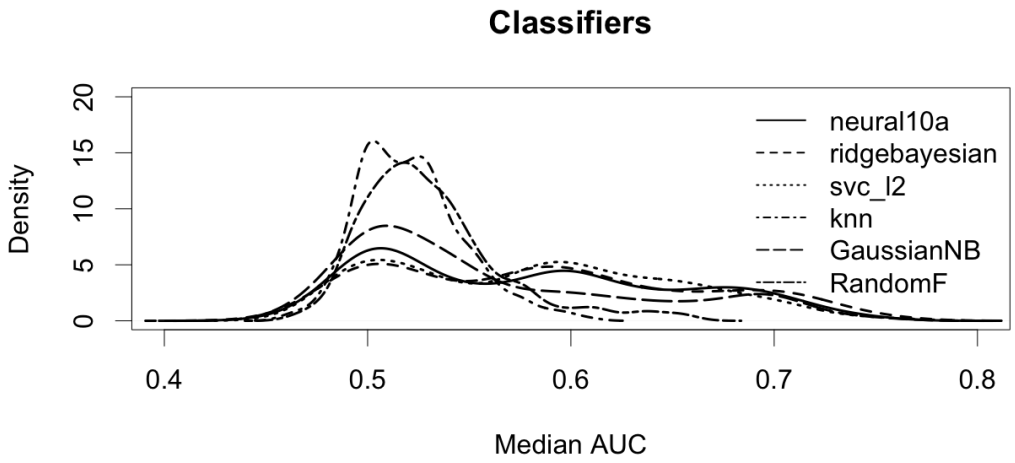

Figure 6.6: Density plots of the median AUC results achieved from the different classifiers tested in the experiments. Neural10a =10 hidden layers MLP trained with adam procedure, SVC L2= non sparse SVC, b_ridge=bayesian ridge regression, GNB=gaussian naive Bayes, RF=random forest.

Table 6.4: One sided (row>column) Wilcoxon's rank sum test p-values between median AUC results achieved by the diverse kind of classifiers experimented with. Neural10a =10 hidden layers MLP trained with adam procedure, SVC ℓ_2= non sparse SVC, b_ridge=bayesian ridge regression, GNB=gaussian naive Bayes, RF=random forest.

	neural10a	SVC ℓ_2	b_ridge	kNN	RF	GNB	max AUC
neural10a		0.963	0.817	2.547e-47	1.481e-06	2.143e-30	0.75
SVC ℓ_2	0.036		0.192	5.789e-62	0.841e-11	1.264e-43	0.761
b_ridge	0.182	0.807		1.438e-61	1.407e-09	1.594e-42	0.761
kNN	1	1	1		1	1	0.61
RF	1	1	1	7.701e-20		2.036e-08	0.756
GNB	1	1	1	6.782e-07	1		0.66

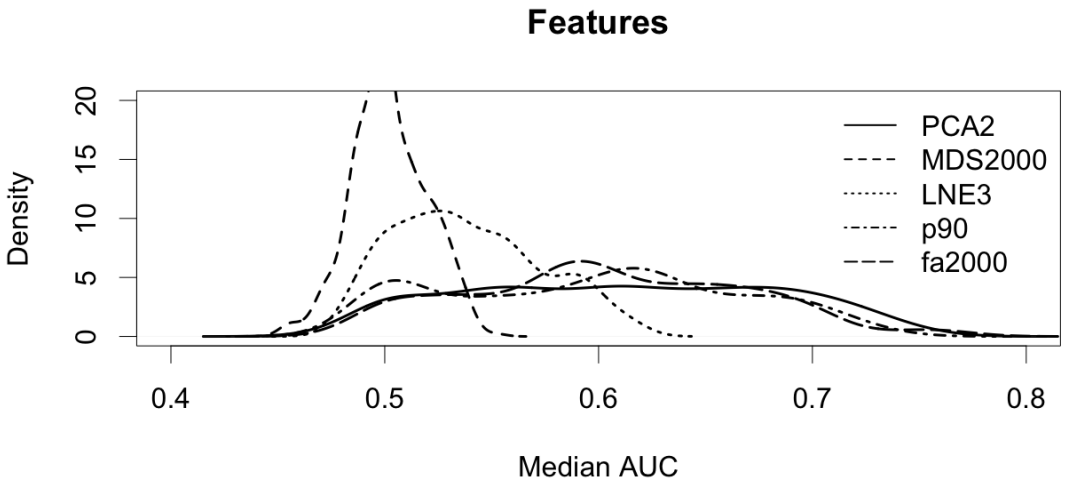

Figure 6.7: Density plots of the median AUC results achieved from the different feature extraction approaches. PCA2 = PCA retaining only half of the features, MDS2000, fa2000= MDS, FA retaining 2000 features, LNE3=LNE retaining one third of the features, p90= PCC selection 90% percentile.

Table 6.5: One sided (row>column) Wilcoxon's rank sum test p-values between median AUC results achieved from the different best versions of the feature extraction algorithms. PCA2 = PCA retaining only half of the features, MDS2000, fa2000= MDS, FA retaining 2000 features, LNE3=LNE retaining one third of the transformed features.

	PCA2	MDS2000	LNE3	p90	fa2000	Max AUC
PCA2		1.248e-116	8.525e-55	0.0029	0.078	0.75
MDS2000	1		1	1	1	0.55
LNE3	1	4.878e-66		1	1	0.62
fa200	0.921	1.577e-122	6.900e-59	0.0833		0.76

groups of classifiers can be easily identified visually, one group of less performing classifiers whose mass of results is centered around median AUC=0.5, and the other that achieve better responses. The results of the one-sided Wilcoxon's rank sum test in Table 6.4 provide confirmation of the qualitative identification of two groups of classifiers. Top performing are sparse SVC ℓ_2, ridge classifier and the MLP with 10 hidden layers. Among them, the sparse SVC has an almost significant improvement over the other two. These results are in agreement with state of the art results.

6.6 Effect of the feature extraction/selection

Feature extraction consists of a data space transformation where the new variables lose the meaning of the original space, i.e. the anatomical localization of the effects. Feature selection (such as the PCC based connection selection) preserves the meaning of the original variables, because the selected variables are not transformed. Feature selection is the preferred approach for the medical researchers because they can explain and compare the found biomarkers in the framework of the medical literature.

We have explored the effect of the feature extraction and feature selection procedures described above. The Isometric Map has been discarded as its results were far worse than any other feature extraction method. For the other methods we have made an exploration of the performance achieved when varying the number of features retained, finding slight significant improvements leading to specific selections for each approach that are compared in Table 6.5 using the one sided Wilkoxon's rank sum test as the density functions plotted in Figure 6.7 are far from Gaussian in most cases (exception made of MDS which appears to be almost Gaussian). PCA2 has an almost uniform distribution in the interval [0.5,0.7] of AUC values. Regarding Table 6.5, PCA2 improves significantly over the other procedures, althought the significance of the improvement over FA is short.

6.7 Best results

One of the conclusions that can be extracted from the previous sections is that finding good performing pipelines requires exploration of many computational choices where most of them will not achieve good results. Here we have selected the best performing pipelines found by exhaustive search over our experimental results, some of them improving over most of the results reported in the state of the art of Table 3.2. Table 6.6 gives the best median AUC scores found, together with the 5% and 95% percentiles of the cross-validation results in our experiments for comparison with the most comprehensive exploration of results to date [176], where the best reported results are 0.66, 0.711, and 0.756 for the 5%, 50%, 95% percentiles of median

Table 6.6: Best median AUC scores found in cross-validation repetitions, with corresponding settings (parcellation, feature extraction, classifier, and connectivity measure) that achieved it.

Settings				AUC percentiles		
Parcel.	Feat. extr.	Classifier	conn. meas.	5%	median	95%
cc200	fa	logistic ℓ_1	tangent	0.733	0.765	0.803
cc200	pca	logistic ℓ_2	tangent	0.739	0.765	0.801
cc200	fa	svc ℓ_1	tangent	0.739	0.764	0.803
cc200	fa1000	logistic ℓ_1	tangent	0.733	0.765	0.803
cc200	pca	svc ℓ_1	tangent	0.735	0.767	0.805
cc200	fa2000	logistic ℓ_1	tangent	0.733	0.765	0.803
cc200	fa2000	svc ℓ_1	tangent	0.739	0.764	0.803
Best reported to date [176]				0.66	0.711	0.756

Table 6.7: Best Acc scores found in cross-validation, with corresponding settings (parcellation, feature selection, classifier, and connectivity measure) that achieved it.

Settings				Acc percentiles		
parcel.	Feat. ext.	Classifier	conn. meas.	5%	median	95%
cc200	fa	logistic ℓ_1	tangent	66.9	69.9	72.3
cc200	fa	svc ℓ_1	tangent	65.7	69.9	72.8
cc200	fa1000	logistic ℓ_1	tangent	66.9	69.9	72.3
cc200	fa1000	svc ℓ_1	tangent	65.7	69.9	72.8
cc200	fa2000	logistic ℓ_1	tangent	66.9	69.9	72.3
cc200	fa2000	svc ℓ_1	tangent	65.7	69.9	72.8
cc200	pca	logistic ℓ_2	tangent	67.3	70.5	72.1
cc200	pca	svc ℓ_1	tangent	65.9	70.1	72.1
Best reported to date [203]				-	-	77

AUC distribution across all repetitions of the cross-validation experiments. This comparison shows the impact of feature extraction approaches to enhance classification results. Because many of the results in the literature are reported in terms of accuracy, we include here the corresponding accuracy tables. Table 6.7 gives the instances with the best accuracy results of our experiments, comparing favorably with the results gathered in Table 3.2. Some recent results [199, 203] have been achieved using brain parcellations that are not accessible, hence direct comparison against them is not possible for us.

Chapter 7

Results of Deep Learning Approaches

In this Chapter we report two experiences on the application of Deep Learning (DL) to the ASC discrimination based on the connectivity matrices. The first was implemented in Matlab and reported in Section 7.1. Section 7.2 tells our last experience using the Google Codelabs environment to apply DL, and transfer learning to this problem. Section 7.3 gives some comments on our attempts to apply DL to this problem.

7.1 Matlab implementation

We report a series experiments on the application of CNNs [264,311] over the connectivity matrices obtained with the diverse parcellations and connectivity measures. CNNs carry out induction of feature extraction filters at diverse abstraction levels, hence no feature extraction have been included in the experiment. We have used the Matlab implementation of CNNs, publishing the code and the data in zenodo [1]. The number of the experiments is limited by available computing resources.Table 7.1 gives the best results achieved by each CNN topology after 10 repetitions of 10-fold crossvalidation with each setting. One of the difficulties of the application

[1] `https://zenodo.org/record/4121200`

Table 7.1: Results of explored CNN topologies. We report median accuracy, brain parcellation (parcel.) and connectivity measure (conn. meas.) with best results. n@m denotes a convolution layer with n filters of size m. full denotes full connectivity layer. Output is always a softmax of two units. E denotes the number of CNNs in an ensemble.

Settings			Acc percentiles		
CNN topology	parcel.	conn. meas.	5%	median	95%
20@5, full	TT	correlation	48.30	54.55	62.50
20@5,20@5,full	EZ	correlation	51,14	60.23	67,61
20@5,20@5,20@5,full	HO	correlation	54.55	63.64	72.73
20@5,20@5,20@5,20@5,full	AAL	correlation	55.93	64.04	72.16
20@5,20@5,20@5,20@5,20@3,full	AAL	correlation	53.93	61.36	68.18
20@5,20@5,20@5,20@5,full,E=11	AAL	correlation	57.95	66.29	74.58
20@9,20@7,20@5,full	HO	correlation	55.68	64.77	72.73
20@11,20@59,20@7,20@5,full	AAL	correlation	55.68	64.77	71.19
20@11,20@59,20@7,20@5,full,E=11	AAL	correlation	58.43	66.29	74.01

of DL approaches is the finding the optimal topology of the network, which can be very tricky. For our experiments using Matlab environment we have followed the strategy of increasing the depth of the network and changing the size of the filters following a pyramid structure, broader filters at the bottom layers and smaller ones at the top layers. We have also tested ensembles of CNNs, though not very big for lack of computational resources. We found that adding layers provided some improvements, reaching kind of overfitting situation when we applied a five layers topology. Using an ensemble of 11 CNNs provided a small improvement, lack of computational resources and time prevented experimentation with larger ensembles. The use of a pyramidal strategy in the definition of the filters did not provide significant improvements. Comparison with results in Table 6.7 show that the examined CNN topologies do not provide any improvement over conventional feature selection and classification methods. This observation does not preclude the existence some specific CNN topology that improves over conventional approaches on this dataset, however the ingenuity and computational resources to find it is beyond our current capabilities. Another observation from the results in Table 7.1 is that the 5-95% percentile interval is much larger than in Table 6.7, likely due to the stochastic learning characteristics.

7.2 Google codelab implementation

Using the resources provided by Google Codelabs[2] we carried out some experiments with little success. Transfer learning using as base network the VGG16, MobileNet and Resnet50 networks achieved very poor results of average accuracy 0.4615, independently of the brain parcellation used. Fully trained CNN on the connectivity matrix obtained from the AAL and CC200 atlas increased to Acc = 54.00.

The model was expected to improve around the predefined repositories and architecture with Tensorflow and Keras (https://tfhub.dev/), but having tested with images given the existing example-based tests, these improve up to 20%. In our case, its applicability and existing information is almost null. On the other hand, this occurs with the tensorflow 2.0 version, the previous reviews and comments were given with the Tensorflow 1.0 version. It is interesting to mention that there are significant differences between both versions at the time of their execution, this is due to the updating of the libraries, improvements to the development model or others that do not facilitate continuity in order to generate a robust model.

7.3 Conclussions on DL performance

Our conclussions on the applicability of DL to ASC discrimination based on brain connectivity are very negative. It does not seem evident that DL will be providing much better results than the conventional machine learning approaches. Besides our experience reported above the literature has several examples of attempts to apply DL to ASC prediction on the ABIDE dataset. In order to discuss comparative results we face the issue of the diversity of the underlying pipeline selections and DL design pecularities. We have not found in the literature an exhaustive exploration of DL approaches over the brain parcellations and connectivity measures comparable to ours. However, we have shown that they have quite significant effect on the predictive performance. For instance, experiments involving a large ensamble of 300 CNNs [203] was carried out on a very specific irreproducible brain parcella-

[2] `https://codelabs.developers.google.com/?cat=all`

tion and connectivity matrix constructions, with ad hoc simplified CNN topologies found by after a long trial and error process with little succes (Acc=67). A greater computational (irreproducible) tour de force of training an ensemble of 3D CNN applied on the normalized rs-fMRI data [199] provided a small improvement (Acc=72). The use of recurrent networks such as the LSTM [194] did not achieve better results than the conventional approaches (Acc=68%). Graph convolutional networks (GCN) [189, 191] did not provide significant improvement over conventional results in Table 6.7 achieving the best result Acc=70 adding ancilliary information to the connectivity data. Even using ensembles of GCN [192] did not add significant benefits. Using autoencoders for feature extraction combined with conventional MLP classifier provided one of the best reported results [206] .

Chapter 8

Conclusions and future work

In this Chapter we provide summarized conclussions of the work carried out in Section (8.1) and some lines of future work in Section (8.1).

8.1 Conclusions

The predictive approach to the analysis of brain connectivity from rs-fMRI data is gaining importance in recent studies. In this approach, brain connectivity biomarkers are confirmed by the predictive performance in the classification between target populations. Up to this date there is no comprehensive study of the impact of the choices that can be made while building the machine learning pipelines, hence we have carried out a comprehensive assessment on the ABIDE I dataset, finding that some feature extraction procedures provide a boost on the performance of the classifiers across several connectivity matrix building approaches, namely the classical principal component analysis (PCA) and factor analysis (FA).

A key issue is the reproducibility of the results, that depends on the availability of the data and the precise computational resources to other researchers in the community. For this reason, we emphasize the public availability of the data and programming resources used for this study via github[1] and zenodo[2] repositories.

[1] `https://github.com/mmscnet/Impact-feature-extraction-in-Autism`
[2] `https://zenodo.org/record/4121200`

8.2 Future work

Future work should address the extension of the computational experiments to the full extent of the ABIDE II dataset. Other conectomics datasets collecting subjects and controls from connectivity analysis regarding other diseases will also be considered. Additionally, innovative machine learning approaches [312–315] will be explored. The instability of the validation of the predictive approaches in many instances of neuroscience datasets is an issue of methodological concern. In the case of the ABIDE dataset the sources of this instability are the heterogeneity of the subjects, diagnostic criteria implementation, and the data capture differences among sites. Future work will explore the relevance of novel validation approaches such as the works underlying the statistical agnostic mapping [316] to provide more robust performance predictions leading to better grounded biomarker identification.

Bibliography

[1] M. Lindquist. 1 principles of functional magnetic resonance imaging. 2014.

[2] J. Ashburner and K.J. Friston. Voxel based morphometry. In *Encyclopedia of Neuroscience*, pages 471–477. Elsevier, 2009.

[3] Mohammad-Parsa Hosseini, Mohammad-Reza Nazem-Zadeh, Dario Pompili, Kourosh Jafari-Khouzani, Kost Elisevich, and Hamid Soltanian-Zadeh. Comparative performance evaluation of automated segmentation methods of hippocampus from magnetic resonance images of temporal lobe epilepsy patients. *Medical Physics*, 43(1):538–553, jan 2016.

[4] Pei Huang, Johan D. Carlin, Richard N. Henson, and Marta M. Correia. Improved motion correction of submillimetre 7t fMRI time series with boundary-based registration (BBR). *NeuroImage*, 210:116542, apr 2020.

[5] Martin A. Lindquist, Ji Meng Loh, and Yu (Ryan) Yue. Adaptive spatial smoothing of fMRI images. *Statistics and Its Interface*, 3(1):3–13, 2010.

[6] Sebastian Ruder. *Neural Transfer Learning for Natural Language Processing*. PhD thesis, National University of Ireland, Galway, 2019.

[7] Karen Simonyan and Andrew Zisserman. Very deep convolutional networks for large-scale image recognition. September 2014.

[8] Catherine Lord, Traolach S. Brugha, Tony Charman, James Cusack, Guillaume Dumas, Thomas Frazier, Emily J. H. Jones, Rebecca M. Jones, Andrew Pickles, Matthew W. State, Julie Lounds Taylor, and Jeremy Veenstra-

VanderWeele. Autism spectrum disorder. *Nature Reviews Disease Primers*, 6(1):5, 2020.

[9] Shreya Bhat, U Rajendra Acharya, Hojjat Adeli, G Muralidhar Bairy, and Amir Adeli. Autism: cause factors, early diagnosis and therapies. *Rev Neurosci*, 25(6):841–850, 2014.

[10] National Center on Birth Defects, Developmental (Centers for Disease Control, Prevention). Division of Congenital, Developmental Disorders., Deborah L. Christensen, Jon Baio, Kim Van Naarden Braun, Deborah Bilder, Jane Charles, John N. Constantino, Julie Daniels, Maureen S. Durkin, Robert T. Fitzgerald, Margaret Kurzius-Spencer, Li-Ching Lee, Sydney Pettygrove, Cordelia Robinson, Eldon Schulz, Chris Wells, Martha S. Wingate, Walter Zahorodny, and Marshalyn Yeargin-Allsopp. Mmwr. surveillance summaries : Morbidity and mortality weekly report. surveillance summaries ; v. 65, no. ss-13. 65(13), November 16, 2018.

[11] Meng-Chuan Lai, Michael V. Lombardo, John Suckling, Amber N. V. Ruigrok, Bhismadev Chakrabarti, Christine Ecker, Sean C. L. Deoni, Michael C. Craig, Declan G. M. Murphy, Edward T. Bullmore, MRC AIMS Consortium, and Simon Baron-Cohen. Biological sex affects the neurobiology of autism. *Brain*, 136(9):2799–2815, 08 2013.

[12] Meng-Chuan Lai, Michael V Lombardo, Bonnie Auyeung, Bhismadev Chakrabarti, and Simon Baron-Cohen. Sex/gender differences and autism: setting the scene for future research. *J Am Acad Child Adolesc Psychiatry*, 54(1):11–24, Jan 2015.

[13] Meng-Chuan Lai, Michael V Lombardo, and Simon Baron-Cohen. Autism. *The Lancet*, 383(9920):896–910, 2013.

[14] Laurent Mottron and Danilo Bzdok. Autism spectrum heterogeneity: fact or artifact? *Molecular Psychiatry*, 2020.

[15] C Ecker, DS Andrews, CM Gudbrandsen, and et al. Association between the probability of autism spectrum disorder and normative sex-related phenotypic diversity in brain structure. *JAMA Psychiatry*, 74(4):329–338, 2017.

[16] Catherine Lord, Eva Petkova, Vanessa Hus, Weijin Gan, Feihan Lu, Donna M. Martin, Opal Ousley, Lisa Guy, Raphael Bernier, Jennifer Gerdts, Molly Algermissen, Agnes Whitaker, James S. Sutcliffe, Zachary Warren, Ami Klin, Celine Saulnier, Ellen Hanson, Rachel Hundley, Judith Piggot, Eric Fombonne, Mandy Steiman, Judith Miles, Stephen M. Kanne, Robin P. Goin-Kochel, Sarika U. Peters, Edwin H. Cook, Stephen Guter, Jennifer Tjernagel, Lee Anne Green-Snyder, Somer Bishop, Amy Esler, Katherine Gotham, Rhiannon Luyster, Fiona Miller, Jennifer Olson, Jennifer Richler, and Susan Risi. A Multisite Study of the Clinical Diagnosis of Different Autism Spectrum Disorders. *Archives of General Psychiatry*, 69(3):306–313, 03 2012.

[17] Shreya Bhat, U. Rajendra Acharya, Hojjat Adeli, G. Muralidhar Bairy, and Amir Adeli. Automated diagnosis of autism: in search of a mathematical marker. *Reviews in the Neurosciences*, 25(6):851 – 861, 2014.

[18] Tao Chen, Ye Chen, Mengxue Yuan, Mark Gerstein, Tingyu Li, Huiying Liang, Tanya Froehlich, and Long Lu. The development of a practical artificial intelligence tool for diagnosing and evaluating autism spectrum disorder: Multicenter study. *JMIR Med Inform*, 8(5):e15767, May 2020.

[19] Hidir Selcuk Nogay and Hojjat Adeli. Machine learning (ml) for the diagnosis of autism spectrum disorder (asd) using brain imaging. *Reviews in the Neurosciences*, (0):000010151520200043, 2020.

[20] Fermín Segovia, Rosemary Holt, Michael Spencer, Juan M. Górriz, Javier Ramírez, Carlos G. Puntonet, Christophe Phillips, Lindsay Chura, Simon Baron-Cohen, and John Suckling. Identifying endophenotypes of autism: a multivariate approach. *Frontiers in Computational Neuroscience*, 8:60, 2014.

[21] L Q Uddin, D R Dajani, W. Voorhies, H. Bednarz, and R K Kana. Progress and roadblocks in the search for brain-based biomarkers of autism and

attention-deficit/hyperactivity disorder. *Translational Psychiatry*, 7(8):e1218–e1218, 2017.

[22] A Di Martino, C-G Yan, Q Li, E Denio, F X Castellanos, K Alaerts, J S Anderson, M Assaf, S Y Bookheimer, M Dapretto, B Deen, S Delmonte, I Dinstein, B Ertl-Wagner, D A Fair, L Gallagher, D P Kennedy, C L Keown, C Keysers, J E Lainhart, C Lord, B Luna, V Menon, N J Minshew, C S Monk, S Mueller, R-A Müller, M B Nebel, J T Nigg, K O'Hearn, K A Pelphrey, S J Peltier, J D Rudie, S Sunaert, M Thioux, J M Tyszka, L Q Uddin, J S Verhoeven, N Wenderoth, J L Wiggins, S H Mostofsky, and M P Milham. The autism brain imaging data exchange: towards a large-scale evaluation of the intrinsic brain architecture in autism. *Molecular Psychiatry*, 19:659 EP –, 06 2013.

[23] Adriana Di Martino, David O'Connor, Bosi Chen, Kaat Alaerts, Jeffrey S. Anderson, Michal Assaf, Joshua H. Balsters, Leslie Baxter, Anita Beggiato, Sylvie Bernaerts, Laura M. E. Blanken, Susan Y. Bookheimer, B. Blair Braden, Lisa Byrge, F. Xavier Castellanos, Mirella Dapretto, Richard Delorme, Damien A. Fair, Inna Fishman, Jacqueline Fitzgerald, Louise Gallagher, R. Joanne Jao Keehn, Daniel P. Kennedy, Janet E. Lainhart, Beatriz Luna, Stewart H. Mostofsky, Ralph-Axel Müller, Mary Beth Nebel, Joel T. Nigg, Kirsten O'Hearn, Marjorie Solomon, Roberto Toro, Chandan J. Vaidya, Nicole Wenderoth, Tonya White, R. Cameron Craddock, Catherine Lord, Bennett Leventhal, and Michael P. Milham. Enhancing studies of the connectome in autism using the autism brain imaging data exchange ii. *Scientific Data*, 4:170010 EP –, 03 2017.

[24] Benjamin Gutierrez Becker, Tassilo Klein, and Christian Wachinger. Gaussian process uncertainty in age estimation as a measure of brain abnormality. *NeuroImage*, 175:246 – 258, 2018.

[25] Thomas Wolfers, Dorothea L. Floris, Richard Dinga, Daan van Rooij, Christina Isakoglou, Seyed Mostafa Kia, Mariam Zabihi, Alberto Llera, Rajanikanth Chowdanayaka, Vinod J. Kumar, Han Peng, Charles Laidi, Dafnis

Batalle, Ralica Dimitrova, Tony Charman, Eva Loth, Meng-Chuan Lai, Emily Jones, Sarah Baumeister, Carolin Moessnang, Tobias Banaschewski, Christine Ecker, Guillaume Dumas, Jonathan O'Muircheartaigh, Declan Murphy, Jan K. Buitelaar, Andre F. Marquand, and Christian F. Beckmann. From pattern classification to stratification: towards conceptualizing the heterogeneity of autism spectrum disorder. *Neuroscience & Biobehavioral Reviews*, 104:240 – 254, 2019.

[26] Mehran Ahmadlou, Hojjat Adeli, and Amir Adeli. Improved visibility graph fractality with application for the diagnosis of autism spectrum disorder. *Physica A: Statistical Mechanics and its Applications*, 391(20):4720 – 4726, 2012.

[27] Mehran Ahmadlou and Hojjat Adeli. Complexity of weighted graph: A new technique to investigate structural complexity of brain activities with applications to aging and autism. *Neuroscience Letters*, 650:103 – 108, 2017.

[28] Mehran Ahmadlou, Hojjat Adeli, and Amir Adeli. Fuzzy synchronization likelihood-wavelet methodology for diagnosis of autism spectrum disorder. *Journal of Neuroscience Methods*, 211(2):203 – 209, 2012.

[29] E. Puerto, J. Aguilar, C. López, and D. Chávez. Using multilayer fuzzy cognitive maps to diagnose autism spectrum disorder. *Applied Soft Computing*, 75:58 – 71, 2019.

[30] Alicia d'Anjou, Manuel Graña, and Francois Moutet. Brief survey about the search for biomarkers and computer aided diagnosis of autism spectrum disorder. Technical Report http://doi.org/10.5281/zenodo.1408202, Zenodo, 2018.

[31] Alex M. Pagnozzi, Eugenia Conti, Sara Calderoni, Jurgen Fripp, and Stephen E. Rose. A systematic review of structural mri biomarkers in autism spectrum disorder: A machine learning perspective. *International Journal of Developmental Neuroscience*, 71:68 – 82, 2018.

[32] Stephanie H. Ameis and Marco Catani. Altered white matter connectivity as a neural substrate for social impairment in autism spectrum disorder. *Cortex*,

62:158 – 181, 2015. Special issue: The clinical anatomy of the limbic lobe and connected structures.

[33] Xin Di, Azeezat Azeez, Xiaobo Li, Emad Haque, and Bharat B. Biswal. Disrupted focal white matter integrity in autism spectrum disorder: A voxel-based meta-analysis of diffusion tensor imaging studies. *Progress in Neuro-Psychopharmacology and Biological Psychiatry*, 82:242 – 248, 2018.

[34] Joshua H. Balsters, Dante Mantini, and Nicole Wenderoth. Connectivity-based parcellation reveals distinct cortico-striatal connectivity fingerprints in autism spectrum disorder. *NeuroImage*, 170:412 – 423, 2018. Segmenting the Brain.

[35] Salim Arslan, Sofia Ira Ktena, Antonios Makropoulos, Emma C. Robinson, Daniel Rueckert, and Sarah Parisot. Human brain mapping: A systematic comparison of parcellation methods for the human cerebral cortex. *NeuroImage*, 170:5 – 30, 2018. Segmenting the Brain.

[36] Neil D. Woodward and Carissa J. Cascio. Resting-State Functional Connectivity in Psychiatric Disorders. *JAMA Psychiatry*, 72(8):743–744, 08 2015.

[37] Manuel Graña, Leire Ozaeta, and Darya Chyzhyk. Resting state effective connectivity allows auditory hallucination discrimination. *International Journal of Neural Systems*, 27(05):1750019, 2017. PMID: 28274168.

[38] Priya Aggarwal and Anubha Gupta. Multivariate graph learning for detecting aberrant connectivity of dynamic brain networks in autism. *Medical Image Analysis*, 56:11 – 25, 2019.

[39] Zening Fu, Yiheng Tu, Xin Di, Yuhui Du, Jing Sui, Bharat B. Biswal, Zhiguo Zhang, N. de Lacy, and V.D. Calhoun. Transient increased thalamic-sensory connectivity and decreased whole-brain dynamism in autism. *NeuroImage*, 190:191 – 204, 2019. Mapping diseased brains.

[40] Andry Andriamananjara, Rayan Muntari, and Alessandro Crimi. Overlaps in brain dynamic functional connectivity between schizophrenia and autism spectrum disorder. *Scientific African*, 2:e00019, 2019.

[41] Dana Mastrovito, Catherine Hanson, and Stephen Jose Hanson. Differences in atypical resting-state effective connectivity distinguish autism from schizophrenia. *NeuroImage: Clinical*, 18:367 – 376, 2018.

[42] Maya A. Reiter, Lisa E. Mash, Annika C. Linke, Christopher H. Fong, Inna Fishman, and Ralph-Axel Müller. Distinct patterns of atypical functional connectivity in lower-functioning autism. *Biological Psychiatry: Cognitive Neuroscience and Neuroimaging*, 4(3):251 – 259, 2019.

[43] Joanna Granich, Alena Dass, Margherita Busacca, Dennis Moore, Angelika Anderson, Svetha Venkatesh, Thi Duong, Pratibha Vellanki, Amanda Richdale, David Trembath, Darin Cairns, Wendy Marshall, Tania Rodwell, Madeleine Rayner, and Andrew J. O. Whitehouse. Randomised controlled trial of an ipad based early intervention for autism: Toby playpad study protocol. *BMC Pediatrics*, 16(1):167, Oct 2016.

[44] Silvana E Mengoni, Karen Irvine, Deepshikha Thakur, Garry Barton, Kerstin Dautenhahn, Karen Guldberg, Ben Robins, David Wellsted, and Shivani Sharma. Feasibility study of a randomised controlled trial to investigate the effectiveness of using a humanoid robot to improve the social skills of children with autism spectrum disorder (kaspar rct): a study protocol. *BMJ Open*, 7(6), 2017.

[45] Dennis W. Moore, Svetha Venkatesh, Angelika Anderson, Stewart Greenhill, Dinh Phung, Thi Duong, Darin Cairns, Wendy Marshall, and Andrew J. O. Whitehouse. Toby play-pad application to teach children with asd – a pilot trial. *Developmental Neurorehabilitation*, 18(4):213–217, 2015. PMID: 23869435.

[46] IP Oono, EJ Honey, and H McConachie. Parent mediated early intervention for young children with autism spectrum disorders (asd). *Cochrane Database of Systematic Reviews*, (4), 2013.

[47] B Reichow, K Hume, EE Barton, and BA Boyd. Early intensive behavioral intervention (EIBI) for young children with autism spectrum disorders (ASD). *Cochrane Database of Systematic Reviews*, (5), 2018.

[48] Andrew J.O. Whitehouse, Joanna Granich, Gail Alvares, Margherita Busacca, Matthew N. Cooper, Alena Dass, Thi Duong, Rajes Harper, Wendy Marshall, Amanda Richdale, Tania Rodwell, David Trembath, Pratibha Vellanki, Dennis W. Moore, and Angelika Anderson. A randomised controlled trial of an ipad-based application to complement early behavioural intervention in autism spectrum disorder. *Journal of Child Psychology and Psychiatry*, 58(9):1042–1052, 2017.

[49] Elena Cravedi, Emmanuelle Deniau, Marianna Giannitelli, Hugues Pellerin, Virginie Czernecki, Tiphanie Priou, Jean Xavier, Angele Consoli, Andreas Hartmann, and David Cohen. Disentangling tourette syndrome heterogeneity through hierarchical ascendant clustering. *Dev Med Child Neurol*, 2018.

[50] Pashalina Lialiou, Dimitrios Zikos, and John Mantas. *Quality of Life through Quality of Information*, volume 180 of *Studies in Health Technology and Informatics*, chapter Development and Evaluation of an Expert System for the Diagnosis of Child Autism, pages 1185 – 1187. IOS Press, 2012.

[51] Maryam Akhavan Aghdam, Arash Sharifi, and Mir Mohsen Pedram. Combination of rs-fMRI and sMRI data to discriminate autism spectrum disorders in young children using deep belief network. *Journal of Digital Imaging*, May 2018.

[52] Bhaskar Sen, Neil C. Borle, Russell Greiner, and Matthew R. G. Brown. A general prediction model for the detection of ADHD and autism using structural and functional mri. *PLOS ONE*, 13(4):1–28, 04 2018.

[53] Ridha Djemal, Khalil AlSharabi, Sutrisno Ibrahim, and Abdullah Alsuwailem. EEG-based computer aided diagnosis of autism spectrum disorder using wavelet, entropy, and ann. *BioMed Research International*, 2017:9, 2017.

[54] Shilan S. Hameed, Rohayanti Hassan, and Fahmi F. Muhammad. Selection and classification of gene expression in autism disorder: Use of a combination of statistical filters and a gbpso-svm algorithm. *PLOS ONE*, 12(11):1–25, 11 2017.

[55] Tomasz Latkowski and Stanislaw Osowski. Computerized system for recognition of autism on the basis of gene expression microarray data. *Computers in Biology and Medicine*, 56:82 – 88, 2015.

[56] Genyuan Li, Olivia Lee, and Herschel Rabitz. High efficiency classification of children with autism spectrum disorder. *PLOS ONE*, 13(2):1–23, 02 2018.

[57] Changchun Liu, Karla Conn, Nilanjan Sarkar, and Wendy Stone. Physiology-based affect recognition for computer-assisted intervention of children with autism spectrum disorder. *International Journal of Human-Computer Studies*, 66(9):662 – 677, 2008.

[58] Anurag Sharma, Arun Khosla, Mamta Khosla, and Yogeswara Rao. Fast and accurate diagnosis of autism (fada): a novel hierarchical fuzzy system based autism detection tool. *Australasian Physical & Engineering Sciences in Medicine*, Jul 2018.

[59] Tomasz Latkowski and Stanislaw Osowski. Gene selection in autism – comparative study. *Neurocomputing*, 250:37 – 44, 2017. Applications in Computational Intelligence (Selected an improved papers of the 13th International Work-Conference on Artificial Neural Networks, IWANN2015).

[60] Mahmoud Mansouri, Ann-Charlotte Thuresson, Catalina Betancur, Marion Leboyer, Christopher Gillberg, Cordelia Langford, and Niklas Dahl. P3: Array-cgh for the identification of autism susceptibility loci. *European Journal of Medical Genetics*, 48(4):449 – 450, 2005. Includes programme and

abstracts of the Marie Curie Conferences and Training Courses on arrayCGH and Molecular Cytogenetics.

[61] Erin D. Bigler. Structural image analysis of the brain in neuropsychology using magnetic resonance imaging (mri) techniques. *Neuropsychology Review*, 25(3):224–249, 2015.

[62] Andrew J. Steven, Jiachen Zhuo, and Elias R. Melhem. Diffusion kurtosis imaging: An emerging technique for evaluating the microstructural environment of the brain. *American Journal of Roentgenology*, 202(1):W26–W33, 2018/05/31 2013.

[63] Nan-kuei Chen, Hing-Chiu Chang, Ali Bilgin, Adam Bernstein, and Theodore P. Trouard. A diffusion-matched principal component analysis (dm-pca) based two-channel denoising procedure for high-resolution diffusion-weighted mri. *PLOS ONE*, 13(4):e0195952–, 04 2018.

[64] Geetha Soujanya Chilla, Cher Heng Tan, Chenjie Xu, and Chueh Loo Poh. Diffusion weighted magnetic resonance imaging and its recent trend—a survey. *Quantitative Imaging in Medicine and Surgery*, 5(3):407–422, 06 2015.

[65] Aurobrata Ghosh and Rachid Deriche. A survey of current trends in diffusion mri for structural brain connectivity. *Journal of Neural Engineering*, 13(1):011001, 2016.

[66] Rajesh K. Kana, Lucina Q. Uddin, Tal Kenet, Diane Chugani, and Ralph-Axel Müller. Brain connectivity in autism. *Frontiers in Human Neuroscience*, 8:349, 2014.

[67] Maggie S M Chow, Sharon L Wu, Sarah E Webb, Katie Gluskin, and D T Yew. Functional magnetic resonance imaging and the brain: A brief review. *World Journal of Radiology*, 9(1):5–9, 01 2017.

[68] Jodie R. Gawryluk, Erin L. Mazerolle, and Ryan C. N. D'Arcy. Does functional mri detect activation in white matter? a review of emerging evidence, issues, and future directions. *Frontiers in Neuroscience*, 8:239, 2014.

[69] KA Smitha, K Akhil Raja, KM Arun, PG Rajesh, Bejoy Thomas, TR Kapilamoorthy, and Chandrasekharan Kesavadas. Resting state fmri: A review on methods in resting state connectivity analysis and resting state networks. *The Neuroradiology Journal*, 30(4):305–317, 2018/05/25 2017.

[70] H. Lv, Z. Wang, E. Tong, L. M. Williams, G. Zaharchuk, M. Zeineh, A. N. Goldstein-Piekarski, T. M. Ball, C. Liao, and M. Wintermark. Resting-state functional mri: Everything that nonexperts have always wanted to know. *American Journal of Neuroradiology*, 01 2018.

[71] Bharat B. Biswal. Resting state fmri: A personal history. *NeuroImage*, 62(2):938–944, 2012.

[72] Alexander Westphal, Avery Voos, and Kevin Pelphrey. Chapter 8 - functional magnetic resonance imaging as a biomarker for the diagnosis, progression, and treatment of autistic spectrum disorders. In Robert A. McArthur, editor, *Translational Neuroimaging*, pages 221 – 243. Academic Press, 2013.

[73] V. J. Wedeen, R. P. Wang, J. D. Schmahmann, T. Benner, W. Y. I. Tseng, G. Dai, D. N. Pandya, P. Hagmann, H. D'Arceuil, and A. J. de Crespigny. Diffusion spectrum magnetic resonance imaging (dsi) tractography of crossing fibers. *NeuroImage*, 41(4):1267–1277, 2008.

[74] J. Wedeen Van, Patric Hagmann, Isaac Tseng Wen-Yih, G. Reese Timothy, and M. Weisskoff Robert. Mapping complex tissue architecture with diffusion spectrum magnetic resonance imaging. *Magnetic Resonance in Medicine*, 54(6):1377–1386, 2018/05/29 2005.

[75] G Russell Glenn, Li-Wei Kuo, Yi-Ping Chao, Chu-Yu Lee, Joseph A Helpern, and Jens H Jensen. Mapping the orientation of white matter fiber bundles: A comparative study between diffusion tensor imaging (dti), diffusional kurtosis imaging (dki), and diffusion spectrum imaging (dsi). *AJNR. American journal of neuroradiology*, 37(7):1216–1222, 07 2016.

[76] Andre Santos Ribeiro, Luis Miguel Lacerda, Hugo Alexandre Ferreira, and Alessandro Tavano. Multimodal imaging brain connectivity analysis (mibca) toolbox. *PeerJ*, 3:e1078, 2015.

[77] Corinne E Jung, Lars Strother, David J Feil-Seifer, and Jeffrey J Hutsler. Atypical asymmetry for processing human and robot faces in autism revealed by fnirs. *PLoS One*, 11(7):e0158804–e0158804, 2016.

[78] Penny Stribling, John Rae, and Paul Dickerson. Using conversation analysis to explore the recurrence of a topic in the talk of a boy with an autism spectrum disorder. *Clin Linguist Phon*, 23(8):555–582, 2009.

[79] Baihua Li, Arjun Sharma, James Meng, Senthil Purushwalkam, and Emma Gowen. Applying machine learning to identify autistic adults using imitation: An exploratory study. *PLOS ONE*, 12(8):1–19, 08 2017.

[80] Anna Anzulewicz, Krzysztof Sobota, and Jonathan T. Delafield-Butt. Toward the autism motor signature: Gesture patterns during smart tablet gameplay identify children with autism. *Scientific Reports*, 6:31107 EP –, 08 2016.

[81] Joon Young Kang, Ryunhyung Kim, Hyunsun Kim, Yeonjune Kang, Susan Hahn, Zhengrui Fu, Mamoon I. Khalid, Enja Schenck, and Thomas Thesen. Automated tracking and quantification of autistic behavioral symptoms using microsoft kinect. In J.D. Westwood et al., editor, *Medicine Meets Virtual Reality 22*, volume 220 of *Studies in Health Technology and Informatics*. IOS Press, 2016.

[82] Valentina Focaroli, Fabrizio Taffoni, Shelby M. Parsons, Flavio Keller, and Jana M. Iverson. Performance of motor sequences in children at heightened vs. low risk for asd: A longitudinal study from 18 to 36 months of age. *Frontiers in Psychology*, 7:724, 2016.

[83] M. Del Coco, M. Leo, P. Carcagnì, F. Famà, L. Spadaro, L. Ruta, G. Pioggia, and C. Distante. Study of mechanisms of social interaction stimulation in autism spectrum disorder by assisted humanoid robot. *IEEE Transactions on Cognitive and Developmental Systems*, pages 1–1, 2018.

[84] J. Noel, M. De Niear, N. S. Lazzara, and M. T. Wallace. Uncoupling between multisensory temporal function and non-verbal turn-taking in autism spectrum disorder. *IEEE Transactions on Cognitive and Developmental Systems*, pages 1–1, 2018.

[85] Bi Ge, Hae Won Park, and Ayanna M. Howard. Identifying engagement from joint kinematics data for robot therapy prompt interventions for children with autism spectrum disorder. In Arvin Agah, John-John Cabibihan, Ayanna M. Howard, Miguel A. Salichs, and Hongsheng He, editors, *Social Robotics. ICSR 2016*, volume Lecture Notes in Computer Science, vol 9979, pages 531–540, Cham, 2016. Springer International Publishing.

[86] Nuno Gonçalves, José L. Rodrigues, Sandra Costa, and Filomena Soares. Automatic detection of stereotypical motor movements. *Procedia Engineering*, 47:590 – 593, 2012. 26th European Conference on Solid-State Transducers, EUROSENSOR 2012.

[87] José L. Rodrigues, Nuno Gonçalves, Sandra Costa, and Filomena Soares. Stereotyped movement recognition in children with asd. *Sensors and Actuators A: Physical*, 202:162 – 169, 2013. Selected Papers from the 26th European Conference on Solid-State Transducers Kraków, Poland, 9-12 September 2012.

[88] K. S. Lohan, E. Sheppard, G. E. Little, and G. Rajendran. Towards improved child robot interaction by understanding eye movements. *IEEE Transactions on Cognitive and Developmental Systems*, pages 1–1, 2018.

[89] Anwesha Banerjee, Monalisa Pal, Shreyasi Datta, D.N. Tibarewala, and Amit Konar. Eye movement sequence analysis using electrooculogram to assist autistic children. *Biomedical Signal Processing and Control*, 14:134 – 140, 2014.

[90] K. A. A. Mamun, S. Bardhan, M. A. Ullah, E. Anagnostou, J. Brian, S. Akhter, and M. G. Rabbani. Smart autism — a mobile, interactive and integrated framework for screening and confirmation of autism. In *2016 38th Annual International Conference of the IEEE Engineering in Medicine and Biology Society (EMBC)*, pages 5989–5992, Aug 2016.

[91] W. Liu, T. Zhou, C. Zhang, X. Zou, and M. Li. Response to name: A dataset and a multimodal machine learning framework towards autism study. In *2017 Seventh International Conference on Affective Computing and Intelligent Interaction (ACII)*, pages 178–183, Oct 2017.

[92] Giuseppe Di Cesare, Laura Sparaci, Annalisa Pelosi, Luigi Mazzone, Giulia Giovagnoli, Deny Menghini, Emanuele Ruffaldi, and Stefano Vicari. Differences in action style recognition in children with autism spectrum disorders. *Front Psychol*, 8:1456–1456, 2017.

[93] T. Kujala, S. Kuuluvainen, S. Saalasti, E. Jansson-Verkasalo, L. von Wendt, and T. Lepistö. Speech-feature discrimination in children with asperger syndrome as determined with the multi-feature mismatch negativity paradigm. *Clinical Neurophysiology*, 121(9):1410 – 1419, 2010.

[94] Bora Han, Charles Tijus, Florence Le Barillier, and Jacqueline Nadel. Morphing technique reveals intact perception of object motion and disturbed perception of emotional expressions by low-functioning adolescents with autism spectrum disorder. *Res Dev Disabil*, 47:393–404, 2015.

[95] Basilio Noris, Karim Benmachiche, Julien Meynet, Jean-Philippe Thiran, and Aude G. Billard. Analysis of head-mounted wireless camera videos for early diagnosis of autism. In Marek Kurzynski, Edward Puchala, Michal Wozniak, and Andrzej Zolnierek, editors, *Computer Recognition Systems 2*, pages 663–670, Berlin, Heidelberg, 2007. Springer Berlin Heidelberg.

[96] Frano Petric, Domagoj Tolić, Damjan Miklić, Zdenko Kovačić, Maja Cepanec, and Sanja Šimleša. Towards a robot-assisted autism diagnostic protocol: Modelling and assessment with pomdp. In Honghai Liu, Naoyuki Kubota, Xiangyang Zhu, Rüdiger Dillmann, and Dalin Zhou, editors, *Intelligent Robotics and Applications*, pages 82–94, Cham, 2015. Springer International Publishing.

[97] Elisabeth Söchting, Johannes Hartl, Martin Riederer, Christian Schönauer, Hannes Kaufmann, and Claus Lamm. Development of tests to evaluate the sensory abilities of children with autism spectrum disorder. *Procedia Computer*

Science, 67:193 – 203, 2015. Proceedings of the 6th International Conference on Software Development and Technologies for Enhancing Accessibility and Fighting Info-exclusion.

[98] Laura Sparaci, Domenico Formica, Francesca Romana Lasorsa, Luigi Mazzone, Giovanni Valeri, and Stefano Vicari. Untrivial pursuit: Measuring motor procedures learning in children with autism. *Autism Res*, 8(4):398–411, 2015.

[99] Fabrizio Taffoni, Valentina Focaroli, Domenico Formica, Eugenio Gugliemelli, Flavio Keller, and Jana M Iverson. Sensor-based technology in the study of motor skills in infants at risk for asd. *Proc IEEE RAS EMBS Int Conf Biomed Robot Biomechatron*, pages 1879–1883, 2012.

[100] Indika B. Wijayasinghe, Isura Ranatunga, Namrata Balakrishnan, Nicoleta Bugnariu, and Dan O. Popa. Human–robot gesture analysis for objective assessment of autism spectrum disorder. *International Journal of Social Robotics*, 8(5):695–707, Nov 2016.

[101] Hanne De Jaegher. Embodiment and sense-making in autism. *Front Integr Neurosci*, 7:15–15, 2013.

[102] Martha D. Kaiser and Kevin A. Pelphrey. Disrupted action perception in autism: Behavioral evidence, neuroendophenotypes, and diagnostic utility. *Developmental Cognitive Neuroscience*, 2(1):25 – 35, 2012.

[103] Marco Turi, Filippo Muratori, Francesca Tinelli, Maria Concetta Morrone, and David C Burr. Autism is associated with reduced ability to interpret grasping actions of others. *Sci Rep*, 7(1):12687–12687, 2017.

[104] John-John Cabibihan, Hifza Javed, Mohammed Aldosari, Thomas W Frazier, and Haitham Elbashir. Sensing technologies for autism spectrum disorder screening and intervention. *Sensors (Basel)*, 17(1), 2016.

[105] Domenico Campolo, Massimo Molteni, Eugenio Guglielmelli, Flavio Keller, Cecilia Laschid, and Paolo Dario. Towards development of biomechatronic

tools for early diagnosis of neurodevelopmental disorders. *Conf Proc IEEE Eng Med Biol Soc*, 1:3242–3245, 2006.

[106] Marco Leo, Marco Del Coco, Pierluigi Carcagnì, Pier Luigi Mazzeo, Paolo Spagnolo, and Cosimo Distante. Intelligent vision system for asd diagnosis and assessment. In Jacques Blanc-Talon, Cosimo Distante, Wilfried Philips, Dan Popescu, and Paul Scheunders, editors, *Advanced Concepts for Intelligent Vision Systems*, pages 534–546, Cham, 2016. Springer International Publishing.

[107] Mollie K Marko, Deana Crocetti, Thomas Hulst, Opher Donchin, Reza Shadmehr, and Stewart H Mostofsky. Behavioural and neural basis of anomalous motor learning in children with autism. *Brain*, 138(Pt 3):784–797, 2015.

[108] Anthony Haffey, Clare Press, Garret O'Connell, and Bhismadev Chakrabarti. Autistic traits modulate mimicry of social but not nonsocial rewards. *Autism Res*, 6(6):614–620, 2013.

[109] Shreya Bhat, U. Rajendra Acharya, Hojjat Adeli, G. Muralidhar Bairy, and Amir Adeli. Automated diagnosis of autism: in search of a mathematical marker. 25:851, 2018-07-17T14:19:44.285+02:00 2014.

[110] Enzo Grossi, Chiara Olivieri, and Massimo Buscema. Diagnosis of autism through EEG processed by advanced computational algorithms: A pilot study. *Computer Methods and Programs in Biomedicine*, 142:73 – 79, 2017.

[111] Christian O'Reilly, John D. Lewis, and Mayada Elsabbagh. Is functional brain connectivity atypical in autism? a systematic review of EEG and MEG studies. *PLOS ONE*, 12(5):1–28, 05 2017.

[112] B. A. Cociu, S. Das, L. Billeci, W. Jamal, K. Maharatna, S. Calderoni, A. Narzisi, and F. Muratori. Multimodal functional and structural brain connectivity analysis in autism: A preliminary integrated approach with eeg, fmri and dti. *IEEE Transactions on Cognitive and Developmental Systems*, pages 1–1, 2017.

[113] N Mikita, E Simonoff, D S Pine, R Goodman, E Artiges, T Banaschewski, A L Bokde, U Bromberg, C Büchel, A Cattrell, P J Conrod, S Desrivières, H Flor, V Frouin, J Gallinat, H Garavan, A Heinz, B Ittermann, S Jurk, J L Martinot, M L Paillère Martinot, F Nees, D Papadopoulos Orfanos, T Paus, L Poustka, M N Smolka, H Walter, R Whelan, G Schumann, and A Stringaris. Disentangling the autism-anxiety overlap: fmri of reward processing in a community-based longitudinal study. *Translational Psychiatry*, 6:e845 EP –, 06 2016.

[114] M.T. Ismail Marwa, S. Keynton Robert, M. M. O. Mostapha Mahmoud, Ahmed H. ElTanboly, Manuel F. Casanova, L. Gimel'farb Georgy, and Ayman El-Baz. Studying autism spectrum disorder with structural and diffusion magnetic resonance imaging: A survey. *Frontiers in Human Neuroscience*, 10:211, 2016.

[115] Brittany G. Travers, Nagesh Adluru, Chad Ennis, Do P. M. Tromp, Dan Destiche, Sam Doran, Erin D. Bigler, Nicholas Lange, Janet E. Lainhart, and Andrew L. Alexander. Diffusion tensor imaging in autism spectrum disorder: A review. *Autism Research*, 5(5):289–313, 2012.

[116] Nicha C. Dvornek, Pamela Ventola, Kevin A. Pelphrey, and James S. Duncan. Identifying autism from resting-state fmri using long short-term memory networks. In Qian Wang, Yinghuan Shi, Heung-Il Suk, and Kenji Suzuki, editors, *Machine Learning in Medical Imaging*, pages 362–370, Cham, 2017. Springer International Publishing.

[117] Anibal Sólon Heinsfeld, Alexandre Rosa Franco, R. Cameron Craddock, Augusto Buchweitz, and Felipe Meneguzzi. Identification of autism spectrum disorder using deep learning and the abide dataset. *NeuroImage: Clinical*, 17:16–23, 2018.

[118] Maryam Akhavan Aghdam, Arash Sharifi, and Mir Mohsen Pedram. Combination of rs-fmri and smri data to discriminate autism spectrum disorders in young children using deep belief network. *Journal of Digital Imaging*, 2018.

[119] Takamitsu Watanabe and Geraint Rees. Brain network dynamics in high-functioning individuals with autism. *Nature Communications*, 8:16048 EP –, 07 2017.

[120] Colleen P. Chen, Christopher L. Keown, Afrooz Jahedi, Aarti Nair, Mark E. Pflieger, Barbara A. Bailey, and Ralph-Axel Müller. Diagnostic classification of intrinsic functional connectivity highlights somatosensory, default mode, and visual regions in autism. *NeuroImage: Clinical*, 8:238–245, 2015.

[121] Antoine Bernas, Evelien M. Barendse, Albert P. Aldenkamp, Walter H. Backes, Paul A. M. Hofman, Marc P. H. Hendriks, Roy P. C. Kessels, Frans M. J. Willems, Peter H. N. de With, Svitlana Zinger, and Jacobus F. A. Jansen. Brain resting state networks in adolescents with high functioning autism: Analysis of spatial connectivity and temporal neurodynamics. *Brain and Behavior*, 8(2):e00878, 2018/05/25 2018.

[122] Maryam Falahpour, Wesley K.Thompson, Angela E.Abbott, Afrooz Jahedi, Mark E.Mulvey, Michael Datko, Thomas T.Liu, and Ralph-Axel Muller. Underconnected, but not broken? dynamic functional connectivity mri shows underconnectivity in autism is linked to increased intra-individual variability across time. *Brain Connectivity*, 6(5), 2016.

[123] Lauren E Libero, Thomas P DeRamus, Adrienne C Lahti, Gopikrishna Deshpande, and Rajesh K Kana. Multimodal neuroimaging based classification of autism spectrum disorder using anatomical, neurochemical, and white matter correlates. *Cortex*, 66:46–59, 05 2015.

[124] Xin Di, Azeezat Azeez, Xiaobo Li, Emad Haque, and Bharat Biswal. Disrupted focal white matter integrity in autism spectrum disorder: A voxel-based meta-analysis of diffusion tensor imaging studies. *Progress in Neuro-Psychopharmacology and Biological Psychiatry*, 82:242–248, 03 2018.

[125] Yuta Aoki, Osamu Abe, Yasumasa Nippashi, and Hidenori Yamasue. Comparison of white matter integrity between autism spectrum disorder subjects and

typically developing individuals: a meta-analysis of diffusion tensor imaging tractography studies. *Molecular Autism*, 4:25–25, 2013.

[126] Sungji Ha, In-Jung Sohn, Namwook Kim, Hyeon Jeong Sim, and Keun-Ah Cheon. Characteristics of brains in autism spectrum disorder: Structure, function and connectivity across the lifespan. *Experimental Neurobiology*, 24(4):273–284, 12 2015.

[127] Anna Pichiecchio and Tiziana Carigi. Brain diffusion tensor imaging and volumetric analysis: Grey and white matter changes in preschool children with autism spectrum disorder. *Autism-Open Access*, 06, 01 2016.

[128] Gajendra J. Katuwal, Stefi A. Baum, Nathan D. Cahill, and Andrew M. Michael. Divide and conquer: Sub-grouping of asd improves asd detection based on brain morphometry. *PLOS ONE*, 11(4):e0153331–, 04 2016.

[129] G. J. Katuwal, N. D. Cahill, S. A. Baum, and A. M. Michael. The predictive power of structural mri in autism diagnosis. In *2015 37th Annual International Conference of the IEEE Engineering in Medicine and Biology Society (EMBC)*, pages 4270–4273, 2015.

[130] Guillaume Chanel, Swann Pichon, Laurence Conty, Sylvie Berthoz, Coralie Chevallier, and Julie Grèzes. Classification of autistic individuals and controls using cross-task characterization of fmri activity. *NeuroImage : Clinical*, 10:78–88, 2016.

[131] K. Nickel, L. Tebartz van Elst, E. Perlov, D. Endres, G. T. Müller, A. Riedel, T. Fangmeier, and S. Maier. Altered white matter integrity in adults with autism spectrum disorder and an iq >100: a diffusion tensor imaging study. *Acta Psychiatrica Scandinavica*, 135(6):573–583, 2017.

[132] Anibal Sólon Heinsfeld, Alexandre Rosa Franco, R. Cameron Craddock, Augusto Buchweitz, and Felipe Meneguzzi. Identification of autism spectrum disorder using deep learning and the abide dataset. *NeuroImage: Clinical*, 17:16 – 23, 2018.

[133] Tetsuya Iidaka. Resting state functional magnetic resonance imaging and neural network classified autism and control. *Cortex*, 63:55 – 67, 2015.

[134] Dongyun Li, Hans-Otto Karnath, and Xiu Xu. Candidate biomarkers in children with autism spectrum disorder: A review of mri studies. *Neuroscience Bulletin*, 33(2):219–237, Apr 2017.

[135] Patrick Chen and Weizhe Hong. Neural circuit mechanisms of social behavior. *Neuron*, 98(1):16 – 30, 2018.

[136] Dorothea L. Floris, Meng-Chuan Lai, Tibor Auer, Michael V. Lombardo, Christine Ecker, Bhismadev Chakrabarti, Sally J. Wheelwright, Edward T. Bullmore, Declan G.M. Murphy, Simon Baron-Cohen, and John Suckling. Atypically rightward cerebral asymmetry in male adults with autism stratifies individuals with and without language delay. *Human Brain Mapping*, 37(1):230–253, 2016.

[137] Elizabeth J Carter, Diane L Williams, Nancy J Minshew, and Jill F Lehman. Is he being bad? social and language brain networks during social judgment in children with autism. *PLoS One*, 7(10):e47241–e47241, 2012.

[138] K. O'Connor. Auditory processing in autism spectrum disorder: A review. *Neuroscience & Biobehavioral Reviews*, 36(2):836 – 854, 2012.

[139] Leanne Chukoskie, Jeanne Townsend, and Marissa Westerfield. Chapter seven - motor skill in autism spectrum disorders: A subcortical view. In Genevieve Konopka, editor, *Neurobiology of Autism*, volume 113 of *International Review of Neurobiology*, pages 207 – 249. Academic Press, 2013.

[140] Lindsay M. Oberman, Edward M. Hubbard, Joseph P. McCleery, Eric L. Altschuler, Vilayanur S. Ramachandran, and Jaime A. Pineda. Eeg evidence for mirror neuron dysfunction in autism spectrum disorders. *Cognitive Brain Research*, 24(2):190 – 198, 2005.

[141] Antonia F. de C. Hamilton. Reflecting on the mirror neuron system in autism: A systematic review of current theories. *Developmental Cognitive Neuroscience*, 3:91–105, 2013.

[142] Manuela Schuetze, Min Tae M Park, Ivy YK Cho, Frank P MacMaster, M Mallar Chakravarty, and Signe L Bray. Morphological alterations in the thalamus, striatum, and pallidum in autism spectrum disorder. *Neuropsychopharmacology*, 41:2627 EP –, 04 2016.

[143] Budhachandra S. Khundrakpam, John D. Lewis, Penelope Kostopoulos, Felix Carbonell, and Alan C. Evans. Cortical thickness abnormalities in autism spectrum disorders through late childhood, adolescence, and adulthood: A large-scale mri study. *Cerebral Cortex*, 27(3):1721–1731, 2017.

[144] Daniel Y.-J. Yang, Danielle Beam, Kevin A. Pelphrey, Sebiha Abdullahi, and Roger J. Jou. Cortical morphological markers in children with autism: a structural magnetic resonance imaging study of thickness, area, volume, and gyrification. *Molecular Autism*, 7(1):11, Jan 2016.

[145] E. Conti, J. Mitra, S. Calderoni, K. Pannek, K. K. Shen, A. Pagnozzi, S. Rose, S. Mazzotti, D. Scelfo, M. Tosetti, F. Muratori, G. Cioni, and A. Guzzetta. Network over-connectivity differentiates autism spectrum disorder from other developmental disorders in toddlers: A diffusion MRI study. *Human Brain Mapping*, 38(5):2333–2344, 2017.

[146] Jocelyn V Hull, Zachary J Jacokes, Carinna M Torgerson, Andrei Irimia, and John Darrell Van Horn. Resting-state functional connectivity in autism spectrum disorders: A review. *Frontiers in Psychiatry*, 7:205, 2016.

[147] Takashi Yamada, Takashi Itahashi, Motoaki Nakamura, Hiromi Watanabe, Miho Kuroda, Haruhisa Ohta, Chieko Kanai, Nobumasa Kato, and Ryuichiro Hashimoto. Altered functional organization within the insular cortex in adult males with high-functioning autism spectrum disorder: evidence from connectivity-based parcellation. *Molecular Autism*, 7(1):41, Oct 2016.

[148] Yuko Okamoto, Ryo Kitada, Hiroki C Tanabe, Masamichi J Hayashi, Takanori Kochiyama, Toshio Munesue, Makoto Ishitobi, Daisuke N Saito, Hisakazu T Yanaka, Masao Omori, Yuji Wada, Hidehiko Okazawa, Akihiro T Sasaki, Tomoyo Morita, Shoji Itakura, Hirotaka Kosaka, and Norihiro Sadato. Attenuation of the contingency detection effect in the extrastriate body area in autism spectrum disorder. *Neurosci Res*, 87:66–76, 2014.

[149] Kevin A Pelphrey and Elizabeth J Carter. Charting the typical and atypical development of the social brain. *Dev Psychopathol*, 20(4):1081–1102, 2008.

[150] Elizabeth Redcay. The superior temporal sulcus performs a common function for social and speech perception: Implications for the emergence of autism. *Neuroscience & Biobehavioral Reviews*, 32(1):123 – 142, 2008.

[151] Thierry Chaminade, David Da Fonseca, Delphine Rosset, Gordon Cheng, and Christine Deruelle. Atypical modulation of hypothalamic activity by social context in asd. *Research in Autism Spectrum Disorders*, 10:41 – 50, 2015.

[152] Clare Gibbard. *Structural connectivity of the brain in autism spectrum disorder*. PhD thesis, UCL (University College London), 2016.

[153] Adonay S. Nunes, Nicholas Peatfield, Vasily Vakorin, and Sam M. Doesburg. Idiosyncratic organization of cortical networks in autism spectrum disorder. *NeuroImage*, 2018.

[154] AE Abbott, A Nair, CL Keown, M Datko, A Jahedi, I Fishman, and RA Muller. Patterns of atypical functional connectivity and behavioral links in autism differ between default, salience, and executive networks. *Cereb Cortex.*, 26(10):4034–45, 2016.

[155] Nair Aarti, Carper Ruth A., Abbott Angela E., Chen Colleen P., Solders Seraphina, Nakutin Sarah, Datko Michael C., Fishman Inna, and Müller Ralph-Axel. Regional specificity of aberrant thalamocortical connectivity in autism. *Human Brain Mapping*, 36(11):4497–4511, 2015.

[156] Kajsa M. Igelstrom, Taylor W. Webb, and Michael S. A. Graziano. Functional connectivity between the temporoparietal cortex and cerebellum in autism spectrum disorder. *Cerebral Cortex*, 27(4):2617–2627, 2017.

[157] J. Wang, Q. Wang, H. Zhang, J. Chen, S. Wang, and D. Shen. Sparse multiview task-centralized ensemble learning for asd diagnosis based on age- and sex-related functional connectivity patterns. *IEEE Transactions on Cybernetics*, 49(8):3141–3154, 2019.

[158] Y Zhu, X Zhu, M Kim, J Yan, and G Wu. A tensor statistical model for quantifying dynamic functional connectivity. *Inf Process Med Imaging.*, 10265:398–410, 2017.

[159] Chong-Yaw Wee, Pew-Thian Yap, and Dinggang Shen. Diagnosis of autism spectrum disorders using temporally distinct resting-state functional connectivity networks. *CNS Neuroscience & Therapeutics*, 22(3):212–219, 2016.

[160] Yingying Zhu, Xiaofeng Zhu, Han Zhang, Wei Gao, Dinggang Shen, and Guorong Wu. Reveal consistent spatial-temporal patterns from dynamic functional connectivity for autism spectrum disorder identification. In Sebastien Ourselin, Leo Joskowicz, Mert R. Sabuncu, Gozde Unal, and William Wells, editors, *Medical Image Computing and Computer-Assisted Intervention – MICCAI 2016*, pages 106–114, Cham, 2016. Springer International Publishing.

[161] Xiang Xiao, Hui Fang, Jiansheng Wu, ChaoYong Xiao, Ting Xiao, Lu Qian, FengJing Liang, Zhou Xiao, Kang Kang Chu, and Xiaoyan Ke. Diagnostic model generated by MRI-derived brain features in toddlers with autism spectrum disorder. *Autism Research*, 10(4):620–630, 2016.

[162] Noriaki Yahata, Jun Morimoto, Ryuichiro Hashimoto, Giuseppe Lisi, Kazuhisa Shibata, Yuki Kawakubo, Hitoshi Kuwabara, Miho Kuroda, Takashi Yamada, Fukuda Megumi, Hiroshi Imamizu, JoséE. Náñez Sr, Hidehiko Takahashi, Yasumasa Okamoto, Kiyoto Kasai, Nobumasa Kato, Yuka Sasaki, Takeo Watanabe, and Mitsuo Kawato. A small number of abnormal brain

connections predicts adult autism spectrum disorder. *Nature Communications*, 7(1):11254, 2016.

[163] Wang Jun, Wang Qian, Peng Jialin, Nie Dong, Zhao Feng, Kim Minjeong, Zhang Han, Wee Chong-Yaw, Wang Shitong, and Shen Dinggang. Multi-task diagnosis for autism spectrum disorders using multi-modality features: A multi-center study. *Human Brain Mapping*, 38(6):3081–3097, 2017.

[164] B J Casey, Tariq Cannonier, May I Conley, Alexandra O Cohen, Deanna M Barch, Mary M Heitzeg, Mary E Soules, Theresa Teslovich, Danielle V Dellarco, Hugh Garavan, Catherine A Orr, Tor D Wager, Marie T Banich, Nicole K Speer, Matthew T Sutherland, Michael C Riedel, Anthony S Dick, James M Bjork, Kathleen M Thomas, Bader Chaarani, Margie H Mejia, Donald J Jr Hagler, M Daniela Cornejo, Chelsea S Sicat, Michael P Harms, Nico U F Dosenbach, Monica Rosenberg, Eric Earl, Hauke Bartsch, Richard Watts, Jonathan R Polimeni, Joshua M Kuperman, Damien A Fair, and Anders M Dale. The adolescent brain cognitive development (abcd) study: Imaging acquisition across 21 sites. *Dev Cogn Neurosci*, 32:43–54, Aug 2018.

[165] FJ Martinez-Murcia, MC Lai, JM Gorriz, J Ramirez, AM Young, SC Deoni, C Ecker, MV Lombardo, MRC AIMS Consortium, S Baron-Cohen, DG Murphy, ET Bullmore, and J Suckling. On the brain structure heterogeneity of autism: Parsing out acquisition site effects with significance–weighted principal component analysis. *Human Brain Mapping*, 38(3):1208–1223, 2018/08/13 2016.

[166] Reem Al-jawahiri, Elizabeth Milne, and Jon Brock. Resources available for autism research in the big data era: a systematic review. *PeerJ*, 5:e2880, 2017.

[167] Adriana Di Martino, Chao-Gan Yan, Qingyang Li, Erin Denio, Francisco X Castellanos, Kaat Alaerts, Jeffrey S Anderson, Michal Assaf, Susan Y Bookheimer, Mirella Dapretto, Ben Deen, Sonja Delmonte, Ilan Dinstein, Birgit Ertl-Wagner, Damien A Fair, Louise Gallagher, Daniel P Kennedy, Christopher L Keown, Christian Keysers, Janet E Lainhart, Catherine Lord,

Beatriz Luna, Vinod Menon, Nancy Minshew, Christopher S Monk, Sophia Mueller, Ralph-Axel Müller, Mary Beth Nebel, Joel T Nigg, Kirsten O'Hearn, Kevin A Pelphrey, Scott J Peltier, Jeffrey D Rudie, Stefan Sunaert, Marc Thioux, J Michael Tyszka, Lucina Q Uddin, Judith S Verhoeven, Nicole Wenderoth, Jillian L Wiggins, Stewart H Mostofsky, and Michael P Milham. The autism brain imaging data exchange: Towards large-scale evaluation of the intrinsic brain architecture in autism. *Molecular psychiatry*, 19(6):659–667, 06 2014.

[168] Adriana Di Martino, David O'Connor, Bosi Chen, Kaat Alaerts, Jeffrey S. Anderson, Michal Assaf, Joshua H. Balsters, Leslie Baxter, Anita Beggiato, Sylvie Bernaerts, Laura M. E. Blanken, Susan Y. Bookheimer, B. Blair Braden, Lisa Byrge, F. Xavier Castellanos, Mirella Dapretto, Richard Delorme, Damien A. Fair, Inna Fishman, Jacqueline Fitzgerald, Louise Gallagher, R. Joanne Jao Keehn, Daniel P. Kennedy, Janet E. Lainhart, Beatriz Luna, Stewart H. Mostofsky, Ralph-Axel Müller, Mary Beth Nebel, Joel T. Nigg, Kirsten O'Hearn, Marjorie Solomon, Roberto Toro, Chandan J. Vaidya, Nicole Wenderoth, Tonya White, R. Cameron Craddock, Catherine Lord, Bennett Leventhal, and Michael P. Milham. Enhancing studies of the connectome in autism using the autism brain imaging data exchange ii. *Scientific Data*, 4:170010 EP –, 03 2017.

[169] Taban Eslami. *High Performance and Machine Learning Algorithms for Brain fMRI Data fMRI Data.* PhD thesis, Western Michigan University Western Michigan Univ, April 2020.

[170] Gary H. Glover. Overview of functional magnetic resonance imaging. *Neurosurgery Clinics of North America*, 22(2):133–139, apr 2011.

[171] WikiBooks. Neuroimaging data processing/realignment. Technical report, WikiBooks, https://en.wikibooks.org/wiki/Neuroimaging$_{D}ata_{P}rocessing/Realignment, April$2021.

[172] Katrin Amunts and Karl Zilles. Architectonic mapping of the human brain beyond brodmann. *Neuron*, 88(6):1086–1107, dec 2015.

[173] Jonathan D. Power, Alexander L. Cohen, Steven M. Nelson, Gagan S. Wig, Kelly Anne Barnes, Jessica A. Church, Alecia C. Vogel, Timothy O. Laumann, Fran M. Miezin, Bradley L. Schlaggar, and Steven E. Petersen. Functional network organization of the human brain. *Neuron*, 72(4):665 – 678, 2011.

[174] Nico U. F. Dosenbach, Binyam Nardos, Alexander L. Cohen, Damien A. Fair, Jonathan D. Power, Jessica A. Church, Steven M. Nelson, Gagan S. Wig, Alecia C. Vogel, Christina N. Lessov-Schlaggar, Kelly Anne Barnes, Joseph W. Dubis, Eric Feczko, Rebecca S. Coalson, John R. Pruett, Deanna M. Barch, Steven E. Petersen, and Bradley L. Schlaggar. Prediction of individual brain maturity using fmri. *Science*, 329(5997):1358–1361, 2010.

[175] Alexandre Abraham, Michael P. Milham, Adriana Di Martino, R. Cameron Craddock, Dimitris Samaras, Bertrand Thirion, and Gael Varoquaux. Deriving reproducible biomarkers from multi-site resting-state data: An autism-based example. *NeuroImage*, 147:736 – 745, 2017.

[176] Kamalaker Dadi, Mehdi Rahim, Alexandre Abraham, Darya Chyzhyk, Michael Milham, Bertrand Thirion, and Gaël Varoquaux. Benchmarking functional connectome-based predictive models for resting-state fMRI. *NeuroImage*, 192:115–134, may 2019.

[177] Simon B. Eickhoff, Tomas Paus, Svenja Caspers, Marie-Helene Grosbras, Alan C. Evans, Karl Zilles, and Katrin Amunts. Assignment of functional activations to probabilistic cytoarchitectonic areas revisited. *NeuroImage*, 36(3):511 – 521, 2007.

[178] Rahul S. Desikan, Florent Ségonne, Bruce Fischl, Brian T. Quinn, Bradford C. Dickerson, Deborah Blacker, Randy L. Buckner, Anders M. Dale, R. Paul Maguire, Bradley T. Hyman, Marilyn S. Albert, and Ronald J. Killiany. An automated labeling system for subdividing the human cerebral cortex on mri scans into gyral based regions of interest. *NeuroImage*, 31(3):968 – 980, 2006.

[179] Edmund T. Rolls, Chu-Chung Huang, Ching-Po Lin, Jianfeng Feng, and Marc Joliot. Automated anatomical labelling atlas 3. *NeuroImage*, page 116189, 2019.

[180] N. Tzourio-Mazoyer, B. Landeau, D. Papathanassiou, F. Crivello, O. Etard, N. Delcroix, B. Mazoyer, and M. Joliot. Automated anatomical labeling of activations in spm using a macroscopic anatomical parcellation of the mni mri single-subject brain. *NeuroImage*, 15(1):273 – 289, 2002.

[181] R. Cameron Craddock, G.Andrew James, Paul E. Holtzheimer III, Xiaoping P. Hu, and Helen S. Mayberg. A whole brain fmri atlas generated via spatially constrained spectral clustering. *Human Brain Mapping*, 33(8):1914–1928, 2012.

[182] Wieslaw L Nowinski and Dmitry Belov. The cerefy neuroradiology atlas: a talairach–tournoux atlas-based tool for analysis of neuroimages available over the internet. *NeuroImage*, 20(1):50–57, sep 2003.

[183] R. Cameron Craddock, G.Andrew James, Paul E. Holtzheimer, Xiaoping P. Hu, and Helen S. Mayberg. A whole brain fMRI atlas generated via spatially constrained spectral clustering. *Human Brain Mapping*, 33(8):1914–1928, jul 2011.

[184] Olivier Ledoit and Michael Wolf. A well-conditioned estimator for large-dimensional covariance matrices. *Journal of Multivariate Analysis*, 88(2):365 – 411, 2004.

[185] Karl Pearson. Notes on regression and inheritance in the case of two parents. *Proceedings of the Royal Society of London*, 58:240–242, 1895.

[186] Andrew Zalesky, Alex Fornito, and Ed Bullmore. On the use of correlation as a measure of network connectivity. *NeuroImage*, 60(4):2096 – 2106, 2012.

[187] Stephen M. Smith, Karla L. Miller, Gholamreza Salimi-Khorshidi, Matthew Webster, Christian F. Beckmann, Thomas E. Nichols, Joseph D. Ramsey, and Mark W. Woolrich. Network modelling methods for fmri. *NeuroImage*, 54(2):875 – 891, 2011.

[188] G. Varoquaux, F. Baronnet, A. Kleinschmidt, P. Fillard, and B. Thirion. Detection of brain functional-connectivity difference in post-stroke patients using group-level covariance modeling. In *MICCAI*, 2010.

[189] Sarah Parisot, Sofia Ira Ktena, Enzo Ferrante, Matthew Lee, Ricardo Guerrero, Ben Glocker, and Daniel Rueckert. Disease prediction using graph convolutional

networks: Application to autism spectrum disorder and alzheimer's disease. *Medical Image Analysis*, 48:117 – 130, 2018.

[190] Sofia Ira Ktena, Sarah Parisot, Enzo Ferrante, Martin Rajchl, Matthew Lee, Ben Glocker, and Daniel Rueckert. Distance metric learning using graph convolutional networks: Application to functional brain networks, 2017.

[191] Sarah Parisot, Sofia Ira Ktena, Enzo Ferrante, Matthew Lee, Ricardo Guerrerro Moreno, Ben Glocker, and Daniel Rueckert. Spectral graph convolutions for population-based disease prediction, 2017.

[192] R. Anirudh and J. J. Thiagarajan. Bootstrapping graph convolutional neural networks for autism spectrum disorder classification. In *ICASSP 2019 - 2019 IEEE International Conference on Acoustics, Speech and Signal Processing (ICASSP)*, pages 3197–3201, May 2019.

[193] M. N. Parikh, H. Li, and L. He. Enhancing Diagnosis of Autism With Optimized Machine Learning Models and Personal Characteristic Data. *Front Comput Neurosci*, 13:9, 2019.

[194] Nicha C. Dvornek, Pamela Ventola, Kevin A. Pelphrey, and James S. Duncan. Identifying autism from resting-state fmri using long short-term memory networks. In Qian Wang, Yinghuan Shi, Heung-Il Suk, and Kenji Suzuki, editors, *Machine Learning in Medical Imaging*, pages 362–370, Cham, 2017. Springer International Publishing.

[195] Ravi Tejwani, Adam Liska, Hongyuan You, Jenna Reinen, and Payel Das. Autism classification using brain functional connectivity dynamics and machine learning. 2017.

[196] Julia Leonard, John Flournoy, Christine Paula Lewis de los Angeles, and Kirstie Whitaker. How much motion is too much motion? determining motion thresholds by sample size for reproducibility in developmental resting-state MRI. *Research Ideas and Outcomes*, 3:e12569, mar 2017.

[197] Swati Rane, Eshin Jolly, Anne Park, Hojin Jang, and Cameron Craddock. Developing predictive imaging biomarkers using whole-brain classifiers: Application to the ABIDE i dataset. *Research Ideas and Outcomes*, 3:e12733, mar 2017.

[198] Chandan Singh, Beilun Wang, and Yanjun Qi. A constrained, weighted-l1 minimization approach for joint discovery of heterogeneous neural connectivity graphs. 2017.

[199] Meenakshi Khosla, Keith Jamison, Amy Kuceyeski, and Mert R. Sabuncu. Ensemble learning with 3d convolutional neural networks for functional connectome-based prediction. *NeuroImage*, 199:651–662, oct 2019.

[200] Colin J. Brown, Steven P. Miller, Brian G. Booth, Jill G. Zwicker, Ruth E. Grunau, Anne R. Synnes, Vann Chau, and Ghassan Hamarneh. Predictive connectome subnetwork extraction with anatomical and connectivity priors. *Computerized Medical Imaging and Graphics*, 71:67 – 78, 2019.

[201] Qin Li, Benjamin Becker, Xi Jiang, Zhiying Zhao, Qiong Zhang, Shuxia Yao, and Keith M. Kendrick. Decreased interhemispheric functional connectivity rather than corpus callosum volume as a potential biomarker for autism spectrum disorder. *Cortex*, 119:258 – 266, 2019.

[202] Sofia Ira Ktena, Sarah Parisot, Enzo Ferrante, Martin Rajchl, Matthew Lee, Ben Glocker, and Daniel Rueckert. Metric learning with spectral graph convolutions on brain connectivity networks. *NeuroImage*, 169:431 – 442, 2018.

[203] Matthew Leming, Juan Manuel Górriz, and John Suckling. Ensemble deep learning on large, mixed-site fmri datasets in autism and other tasks. *International Journal of Neural Systems*, online first(0):2050012, 2020. PMID: 32308082.

[204] Abdelbasset Brahim and Nicolas Farrugia. Graph fourier transform of fmri temporal signals based on an averaged structural connectome for the classification of neuroimaging. *Artificial Intelligence in Medicine*, 106:101870, 2020.

[205] Vigneshwaran Subbaraju, Mahanand Belathur Suresh, Suresh Sundaram, and Sundararajan Narasimhan. Identifying differences in brain activities and an accurate

detection of autism spectrum disorder using resting state functional-magnetic resonance imaging : A spatial filtering approach. *Medical Image Analysis*, 35:375 – 389, 2017.

[206] Mladen Rakić, Mariano Cabezas, Kaisar Kushibar, Arnau Oliver, and Xavier Lladó. Improving the detection of autism spectrum disorder by combining structural and functional mri information. *NeuroImage: Clinical*, 25:102181, 2020.

[207] M. Wang, D. Zhang, J. Huang, P. Yap, D. Shen, and M. Liu. Identifying autism spectrum disorder with multi-site fmri via low-rank domain adaptation. *IEEE Transactions on Medical Imaging*, 39(3):644–655, 2020.

[208] Juan M. Gorriz, Javier Ramirez, Andres Ortiz, Francisco J. Martinez-Murcia, Fermin Segovia, John Suckling, Matthew Leming, Yu-Dong Zhang, Jose Ramon Alvarez-Sanchez, Guido Bologna, Paula Bonomini, Fernando E. Casado, David Charte, Francisco Charte, Ricardo Contreras, Alfredo Cuesta-Infante, Richard J. Duro, Antonio Fernandez-Caballero, Eduardo Fernandez-Jover, Pedro Gomez-Vilda, Manuel Graña, Francisco Herrera, Roberto Iglesias, Anna Lekova, Javier de Lope, Ezequiel Lopez-Rubio, Rafael Martinez-Tomas, Miguel A. Molina-Cabello, Antonio S. Montemayor, Paulo Novais, Daniel Palacios-Alonso, Juan J. Pantrigo, Bryson R. Payne, Felix de la Paz Lopez, Maria Angelica Pinninghoff, Mariano Rincon, Jose Santos, Karl Thurnhofer-Hemsi, Athanasios Tsanas, Ramiro Varela, and Jose M. Ferrandez. Artificial intelligence within the interplay between natural and artificial computation: Advances in data science, trends and applications. *Neurocomputing*, 410:237 – 270, 2020.

[209] Sun Jae Moon, Jinseub Hwang, Rajesh Kana, John Torous, and Jung Won Kim. Accuracy of machine learning algorithms for the diagnosis of autism spectrum disorder: Systematic review and meta-analysis of brain magnetic resonance imaging studies. *JMIR Ment Health*, 6(12):e14108, Dec 2019.

[210] Juan M. Górriz, Javier Ramírez, F. Segovia, Francisco J. Martínez, Meng-Chuan Lai, Michael V. Lombardo, Simon Baron-Cohen, and John Suckling and. A machine

learning approach to reveal the NeuroPhenotypes of autisms. *International Journal of Neural Systems*, 29(07):1850058, aug 2019.

[211] Vigneshwaran Subbaraju, Suresh Sundaram, Sundararajan Narasimhan, and Mahanand Belathur Suresh. Accurate detection of autism spectrum disorder from structural mri using extended metacognitive radial basis function network. *Expert Systems with Applications*, 42(22):8775 – 8790, 2015.

[212] Hossein Shahamat and Mohammad Saniee Abadeh. Brain mri analysis using a deep learning based evolutionary approach. *Neural Networks*, 126:218 – 234, 2020.

[213] Francisco Jesus Martinez-Murcia, Meng-Chuan Lai, Juan Manuel Gorriz, Javier Ramirez, Adam M. H. Young, Sean C. L. Deoni, Christine Ecker, Michael V. Lombardo, MRC AIMS Consortium, Simon Baron-Cohen, Declan G. M. Murphy, Edward T. Bullmore, and John Suckling. On the brain structure heterogeneity of autism: Parsing out acquisition site effects with significance-weighted principal component analysis. *Human Brain Mapping*, 38(3):1208–1223, 2017.

[214] Lucina Q. Uddin, Kaustubh Supekar, Charles J. Lynch, Amirah Khouzam, Jennifer Phillips, Carl Feinstein, Srikanth Ryali, and Vinod Menon. Salience Network–Based Classification and Prediction of Symptom Severity in Children With Autism. *JAMA Psychiatry*, 70(8):869–879, 08 2013.

[215] Robert X. Smith, Kay Jann, Mirella Dapretto, and Danny J. J. Wang. Imbalance of functional connectivity and temporal entropy in resting-state networks in autism spectrum disorder: A machine learning approach. *Frontiers in Neuroscience*, 12:869, 2018.

[216] Xinyu Guo, Kelli C. Dominick, Ali A. Minai, Hailong Li, Craig A. Erickson, and Long J. Lu. Diagnosing autism spectrum disorder from brain resting-state functional connectivity patterns using a deep neural network with a novel feature selection method. *Frontiers in Neuroscience*, 11, aug 2017.

[217] Xiaoxiao Li, Yufeng Gu, Nicha Dvornek, Lawrence H. Staib, Pamela Ventola, and James S. Duncan. Multi-site fmri analysis using privacy-preserving federated learn-

ing and domain adaptation: Abide results. *Medical Image Analysis*, 65:101765, 2020.

[218] Canhua Wang, Zhiyong Xiao, and Jianhua Wu. Functional connectivity-based classification of autism and control using svm-rfecv on rs-fmri data. *Physica Medica*, 65:99 – 105, 2019.

[219] Maciel C. Vidal, João R. Sato, Joana B. Balardin, Daniel Y. Takahashi, and André Fujita. ANOCVA in r: A software to compare clusters between groups and its application to the study of autism spectrum disorder. *Frontiers in Neuroscience*, 11, jan 2017.

[220] Joanne C. Beer, Howard J. Aizenstein, Stewart J. Anderson, and Robert T. Krafty. Incorporating prior information with fused sparse group lasso: Application to prediction of clinical measures from neuroimages. *Biometrics*, June 2019.

[221] Yazhou Kong, Jianliang Gao, Yunpei Xu, Yi Pan, Jianxin Wang, and Jin Liu. Classification of autism spectrum disorder by combining brain connectivity and deep neural network classifier. *Neurocomputing*, 324:63 – 68, 2019. Deep Learning for Biological/Clinical Data.

[222] Seok-Jun Hong, Reinder Vos de Wael, Richard A. I. Bethlehem, Sara Lariviere, Casey Paquola, Sofie L. Valk, Michael P. Milham, Adriana Di Martino, Daniel S. Margulies, Jonathan Smallwood, and Boris C. Bernhardt. Atypical functional connectome hierarchy in autism. *Nature Communications*, 10(1):1022, 2019.

[223] Kenia Martínez, Magdalena Martínez-García, Luis Marcos-Vidal, Joost Janssen, Francisco X. Castellanos, Clara Pretus, Óscar Villarroya, Laura Pina-Camacho, Covadonga M. Díaz-Caneja, Mara Parellada, Celso Arango, Manuel Desco, Jorge Sepulcre, and Susanna Carmona. Sensory-to-cognitive systems integration is associated with clinical severity in autism spectrum disorder. *Journal of the American Academy of Child & Adolescent Psychiatry*, 2019.

[224] Katherine S. Button. Double-dipping revisited. *Nature Neuroscience*, 22(5):688–690, 2019.

[225] Nikolaus Kriegeskorte, W Kyle Simmons, Patrick S F Bellgowan, and Chris I Baker. Circular analysis in systems neuroscience: the dangers of double dipping. *Nature Neuroscience*, 12(5):535–540, 2009.

[226] Miguel A. Molina-Cabello, Rafael Marcos Luque-Baena, Ezequiel Lopez-Rubio, and Karl Thurnhofer-Hemsi. Vehicle type detection by ensembles of convolutional neural networks operating on super resolved images. *Integrated Computer-Aided Engineering*, 25:321–333, 2018.

[227] Peng Wang and Xiangzhi Bai. Regional parallel structure based cnn for thermal infrared face identification. *Integrated Computer-Aided Engineering*, 25:247–260, 2018.

[228] J. F. Torres, A. Galicia, A. Troncoso, and F. Martinez-Alvarez. A scalable approach based on deep learning for big data time series forecasting. *Integrated Computer-Aided Engineering*, 25:335–348, 2018.

[229] F. J. Vera-Olmos, E. Pardo, H. Melero, and N. Malpica. Deepeye: Deep convolutional network for pupil detection in real environments. *Integrated Computer-Aided Engineering*, 26:85–95, 2019.

[230] Tao Yang, Cindy Cappelle, Yassine Ruichek, and Mohammed El Bagdouri. Multi-object tracking with discriminant correlation filter based deep learning tracker. *Integrated Computer-Aided Engineering*, 26:273–284, 2019.

[231] Keisuke Maeda, Sho Takahashi, Takahiro Ogawa, and Miki Haseyama. Convolutional sparse coding-based deep random vector functional link network for distress classification of road structures. *Computer-Aided Civil and Infrastructure Engineering*, 34(8):654–676, 2019.

[232] Seongdeok Bang, Somin Park, Hongjo Kim, and Hyoungkwan Kim. Encoder–decoder network for pixel-level road crack detection in black-box images. *Computer-Aided Civil and Infrastructure Engineering*, 34(8):713–727, 2019.

[233] Gilles Louppe. *UNDERSTANDING RANDOM FORESTS from theory to practice*. PhD thesis, University of LiÃšge, 2014.

[234] Fabian Pedregosa, Gael Varoquaux, Alexandre Gramfort, Vincent Michel, Bertrand Thirion, Olivier Grisel, Mathieu Blondel, Peter Prettenhofer, Ron Weiss, Vincent Dubourg, Jake Vanderplas, Alexandre Passos, David Cournapeau, Matthieu Brucher, Matthieu Perrot, and Edouard Duchesnay. Scikit-learn: Machine learning in python. *JMLR*, 12:2825–2830, 2011.

[235] L. Breiman. Random forests. *Machine Learning*, 45(1):5–32, 2001.

[236] L. Breiman, J. Friedman, R. Olshen, and C. Stone. *Classification and Regression Trees*. Wadsworth, Belmont, CA, 1984.

[237] Matthias Schonlau and Rosie Yuyan Zou. The random forest algorithm for statistical learning. 20:3–29, 2020.

[238] Tin Kam Ho. Random decision forests.

[239] Leo Breiman. 45:5–32, 2001.

[240] R. Tibshirani T. Hastie and J. Friedman. *Elements of Statistical Learning*. Springer, 2009.

[241] Evelyn Fix and J. L. Hodges. Discriminatory analysis. nonparametric discrimination: Consistency properties. *International Statistical Review / Revue Internationale de Statistique*, 57(3):238–247, 1989.

[242] Kevin Zakka. A complete guide to k-nearest-neighbors with applications in python and r. Technical report, https://kevinzakka.github.io/2016/07/13/k-nearest-neighbor/, April 2020.

[243] Ali Haghpanah Jahromi and Mohammad Taheri. A non-parametric mixture of gaussian naive bayes classifiers based on local independent features, 2017.

[244] Liangxiao Jiang, Zhihua Cai, Harry Zhang, and Dianhong Wang. Naive bayes text classifiers: a locally weighted learning approach. 25:273–286, 2013.

[245] C. Hue, M. BoullÃ©, and V. Lemaire. Online learning of a weighted selective naive bayes classifier with non-convex optimization. *Advances in Knowledge Discovery and Management (AKDM-6)*, 665:3–17, 2017.

[246] Andrew Ng and Michael Jordan. On discriminative vs. generative classifiers: A comparison of logistic regression and naive bayes. In T. Dietterich, S. Becker, and Z. Ghahramani, editors, *Advances in Neural Information Processing Systems*, volume 14. MIT Press, 2002.

[247] David Heckerman, Dan Geiger, and David M. Chickering. Learning bayesian networks: The combination of knowledge and statistical data. 20:197–243, 1995.

[248] Philippe Besnard. *Estimating continuous distributions in bayesian classifiers; Uncertainty in artificial intelligence : proceedings of the Eleventh Conference (1995) : August 18-20, 1995.* Morgan Kaufmann Publishers, San Francisco, Calif, 1995.

[249] Nello Cristianini and Elisa Ricci. *Support Vector Machines*, pages 928–932. Springer US, Boston, MA, 2008.

[250] C. Cortes and V. Vapnik. Support-vector network. *Mach. Learn.*, 20:273–297, 1995.

[251] D. R. Cox. *Principles of statistical inference.* Cambridge University Press, Cambridge New York, 2006.

[252] Vladimir Vapnik. *Tong ji xue xi li lun de ben zhi.* Qing hua da xue chu ban she, Beijing, 2000.

[253] Burges Christopher J.C. A tutorial on support vector machines for patternrecognition. 1998.

[254] Vladimir Vapnik, Steven Golowich, and Alex Smola. Support vector method for function approximation, regression estimation and signal processing. In M. C. Mozer, M. Jordan, and T. Petsche, editors, *Advances in Neural Information Processing Systems*, volume 9. MIT Press, 1997.

[255] D.A. Freedman. *Statistical Models: Theory and Practice.* Cambridge University Press, 2009.

[256] Fang-Lan Hsiang-Fu Yu and Chih-Jen Lin Huang. Dual coordinate descent methods for logistic regression and maximum entropy models. *Machine Learning*, 85(1–2):41–75, 2011.

[257] SH Walker and DB Duncan. Estimation of the probability of an event as a function of several independent variables. *Biometrika*, 54:167–178, 1967.

[258] Robert Tibshirani. Regression shrinkage and selection via the lasso. *Journal of the Royal Statistical Society. Series B (methodological)*, 58(1):267–88, 1996.

[259] Scott Shaobing Chen, David L. Donoho, and Michael A. Saunders. Atomic decomposition by basis pursuit. *SIAM Journal on Scientific Computing*, 20(1):33–61, jan 1998.

[260] A.E. Hoerl. Application of ridge analysis to regression problems. *Chemical Engineering Progress*, 58(3):54–59, 1962.

[261] A.N. Tikhonov and V.Y. Arsenin. *Solution of Ill-posed Problems*. Winston & Sons, Washington, 1977.

[262] Arthur E. Hoerl and Robert W. Kennard. Ridge regression: Biased estimation for nonorthogonal problems. *Technometrics*, 12(1):55–67, feb 1970.

[263] M.E. Tipping. Sparse bayesian learning and the relevance vector machine. *Journal of Machine Learning Research*, 1:211–244, 2001.

[264] G.E. Hinton. Connectionist learning procedures. *Artificial intelligence*, 40:185–234, 1989.

[265] W. S. McCulloch and W. Pitts. A logical calculus of the ideas immanent in nervous activity. 1943. *Bulletin of mathematical biology*, 52:99–115; discussion 73–97, 1990.

[266] F. ROSENBLATT. The perceptron: a probabilistic model for information storage and organization in the brain. *Psychological review*, 65:386–408, November 1958.

[267] M. Tipping and C. Bishop. Probabilistic principal component analysis. *Journal of the Royal Statistical Society Series B*, 61(Part 3):611–622, 2002.

[268] I. T. Jolliffe. *Principal Component Analysis*. Springer-Verlag GmbH, November 2002.

[269] H. Hotelling. Analysis of a complex of statistical variables into principal components. *Journal of Educational Psychology*, 24(6):417–441, 1933.

[270] Michael E. Tipping and Christopher M. Bishop. Probabilistic principal component analysis. *Royal Statistical Society, SeriesB, 61, Part 3, pp. 611â622*, 1999.

[271] Karl Pearson. LIII. on lines and planes of closest fit to systems of points in space. *The London, Edinburgh, and Dublin Philosophical Magazine and Journal of Science*, 2(11):559–572, nov 1901.

[272] Joshua B. Tenenbaum, Vin de Silva, and John C. Langford. A global geometric framework for nonlinear dimensionality reduction. *Science*, 290(5500):2319–2323, 2000.

[273] Mukund Balasubramanian and Eric Schwartz. Schwartz, e.l.: The isomap algorithm and topological stability. science 295, 5552. *Science (New York, N.Y.)*, 295:7, 02 2002.

[274] Mira Bernstein, Vin De Silva, John C. Langford, and Joshua B. Tenenbaum. Graph approximations to geodesics on embedded manifolds, 2000.

[275] Thomas Seidl and Hans-Peter Kriegel. Optimal multi-step k-nearest neighbor search. In *Proceedings of the 1998 ACM SIGMOD international conference on Management of data - SIGMOD '98*. ACM Press, 1998.

[276] Amir Najafi, Amir Joudaki, and Emad Fatemizadeh. Nonlinear dimensionality reduction via path-based isometric mapping. *IEEE Transactions on Pattern Analysis and Machine Intelligence*, 38(7):1452–1464, 2016.

[277] Sam T. Roweis and Lawrence K. Saul. Nonlinear dimensionality reduction by locally linear embedding. *Science*, 290(5500):2323–2326, 2000.

[278] WOJCIECH CHOJNACKI and MICHAEL J. BROOKS. A NOTE ON THE LOCALLY LINEAR EMBEDDING ALGORITHM. *International Journal of Pattern Recognition and Artificial Intelligence*, 23(08):1739–1752, dec 2009.

[279] I. Borg and Groenen P. *Modern Multidimensional Scaling - Theory and Applications*. Springer Series in Statistics, 1997.

[280] J. Kruskal. Multidimensional scaling by optimizing goodness of fit to a nonmetric hypothesis. *Psychometrika*, 29(1):1–27, 1964.

[281] J. B. Kruskal. Nonmetric multidimensional scaling: A numerical method. *Psychometrika*, 29(2):115–129, jun 1964.

[282] Roger N. Shepard. The analysis of proximities: Multidimensional scaling with an unknown distance function. i. *Psychometrika*, 27(2):125–140, jun 1962.

[283] Andreas Buja, Deborah F Swayne, Michael L Littman, Nathaniel Dean, Heike Hofmann, and Lisha Chen. Data visualization with multidimensional scaling. *Journal of Computational and Graphical Statistics*, 17(2):444–472, jun 2008.

[284] R.B. Cattell. *Factor analysis.* Harper., New York, 1952.

[285] R.B. Cattell. *Use of Factor Analysis in Behavioral and Life Sciences*. Plenum, New York, 1978.

[286] Tom Fawcett. Roc graphs with instance-varying costs. *Pattern Recognition Letters*, 27(8):882 – 891, 2006. ROC Analysis in Pattern Recognition.

[287] Li Deng. Deep learning: Methods and applications. *Foundations and Trends® in Signal Processing*, 7(3-4):197–387, 2014.

[288] Yoshua Bengio. *Learning Deep Architectures for AI.* Now Publishers Inc, October 2009.

[289] Geoffrey E. Hinton, Simon Osindero, and Yee-Whye Teh. A fast learning algorithm for deep belief nets. *Neural Computation*, 18(7):1527–1554, jul 2006.

[290] Kwang Gi Kim. Book review: Deep learning. *Healthcare Informatics Research*, 22(4):351, 2016.

[291] David Calhas and Rui Henriques. Eeg to fmri synthesis: Is deep learning a candidate? September 2020.

[292] Wutao Yin, Longhai Li, and Fang-Xiang Wu. Deep learning for brain disorder diagnosis based on fMRI images. *Neurocomputing*, oct 2020.

[293] Sandra Vieira, Walter H.L. Pinaya, and Andrea Mechelli. Using deep learning to investigate the neuroimaging correlates of psychiatric and neurological disorders: Methods and applications. *Neuroscience & Biobehavioral Reviews*, 74:58–75, mar 2017.

[294] Sergey M. Plis, Devon R. Hjelm, Ruslan Salakhutdinov, Elena A. Allen, Henry J. Bockholt, Jeffrey D. Long, Hans J. Johnson, Jane S. Paulsen, Jessica A. Turner, and Vince D. Calhoun. Deep learning for neuroimaging: a validation study. *Frontiers in Neuroscience*, 8, aug 2014.

[295] Gerard Martí-Juan, Gerard Sanroma-Guell, and Gemma Piella. A survey on machine and statistical learning for longitudinal analysis of neuroimaging data in alzheimer's disease. *Computer Methods and Programs in Biomedicine*, 189:105348, jun 2020.

[296] Taeho Jo, Kwangsik Nho, and Andrew J. Saykin. Deep learning in alzheimer's disease: Diagnostic classification and prognostic prediction using neuroimaging data. *Frontiers in Aging Neuroscience*, 11, aug 2019.

[297] Guangming Zhu, Bin Jiang, Liz Tong, Yuan Xie, Greg Zaharchuk, and Max Wintermark. Applications of deep learning to neuro-imaging techniques. *Frontiers in Neurology*, 10, aug 2019.

[298] Nianyin Zeng, Hong Qiu, Zidong Wang, Weibo Liu, Hong Zhang, and Yurong Li. A new switching-delayed-PSO-based optimized SVM algorithm for diagnosis of alzheimer's disease. *Neurocomputing*, 320:195–202, dec 2018.

[299] Sinno Jialin Pan and Qiang Yang. A survey on transfer learning. *IEEE Transactions on Knowledge and Data Engineering*, 22(10):1345–1359, oct 2010.

[300] Dipanjan Sarkar. A comprehensive hands-on guide to transfer learning with real-world applications in deep learning. Technical report, Deep Learning on Steroids with the Power of Knowledge Transfer!, November 2018.

[301] Esther Guerra, Juan de Lara, Alessio Malizia, and Paloma Díaz. Supporting user-oriented analysis for multi-view domain-specific visual languages. *Information and Software Technology*, 51(4):769–784, apr 2009.

[302] Will Nash, Tom Drummond, and Nick Birbilis. A review of deep learning in the study of materials degradation. *npj Materials Degradation*, 2(1), nov 2018.

[303] Alex Krizhevsky, Ilya Sutskever, and Geoffrey E. Hinton. ImageNet classification with deep convolutional neural networks. *Communications of the ACM*, 60(6):84–90, may 2017.

[304] Hussain Mujtaba. Introduction to resnet or residual network. Technical report, https://www.mygreatlearning.com/blog/resnet/, September 2020.

[305] Matthew D Zeiler and Rob Fergus. Visualizing and understanding convolutional networks. November 2013.

[306] Kaiming He, Xiangyu Zhang, Shaoqing Ren, and Jian Sun. Deep residual learning for image recognition. In *2016 IEEE Conference on Computer Vision and Pattern Recognition (CVPR)*. IEEE, jun 2016.

[307] Kaiming He and Jian Sun. Convolutional neural networks at constrained time cost. December 2014.

[308] Rupesh Kumar Srivastava, Klaus Greff, and JÃŒrgen Schmidhuber. Highway networks. May 2015.

[309] Craddock Cameron, Benhajali Yassine, Chu Carlton, Chouinard Francois, Evans Alan, Jakab András, Khundrakpam Budhachandra, Lewis John, Li Qingyang, Milham Michael, Yan Chaogan, and Bellec Pierre. The neuro bureau preprocessing initiative: open sharing of preprocessed neuroimaging data and derivatives. *Frontiers in Neuroinformatics*, 7, 2013.

[310] Michael V. Lombardo, Meng-Chuan Lai, Bonnie Auyeung, Rosemary J. Holt, Carrie Allison, Paula Smith, Bhismadev Chakrabarti, Amber N. V. Ruigrok, John Suckling, Edward T. Bullmore, Anthony J. Bailey, Simon Baron-Cohen, Patrick F. Bolton,

Edward T. Bullmore, Sarah Carrington, Marco Catani, Michael C. Craig, Eileen M. Daly, Sean C. L. Deoni, Christine Ecker, Francesca Happé, Julian Henty, Peter Jezzard, Patrick Johnston, Derek K. Jones, Michael V. Lombardo, Anya Madden, Diane Mullins, Clodagh M. Murphy, Declan G. M. Murphy, Greg Pasco, Amber N. V. Ruigrok, Susan A. Sadek, Debbie Spain, Rose Stewart, Sally J. Wheelwright, Steven C. Williams, C. Ellie Wilson, Michael C. Craig, Declan G. M. Murphy, and MRC AIMS Consortium. Unsupervised data-driven stratification of mentalizing heterogeneity in autism. *Scientific Reports*, 6(1):35333, 2016.

[311] Y. LeCun, L. Bottou, Y. Bengio, and P. Haffner. Gradient-based learning applied to document recognition. *Proceedings of the IEEE*, 86(11):2278–2324, November 1998.

[312] Mehran Ahmadlou and Hojjat Adeli. Enhanced probabilistic neural network with local decision circles: A robust classifier. *Integrated Computer-Aided Engineering*, 17:197–210, 2010.

[313] M. H. Rafiei and H. Adeli. A new neural dynamic classification algorithm. *IEEE Transactions on Neural Networks and Learning Systems*, 28(12):3074–3083, 2017.

[314] Danilo R. Pereira, Marco Antonio Piteri, AndreN. Souza, Joao Paulo Papa, and Hojjat Adeli. Fema: a finite element machine for fast learning. *Neural Computing and Applications*, 32(10):6393–6404, 2020.

[315] Kazi Md. Rokibul Alam, Nazmul Siddique, and Hojjat Adeli. A dynamic ensemble learning algorithm for neural networks. *Neural Computing and Applications*, 32(12):8675–8690, 2020.

[316] J.M. Gorriz, C. Jimenez-Mesa, R. Romero-Garcia, F. Segovia, J. Ramirez, D. Castillo-Barnes, F.J. Martinez-Murcia, A. Ortiz, D. Salas-Gonzalez, I.A. Illan, C.G. Puntonet, D. Lopez-Garcia, M. Gomez-Rio, and J. Suckling. Statistical agnostic mapping: A framework in neuroimaging based on concentration inequalities. *Information Fusion*, 66:198 – 212, 2021.